Chapter 2

Literature review

In this chapter, several recent studies have been reviewed to evaluate the potentiality of Mg-Ca silicate-based crystalline bioceramics such as, $MgSiO_3$, Mg_2SiO_4, $CaSiO_3$, Ca_2SiO_4, Ca_3SiO_5, $CaMgSi_2O_6$, $Ca_2MgSi_2O_7$, $Ca_7MgSi_4O_{16}$, $CaMgSiO_4$ and $Ca_3MgSi_2O_8$ as new generation orthopaedic prosthetic implants. The chapter thoroughly reviewed and analyzed the influence of crystal structure, processing parameters/routes and compositional alteration on in vitro/in vivo biocompatibility and degradation behavior of the above ceramics. Further, a correlation between structure, processing and properties has been established. In addition, various stimuli, used to promote the cellular response and inhibit bacterial infection, including surface charge and external electrical stimulation have been critically reviewed.

2.1. Introduction

Recently, the design and development of biodegradable implant materials gained remarkable attention for various clinical applications such as bone repair, regeneration, replacement etc. Such implants seize the possibility of revision surgery for their removal as well as other associated complications [1, 2]. Also, if the degradation rate of implant matches with the growth rate of neo bone tissue, the load transfer from the implant to bone tissue takes place effectively which avoids the stress shielding effect and consequently, preserve the mechanical strength [3-5]. In the past few decades, various class of degradable biomaterials including polymers, metals, ceramics, and their composites have been proposed for orthopedic implant applications [6-10]. However, the compatibility between the degradation rate of metallic and polymeric implants with the rate of formation of neo bone tissue remain among the major concerns. Such incompatibility necessitates revision surgery and sometimes, it leads to other complications [3, 6, 11-16]. Towards this end, the importance of a compatible biomaterial

with reasonable/controlled degradation rate can be realized from both, biochemical as well as clinical perspectives. Few of the biodegradable ceramics have potential to address the above concerns by means of tailored compositional/structural modifications as well as processing.

Recently, a new class of crystalline Mg-Ca silicate - based biodegradable ceramics such as, $MgSiO_3$, Mg_2SiO_4, $CaSiO_3$, Ca_2SiO_4, Ca_3SiO_5, $Ca_2MgSi_2O_7$, $CaMgSiO_4$, Ca_3MgSiO_8 and $Ca_7MgSi_4O_{16}$, attracted significant attention due to their excellent bioactivity and tunable degradability [17-25]. Silicate-based bioceramics have wide range of chemical compositions which possess quite appealing biocompatibility, physical and chemical properties for bone tissue engineering applications [26-29]. Also, some of the silicate bioceramics have been reported to promote the osteogenic differentiation of stem cells by releasing Si-containing ionic products which enhance bone regeneration, *in vivo* i.e., stimulate angiogenesis and osteogenesis [21, 30-35]. The presence of Mg^{2+}, Ca^{2+} and Si^{4+} ions in bioceramics can promote the cell adhesion, proliferation, biomineralization and bone growth [17, 19, 36, 37]. The biocompatibility of Mg-Ca silicates - based ceramics can be tailored by substitution of various ions such as, Sr^{2+}, Zn^{2+}, Ca^{2+}, Mg^{2+} and Zr^{4+} which also influence the dissolution rate of these silicate ceramics. The substitution of Mg^{2+}, Zn^{2+} and Zr^{4+} ions into the binary silicate ceramics decreases their apatite formation ability [38]. However, Sr doping in $CaSiO_3$ decreases its dissolution rate without affecting apatite formation ability. In addition, the substitution of various ions like, Mg^{2+}, Zn^{2+} and Sr^{4+} distorts the crystal structure which reduces the crystallinity and consequently, the densification [39-41].

It has been observed that the crystal structure of these bioceramics also affect the release rate of Mg^{2+}, Ca^{2+} and Si^{4+} ions and consequently, the bioactivity and biocompatibility [42]. Such release rate of ions can be tailored to enhance the adhesion, proliferation and differentiation of stem cells [42]. Mg containing bioactive silicate ceramics significantly induce the bone regeneration as Mg^{2+} ions favor the osteoblast cell proliferation and differentiation [43].

Mg^{2+} ions also play an essential role in maintaining mineral metabolism of biological tissues [44]. $MgSiO_3$ has been reported as a potential substitute for orthopedic application by means of various *in vitro* and *in vivo* studies [21, 45-47]. Additionally, the release of Mg^{2+} and Si^{4+} ions from biodegradable $MgSiO_3$ - based perovskite ceramics increase the differentiation of mesenchymal cells into osteoblast cells which ultimately improve osteogenesis and therefore, the efficacy of such perovskites as bone substitute can be realized [48].

The protein adhesion is the prime requisite for cell-biomaterial interactions [49, 50]. The concentration and type of adsorbed proteins depend on the surface composition of biomaterials [51, 52]. In a recent study, calcium phosphate silicate (CPS) has been demonstrated to reveal significant enhancement in the expression of osteogenic markers, like Alkaline phosphatase (ALP), OPN and Runx-2 than hydroxyapatite (HA) ceramic. A proteomic study was also performed to understand the mechanism of promoted osteogenic activity, in which comparatively larger number of unique proteins were adsorbed on the surface of CPS (171) than HA (101) [50]. It is well known that Ca^{2+} ions play a critical role in various bone metabolic activities [53, 54]. Three primary compounds of Ca-based silicates, i.e., $CaSiO_3$, Ca_2SiO_4 and Ca_3SiO_5, with varying Ca/Si ratio, demonstrate excellent bioactivity [55, 56]. The Ca - based silicate bioceramics are mostly used for bone regeneration, among which $CaSiO_3$ has shown wide acceptability due to its superior osteoconductive and bioresorbable nature as compared to the Ca-phosphate implants [57, 58]. Ca- based silicate bioceramics release Ca^{2+} and Si^{4+} ions in SBF which shows higher bioactivity. In view of the fact that the bioactivity and biocompatibility of these silicate ceramics also dependent on the crystal structure, the present review article initially described the detailed crystal structure of various biocompatible silicate ceramics. The degradation behavior of such bioceramics is among the critical parameters which decides the success of implant and that can be tailored by processing. Towards this end, the present article critically

analyzed various processing parameters/routes to obtain dense and pure Mg - Ca silicate - based bioceramics. In addition, *in vitro* and *in vivo* biocompatibility of Mg-Ca based silicate bioceramics have been discussed elaborately.

2.2. $MgSiO_3$-based perovskite biomaterials

2.2.1. Crystal structure

In general, $MgSiO_3$ exists in five polymorphic forms which occur in two crystal structures, orthorhombic (Portoenstatite) and monoclinic (Clinoenstatite) [59, 60]. Among five polymorphic forms of $MgSiO_3$, such as enstatite, portoenstatite, clinoenstatite, orthoenstatite and high temperature clinoenstatite, portoenstatite (orthorhombic) is stable above the 1000 °C while clinoenstatite (monoclinic) phase is stable below or equivalent to this temperature [22, 59-64]. Portoenstatite and clinoenstatite belong to the space group Pbcn and $P2_1/c$ with lattice parameters as, a = 9.25 Å , b = 8.74 Å and c = 5.32 Å and a = 9.61327 Å, b = 8.82246 Å and c = 5.17455 Å, respectively [62, 65]. In this structure, each of the Mg and Si atoms forms octahedral and tetrahedral coordination with oxygen atoms, respectively where the oxygen atoms occupy four different positions (z = 0.15, 0.35, 0.65, 0.85) [Figure. 2.1 (a, b)].

Furthermore, number of studies suggested that the substitution of various divalent or trivalent cations (Ca^{2+}, Mn^{2+}, Co^{2+}, Zn^{2+}, Ni^{2+}, Fe^{3+} etc.) at Mg^{2+} site in $MgSiO_3$ perovskite, affects the lattice parameters and consequently, the crystal structure [66-71]. Hawthorne and Ito [66] proposed that the substitution of Mn^{2+} (0.075) and Co^{2+} (0.224) at the Mg^{2+} site in $MgSiO_3$ results in orthorhombic structure with Pbca space group [Figure. 2.1 (c, d)].

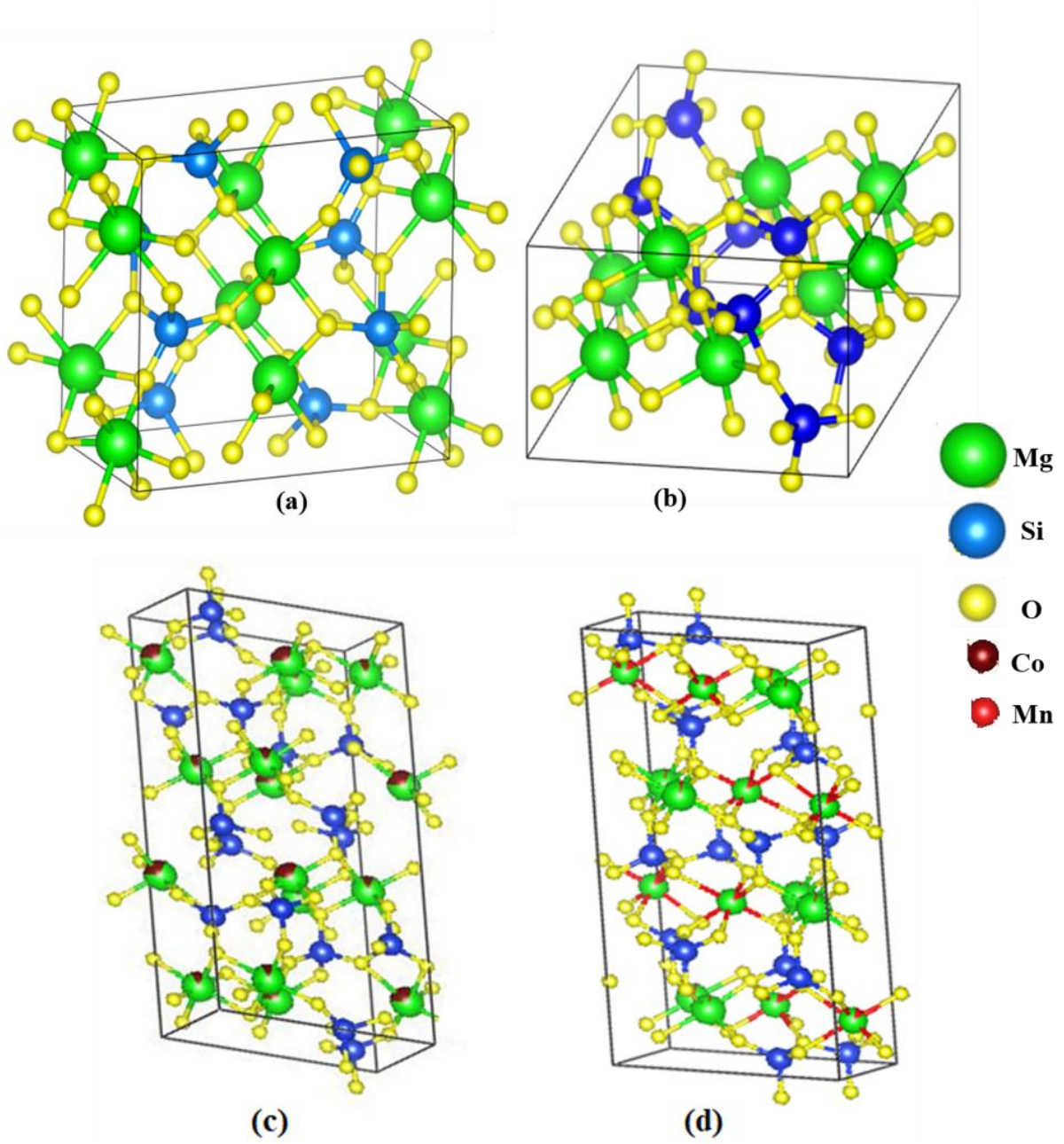

Figure 2.1. Crystal structure of $MgSiO_3$ and Co and Mn substituted $MgSiO_3$. a) Portoenstatite (orthorhombic) with space group Pbcn, b) Clinoenstatite (monoclinic) with space group $P2_1/c$, c) Structure of $(Mg_{0.776}Co_{0.224})$ SiO_3 with space group Pbca and d) Structure of $(Mg_{0.925}Mn_{0.075})$ SiO_3 with space group $(Mg_{0.925}Mn_{0.075})$ SiO_3 [Data taken from refs.62, 63, 65, 66].

Ullah et al. [71] demonstrated that $Mg_{(1-x)}Ni_xSiO_3$ perovskite shows single-phase clinoenstatite (monoclinic, space group $P2_1/c$) structure, formed at $x \leq 0.1$ whereas, the lattice

parameter decreases with increase in the value of x (x = 0 - 0.1). In another study, it has been reported that the substitution of Zn and Co [as, $Mg_{(1-x)}Zn_xSiO_3$ and $Mg_{(1-x)}Co_xSiO_3$] results in increase in the lattice parameters with increase in the value of x as (0 - 0.25) and (0 - 0.3) for Zn and Co, respectively [69, 70]. The cell dimensions and space groups of various polymorphic forms of $MgSiO_3$ are presented in Table 2.1 [62, 65, 72-80].

Table 2.1. Lattice parameters and space group of various polymorphic forms of Mg-Ca silicate based bioceramics with the different crystal structures

Compound	Space group	a (Å)	b (Å)	c (Å)	α (°)	β (°)	γ (°)	Ref.
Portoenstatite ($MgSiO_3$)	Pbcn	9.25	8.74	5.32	90	90	90	62, 65
	Pbcn	9.34	8.79	5.36	90	90	90	
	Pbcn	9.25655	8.7391	5.319	90	90	90	
Clinoenstatite ($MgSiO_3$)	$P2_1/c$	9.61327	8.82246	5.17455	90	108.33	90	72
	$P2_1/c$	9.607	8.815	5.169	90	108.34	90	
Orthoenstatite ($MgSiO_3$)	Pbca	18.225	8.815	5.175	90	90	90	72
High temperature clinoenstatite ($MgSiO_3$)	C2/c	9.864	8.954	5.33	90	110.03	90	73
Wollastonite (β- $CaSiO_3$)	P21/a	15.252	7.224	6.978	90	95.971	90	74
Parawollostenoite ($CaSiO_3$)	P21/a	15.426	7.3200	7.0660	90	95.24	90	75
Pseudowollastonite (α- $CaSiO_3$)	C2/c	6.8394	11.8704	19.6313	90	90.667	90	76
Akermanite ($Ca_2MgSi_2O_7$)	P-42m	7.73	7.73	5.01	90	90	90	77
Diopside ($CaMgSi_2O_6$)	C2/c	9.7456	8.91980	5.25160	90	105.86	90	78
Monticellite ($CaMgSiO_4$)	Pnma	11.1098	6.3839	4.8282	90	90	90	79

Merwinite ($Ca_3MgSi_2O_8$)	$P2_1/a$	13.254	5.293	9.328	90	91.90	90	80

2.2.2. Synthesis of $MgSiO_3$

Number of conventional routes, including dry (solid-state synthesis) and wet (sol-gel, co-precipitation, Pechini method etc.) methods have been adopted to obtain different crystal structures and densification of Mg -based silicate bioceramics. Huang et al. [81] demonstrated that stable orthoenstatite phase of $MgSiO_3$ has been obtained at lower calcination temperature (850 °C for 2 h) using Pechini method. Song et al. [61] fabricated $MgSiO_3$ ceramic using the conventional solid-state method and observed that at lower calcination temperature (< 1200 °C), the additional phase of Mg_2SiO_4 is formed. However, higher temperature (> 1200 °C) leads to the formation of the portoenstatite ($MgSiO_3$) orthorhombic phase. Furthermore, at the higher sintering temperature (1380 °C for 10 h), the Mg_2SiO_4 and SiO_2 phases disappeared and portoenstatite phase is observed with higher densification (98 % of theoretical density, ρ_{th}). However, in earlier studies, it has been reported that the formation of pure enstatite form of $MgSiO_3$ is difficult to achieve using solid-state route as the higher processing temperatures lead to the formation of secondary phases such as, Mg_2SiO_4 and SiO_2 [82-84]. Jin et al. [22] synthesized the $MgSiO_3$ using precipitation route where, $MgSiO_3$ was obtained in two polymorphic forms, clinoenstatite and portoenstatite. The clinoenstatite (monoclinic) phase was formed at lower calcination temperature (< 1000 °C). However, higher calcination temperature (> 1000 °C) leads to the formation of portoenstatite (orthorhombic) phase with the minor presence of clinoenstatite phase. Furthermore, at the higher sintering temperature (1400 °C for 5 h), clinoenstatite phase shows higher densification (82.84 %, ρ_{th}) which is comparatively lower than the densification of portoenstatite, obtained from solid state method. Ullah et al. [69],[85] demonstrated that the substitution of Zn^{2+} (x = 0 - 0.3) and Co^{2+} (x = 0 - 0.25) in $Mg_{(1-x)}B_xSiO_3$ (B = Zn and Co)

reduces the sintering temperature by (~100 ^{0}C) and increases the lattice parameters (a = 9.38949 Å - 9.4045 Å, b = 8.80975 Å - 8.8135 Å, c = 5.18146 Å - 5.1831 Å) with increasing the value of x (0 – 0.3). In addition, doping of Zn^{2+} (x = 0.15) and Co^{2+} (x = 0.15) in $Mg_{(1-x)}B_xSiO_3$ increases the density (97.2 %) of ceramics. From the above studies, it can be concluded that the synthesis of pure $MgSiO_3$ with solid state route is difficult due to the formation of secondary phases at higher sintering temperature. In contrast to the solid-state method, the sol-gel route requires low processing temperature, where the co-existence of multiphases can be eliminated [86]. However, the solid -state method is still important to achieve higher densification which is essential for number of orthopedic implant applications. The densification of $MgSiO_3$ can also be improved by the addition of different dopants such as, Zn, Co and Ni [69-71].

2.2.3. Biocompatibility

2.2.3.1. *In vitro* response

$MgSiO_3$ bioceramics can be suggested as an appealing new class of biodegradable material due to its excellent apatite formulation capability, mechanical and osteogenic properties [32, 45, 48, 87-90].

The cellular response of $MgSiO_3$ has been examined with MC3T3-E1,[45, 48, 91], rat bone marrow mesenchymal stem cells (rBMSCs) [21], bone marrow mesenchymal stem cells **(**BMSCs) [89], MG-63 [92], and mouse fibroblast (L929) [22, 91] cells. Clinoenstatite bioceramics enhance proliferation of L929 and MSCs as compared to HA, due to the release of Mg^{2+} and Si^{4+} ions [22]. Wu et al. [48] reported that mesoporous $MgSiO_3$ (m-$MgSiO_3$) shows better biocompatibility as compared to $MgSiO_3$. The advantageous characteristics of m-$MgSiO_3$ such as, larger specific surface area (451.0 m^2/g) and pore volume (0.41 cm^3/g) as compared to $MgSiO_3$ (75 m^2/g and 0.21 cm^3/g) make mesoporous counterpart more favorable for bone regeneration [48, 93]. Several studies reported that the addition of $MgSiO_3$ in natural

(wheat protein or WP and chitosan or CS) and synthetic (poly (ε-caprolactone) or PCL, poly (ε - ethylene glycol) or PEG, poly (ε-caprolactone) polymers show excellent bioactivity as well as biocompatibility due to the release of Mg^{2+} and Si^{4+} ions from the $MgSiO_3$ - based biocomposites.

Sun et al. [21] demonstrated that $MgSiO_3$ - HA nanowire - chitosan polymer nanosheet i.e., (HA-$MgSiO_3$-CS) nanoporous composite significantly enhances the adhesion of rBMSCs as compared to HA-CS and CS scaffolds after the incubation of 3 days [Figure. 2.2 (a)]. The Mg^{2+} and Si^{4+} ions, released from HA-$MgSiO_3$-CS composite assists in differentiation of rBMSCs into osteoblast cells. Also, HA-CS-$MgSiO_3$ scaffold shows higher angiogenesis and osteogenesis gene expression (RUNX 2, OCN, OPN) as compared to HA-CS and CS scaffolds, while cultured with rBMSCs up to 14 days [Figure. 2.2 (a)] [21]. Feng et al.[45] examined *in vitro* bioactivity and degradability of amorphous mesopores $MgSiO_3$ and natural polymer biocomposites i.e., xm-$MgSiO_3$ - WP (x = 0, 20, 40 wt. %). It has been observed that 40 wt. % m-$MgSiO_3$ - WP composite shows maximum biodegradability and bioactivity [Table 2.2]. Also, the adhesion and differentiation of MC3T3-E1 cells were observed to be enhanced with increasing the fraction of m-$MgSiO_3$ (x = 0, 20, 40 wt.%) [Table 2.2] [45]. Niu et al.[94] demonstrated the biocompatibility of m-$MgSiO_3$ (m-$MgSiO_3$)-PCL- PEG-PCL i.e., (m-MS-PCL-PEG-PCL) composite by varying the proportion of m-$MgSiO_3$ (0, 20, 40 wt.%). The bioactivity, cell proliferation and biodegradation have been observed to be dependent on the m-$MgSiO_3$ content [Table 2.2]. Wu et al. [91] also reported that the biodegradability of m-$MgSiO_3$ (0-40 wt %) - poly (butylene succinate) composites increases with increasing the content of m-$MgSiO_3$, after 84 days while immersed in Tris-HCl solution. Also, enhanced cell attachment, proliferation, and osteogenic differentiation of MC3T3-E1 cells were observed on the surface of composite samples. Another composite scaffold with the amorphous m-$MgSiO_3$, PCL and WP i.e., (m-$MgSiO_3$/PCL/WP), shows enhanced *in vitro*

biodegradability, bioactivity, proliferation and differentiation of L929 and hMSCs cells, respectively [Table 2.2] [95]. Chetagi et al.[89] demonstrated that $MgSiO_3$ coated Ti alloy (Ti-6Al-4V) shows significantly higher cell proliferation as compared to HA-coated Ti alloy, while cultured with BMSCs. In addition, $MgSiO_3$ coated Ti-alloy, cultured with BMSCs illustrates notably higher osteogenesis related genes (ALP, OCN and Collagen 1) as compared to HA-coated Ti alloy [Figure. 2.3 (a)]. It has also been reported that Mg_2SiO_4 bioceramics show excellent biocompatibility, bioactivity and biodegradability [19, 96, 97]. The addition of Zn (0.5 wt. %) in $MgSiO_3$ distorts the crystal structure which reduces the crystallinity and densification and consequently, increases its degradability as compared to pure $MgSiO_3$. $MgSiO_3$ doped with 0.5 wt. % Zn shows higher weight loss (22 %) as compared to pure $MgSiO_3$ after 8 weeks of immersion in SBF. Both of the ceramics show increased attachment and proliferation of MC3T3 cells after 3 days of culture [39, 40]. It has also been demonstrated that Sr (3 wt.%) doped Mg_2SiO_4 bioceramics shows higher weight loss (12 %) as compared to pure Mg_2SiO_4 (9 %) after 8 weeks of immersion in SBF [33].

*2.2.3.*2. *In vivo* response

The bone regeneration capability of $MgSiO_3$-based bioceramics has been reported in several studies. The osteogenic response of $MgSiO_3$ has been examined in combination with synthetic as well as natural polymers [21, 45, 91, 92]. Sun et al.[21] demonstrated that the addition of $MgSiO_3$ into HA nanowire and nanosheet chitosan polymer, i.e., (HA-$MgSiO_3$-CS) nonporous composite scaffold exhibits increased bone regeneration as compared to scaffold without $MgSiO_3$, after 12 weeks of implantation in calvaria defect site of rats [Figure. 2.2 (b)]. The rBMSCs differentiate into osteoblast cells due to release of Mg^{2+} and Si^{4+} ions from composite which consequently, results in enhanced bone regeneration [Figure. 2.2 (c)]. The area and volume of newly formed bone have been found to be higher for HA-$MgSiO_3$-CS (39.41 ± 4.25%, 40.15 ± 6.11%) scaffold than HA-CS (22.99 ± 4.39%, 25.06 ±

3.04%) and CS (3.15 ± 0.84%, 4.92 ± 1.24%) scaffolds [Figure. 2.3 (d)]. Chetagi et al. [89] reported *in vivo* osteogenesis of $MgSiO_3$ coated Ti (Ti-6Al-4V) alloy.

The $MgSiO_3$ coated Ti- alloy shows better osteointegration as compared to HA coated Ti-alloy as well as uncoated Ti -alloy. Also, $MgSiO_3$ coated Ti-alloy shows more neo bone formation (rabbit tibia) and bone implant contact index (BIC) as compared to HA-coated and pure Ti alloy (control) [Figure. 2.3 (b, c and d)]. In another study, augmented (new bone area ~ 90%) bone regeneration has been observed in 40 wt.% m-$MgSiO_3$ incorporated poly (butylene succinate) or PBSu composite scaffolds while implanted in defected femur of rabbit for 12 weeks. Such augmented bone regeneration has been suggested as a consequence of release of Mg^{2+} and Si^{4+} ions [91]. Devi et al. [32, 33] studied *in vivo* osteogenesis of Zn (0.25, 0.5 wt.%) and Sr (1, 2, 3 wt.%) doped Mg_2SiO_4 and pure Mg_2SiO_4 via implantation in rabbit femur defect site for 30 to 90 days. A continuous bone regeneration has been observed on both, Zn (0.5 wt.%) and Sr (3 wt.%) doped Mg_2SiO_4 [Figure. 2.4 (a-h)]. In addition, 0.5 wt.% Zn and 2 wt.% Sr doped Mg_2SiO_4 show significantly higher new bone formation (75 ± 2 % and 80 ± 2 %) as compared to pure Mg_2SiO_4 (42 ± 3 %) after 90 days [Figure. 2.4 (i)][19]. The histological analysis of three major organs such as kidney, liver and heart confirm that the degradation of pure Mg_2SiO_4 and Zn doped Mg_2SiO_4 does not cause any toxic effect to these major organs [Figure. 2.4 (j)]. Again, the release of Mg^{2+} and Si^{4+} ions at the implant's vicinage has been suggested to induce new bone formation [67, 98-104].

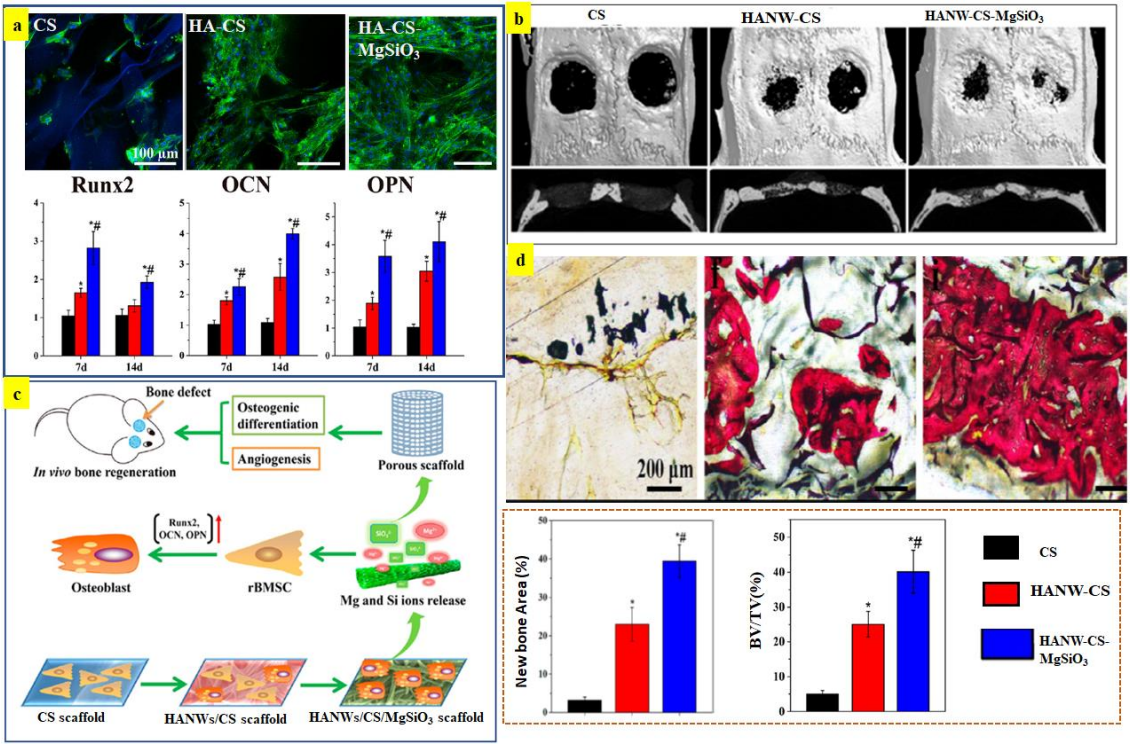

Figure 2.2. In vitro and vivo response of CS, HA-CS and HA-CS-$MgSiO_3$ scaffolds, while cultured with rat bone marrow mesenchymal stem cells (rBMSCs) as well as implanted in calvaria defect site of rat. (a) Cytoskeleton staining after 3 days as well as angiogenesis and osteogenesis gene (Runx2, OCN, OPN) expression, while scaffolds are cultured with rBMSCs for up to 14 days. (b) Micro-CT images of CS, HA-CS and HA-CS-$MgSiO_3$ scaffolds. Coronal and interior images reveal that HA-CS-$MgSiO_3$ scaffold have higher bone regeneration as compared to HA-CS and CS after implantation of 12 weeks. (c) Schematic representing the osteogenic differentiation of rBMSCs into osteoblasts cells. The rBMSCs differentiate into osteoblast cells due to release of Mg^{2+} and Si^{4+}ions from $MgSiO_3$ - based scaffold which consequently, results in enhanced bone regeneration. (d) HA-CS-$MgSiO_3$ demonstrates higher new bone regeneration as compared to CS and HA-CS scaffold. Reproduced with permission from reference [21]. Copyright [2017, American chemical society].

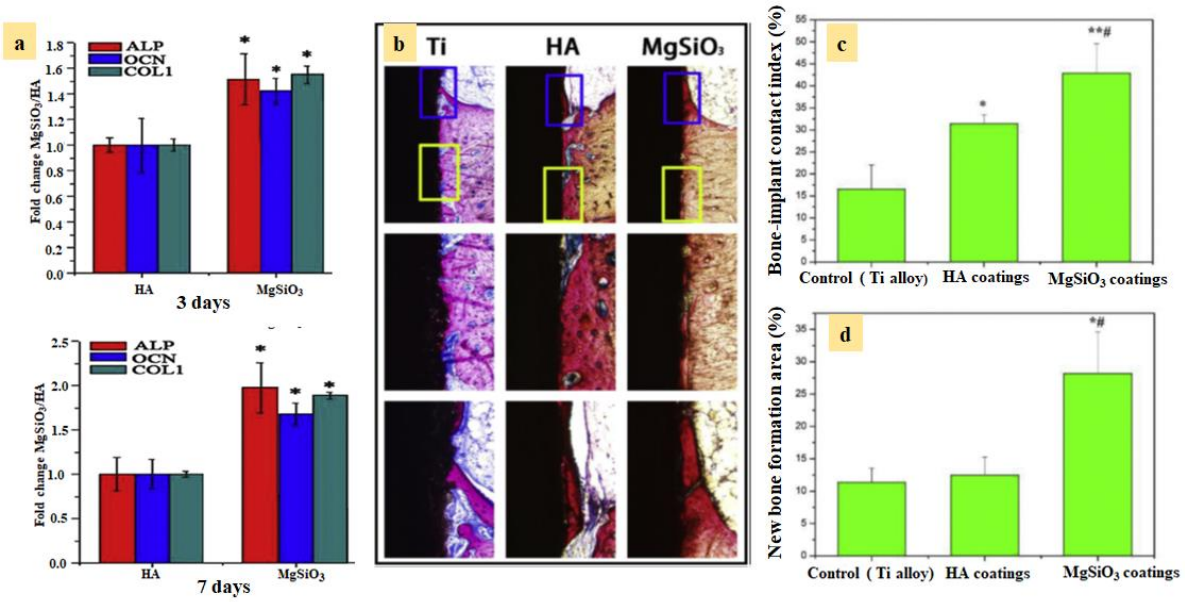

Figure 2.3. In vitro cellular response of $MgSiO_3$ and HA coated Ti- alloy, cultured with BMSCs as well as in vivo response after 8 weeks of implantation in rabbit tibial defect site. (a) $MgSiO_3$ coated Ti-alloy reveals higher osteogenesis related genes (ALP, OCN, COL1) as compared to HA coated Ti- alloy, after 3 and 7 days of culture. (b) Histopathological images, representing neo bone formation (yellow rectangle), while $MgSiO_3$ and HA coated as well as uncoated Ti-alloy are implanted in rabbit tibial defect site upto 8 weeks. (c) Bone- implant contact area and (d) Neo bone formation area for implanted samples with respect to those of control. Reproduced with permission from reference [89]. Copyright [2015, Elsevier].

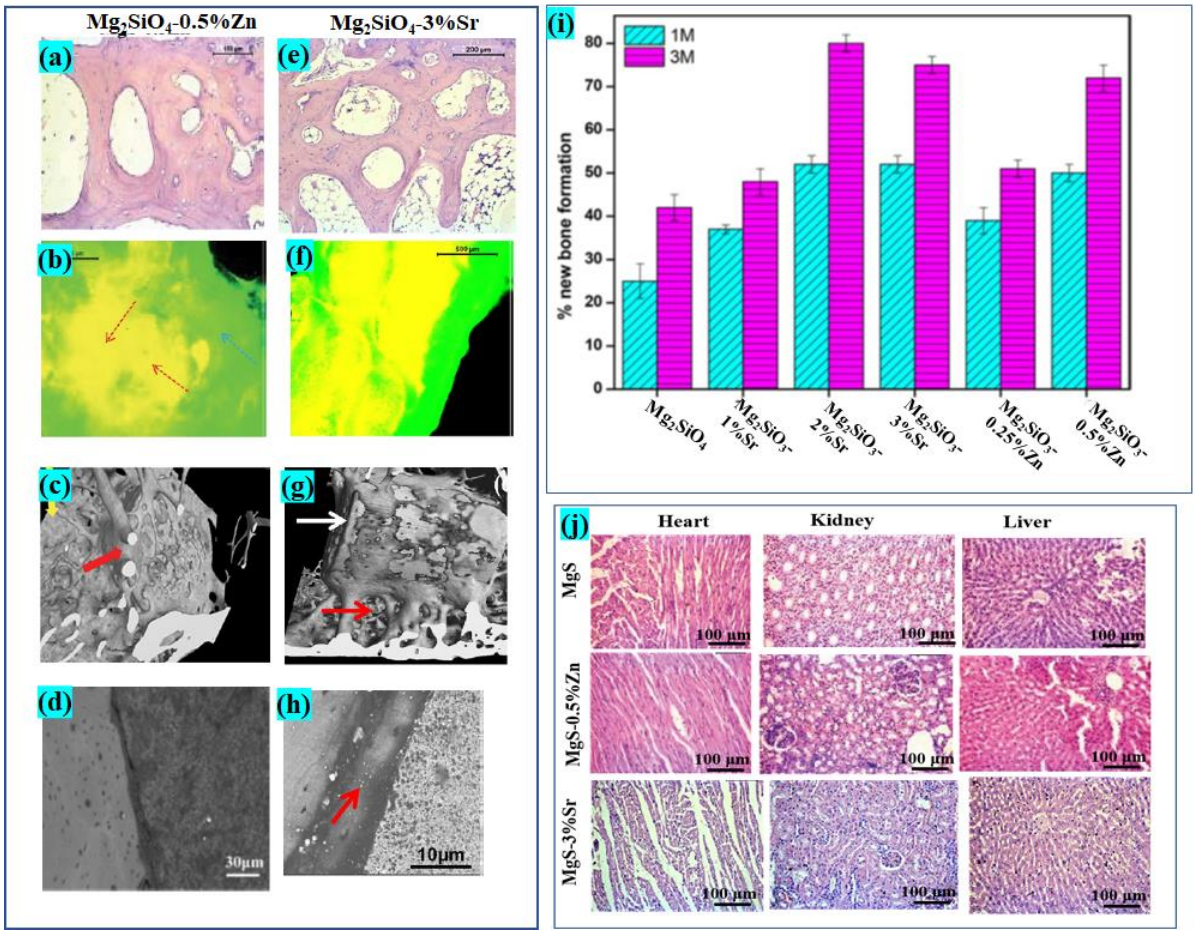

Figure 2.4. In vivo response of Zn and Sr doped Mg_2SiO_4 ceramics, while implanted in rabbit femur defect site. The histological (a, e), fluorescence (b, f), 3D micro -CT (c, g) and scanning electron microscopy (d, h) images of bone - implant interface of Zn and Sr doped Mg_2SiO_4 ceramics, after 90 days of implantation. (i) Formation of neo bone at defect site with varying time and composition of Zn and Sr doped Mg_2SiO_4 [19]. Reproduced with permission from reference [19]. Copyright [2019, Springer Publishing Company]. (j) Implantation of Zn doped Mg_2SiO_4 ceramic does not cause any toxic effect to the three major organs (such as, heart, kidney and lever) of rabbit model up to 90 days [32, 33]. Reproduced with permission from reference [32]. Copyright [2018, American Chemical Society]. Reproduced with permission from reference [33]. Copyright [2018, American Chemical Society.]

From the above discussion, it can be concluded that the inherent biodegradability of $MgSiO_3$ - based scaffolds promote the cellular functionality as well as osteogenesis. However, the

implantation studies are limited upto small animal models due to their uncontrollable degradation behavior [105, 106]. Table 2.2 concisely summarizes the *in vitro* and *in vivo* response of $MgSiO_3$ -based bioceramics [21, 22, 32, 33, 39, 45, 46, 48, 90-92].

Table 2.2. In vitro and in vivo biocompatibility of Mg-based silicate bioceramics

S. N.	**Mg-based silicates**	**Preparation methods**	***In vitro*/ *in vivo* Response**	**Key assessments**	**Ref.**
1	AmorpRs XmMgSiO$_3$-wheat protein polymer composite, X = 0, 20, 40 wt.%	Sol-gel-compression moulding	*In vitro* bioactivity, biodegradability, and cellular response using osteoblast and MC3T3-E1 cells	40 wt. % $MgSiO_3$ reveals maximum weight loss (56 %) after 12 weeks of immersion; Dense apatite layer formation; Increased cell viability and differentiation with increasing the content of $MgSiO_3$ in the composite	45
2	Mesoporous $MgSiO_3$ (m-$MgSiO_3$)	Precipitation centri-fugation	*In vitro* bioactivity, biodegradability, cell proliferation and ALP activity, cultured with MC3T3-E1 cells	Rapid rate apatite formation; Enhanced cell proliferation and ALP activity after 7 days of seeding; 40 % weight loss after 70 days of immersion reflects good biodegradability	48
3	HA-$MgSiO_3$-CS polymer (nanowire HA - nanosheet $MgSiO_3$ -	Porous scaffold prepared through solvothermal method	Bioactivity, cytocompatibility with rBMSCs, 12 weeks implantation in rat bone	Enhanced cell adhesion after 3 days of seeding and higher neo bone area and new bone volume around HA-$MgSiO_3$-CS (39.41±4.25 %, 40.15±6.11 %) as compared to HA-CS (22.99±4.39 %, 25.06±3.04 %) and CS	21

	Chitosan polymer)			(3.15±0.84 %, 4.92±1.24 %) scaffolds in rat bone after 12 weeks of implantation	
4	X (m-$MgSiO_3$)-Poly (Butylene succinate) polymer composite, X = 20, 40 wt. %	Solvent forming-particulate leaching	*In vitro* bioactivity, biodegradability, cellular response and ALP activity with MC3T3-E1 osteoblasts, Implantation in rabbit femur	40 wt. % m-$MgSiO_3$-polymer composite increases weight loss by 4.31 times than scaffold without m-$MgSiO_3$; Highest cell viability and differentiation for 40 wt.% m-$MgSiO_3$ based composite after 5 days; Maximum bone growth observed in 40 m-$MgSiO_3$-polymer composite and 40 wt. % m-$MgSiO_3$-polymer composite shows maximum porosity of 69.7%	91
5	Amorphous m-$MgSiO_3$-PCL-WP	Rapid prototyping technique	*In vitro* hydrophilicity, bioactivity, biodegradability, proliferation, and differentiation of MSCs	Increased hydrophilicity, high biodegradability, and water absorption; Increased cell proliferation and differentiation (after 14 days)	46
6	$MgSiO_3$	Precipitation	*In vitro* cytocompatibility with L929 cells	Enhanced proliferation rate of MEMSCs (after 4 days)	22
7	X(mMgSiO_3)-poly(ε caprolactone)-poly(ε ethylene glycol)-	Solvent casting	*In vitro* bioactivity biodegradability, hydrophilicity, ALP activity with MG-63 cells	40 wt.% m-$MgSiO_3$ polymer composite shows higher hydrophilicity; Formation of dense apatite layer; Higher weight loss (75.6%) and higher cell proliferation as	94

	poly(ε caprolactone), X = 0, 20, 40 wt. %			compared to composite without m-$MgSiO_3$	
8	30 wt. %) m$MgSiO_3$ -(PCL-PEG-PCL) polymer composite	Solvent forming-particulate leaching	Biodegradability, ALP activity, cellular response with MG-63 cells and implantation in the rat femur bone	m-$MgSiO_3$ based polymer composite shows more weight loss (83%) than without m-$MgSiO_3$ based polymer composite (56%), almost double water absorption; Enhanced cell viability; Faster cell differentiation, 1.52 times higher newly formed bone growth in m-$MgSiO_3$ based polymer composite than without m-$MgSiO_3$ based composite	90
9	$MgSiO_3$ coated Ti-6Al-4V alloy	Plasma sprayed	*In vitro* cytocompatibility with Raw 264.7 cells and BMSCs	$MgSiO_3$ coated alloy shows higher cell proliferation; Percentage of new bone formation was higher in $MgSiO_3$ coated alloy (28.19±6.46%) as compared to HA coated (12.51±2.77%) and Ti alloy (11.36±2.19%)	89
10	ZnO (0, 0.25, 0.5 wt.%) doped $MgSiO_3$	Solid - state	*In vitro* cytocompatibility with MC3T3-E1 cells and biodegradation	Higher degradation rate of ZnO doped $MgSiO_3$ (22%) and; Enhanced cell proliferation as compared to pure $MgSiO_3$ and 0.5 wt.%	39

				doped $MgSiO_3$ shows maximum porosity (2.29%) as comperd to pure $MgSiO_3$ (1.15%)	
11	Zn (0, 0.25, 0.5 wt.%) doped Mg_2SiO_4	Solid - state	*In vitro* biodegradation, implantation in rabbit femur	0.5 wt. % Zn doped Mg_2SiO_4 shows the continued degradation, higher porosity (2.53%) and successive bone regeneration after 90 days as compared to Mg_2SiO_4	32
12	Sr (1, 2, 3 wt. %) doped Mg_2SiO_4	Solid-state	*In vitro* bioactivity in BSF, cytocompatibility with MC3T3 cells, implantation in rabbit femur	Higher Sr content in Mg_2SiO_4 facilitates higher weight loss (12%), higher cell proliferation and differentiation; 2 wt. % Sr doping in Mg_2SiO_4 shows higher amount of new bone formation (80±2%) as compared to pure Mg_2SiO_4 (42±2%). The porosity increases from 1.15% - 3.06% with increasing the Sr content from 1 – 3 %.	33

2.3. $CaSiO_3$-based biomaterials

2.3.1. Crystal structure

The $CaSiO_3$ perovskite exists in the two polymorphs, wollastonite (β- $CaSiO_3$) and pseudowollastonite (α- $CaSiO_3$). The β- $CaSiO_3$ phase is stable below 1125 °C. However, α-$CaSiO_3$ phase is sable above 1125 °C. The β-$CaSiO_3$ to α-$CaSiO_3$ phase change occurs at a temperature of 1125 °C [76, 107].

Azarov et al. [108] reported that wollastonite (β- $CaSiO_3$) shows triclinic and monoclinic structures, while pseudowollastonite form possesses monoclinic and pseudohexagonal structures. Primarily, the crystal structure of $CaSiO_3$ is cubic with Pm3m space group [109]. The $CaSiO_3$ exhibits the ideal cubic perovskite structure with Pm-3m space group at the temperature more than 573 °C and low mantle pressure (24-136 GPa) [110]. Felix et al. [111] reported the crystal structure of pseudowollastonite (α-$CaSiO_3$) to be monoclinic with space group $P2_1/a$ and lattice parameters as, a = 15.426 Å, b = 7.3200 Å, c = 7. 0660 Å and β = 94.25° [Figure. 2.5 (a)]. In another study, the crystal structure of pseudowollastonite has been suggested to be monoclinic with space group C2/c and lattice parameters as, a = 6.8394 Å, b = 11.8704 Å, c = 19. 6313 Å, β = 90.667° [Figure. 2.5 (b)] [76]. Earlier, Yamanaka and Mori [112] reported the crystal structure of $CaSiO_3$ to be four-layered triclinic with $C\bar{1}$ space group and lattice parameters as, a = 6.853 Å, b = 11.895 Å, c =19.674Å, α = 90.12°, β = 90.55°, γ = 90.00°.

Some of the theoretical studies suggested that the distortion in cubic phase can produce the tetragonal or orthorhombic symmetries [110, 113-115]. However, Edrees et al. [74] demonstrated that the wollastonite (β- $CaSiO_3$) shows the monocline structure with space group P21/a and lattice parameters such as, a = 15.252 Å , b = 7.22 Å , c = 6.978 Å, β = 95.971°. Moreover, Henriques et al**.** [116] determined the crystal structure of triclinic $CaSiO_3$ with unit cell parameters as, a = 7.63101 Å, b = 6.98062 Å, c = 6.78432 Å and α = 90.0456°, β = 95.5999°, γ = 95.971°. Dörsam et al. [117] suggested the $Ca_{0.43}Sr_{0.57}SiO_3$ structure to be triclinic with P-1 space group and refined lattice parameters as, a = 6.7580 Å, b= 9.46400 Å, c = 6.7507 0 Å, α = 83.22°, β = 76.83°, γ = 70.33° [Figure. 2.5 (c)]. In another study, the crystal structure of α-$(Ca_{1-x}Sr_x)SiO_3$ (x = 0 to 1) has been examined, where, the lattice parameters have been observed to increase (a = 11.9 – 12.3 Å, b = 6.8-7.3 Å , c = 9.8-10.1 Å) with increasing the value of x (0 to 1). The structure was suggested to be monoclinic with

C2/c space group [118]. The crystal structures of $CaSiO_3$ and Sr doped $CaSiO_3$ are shown as Figure. 2.5.

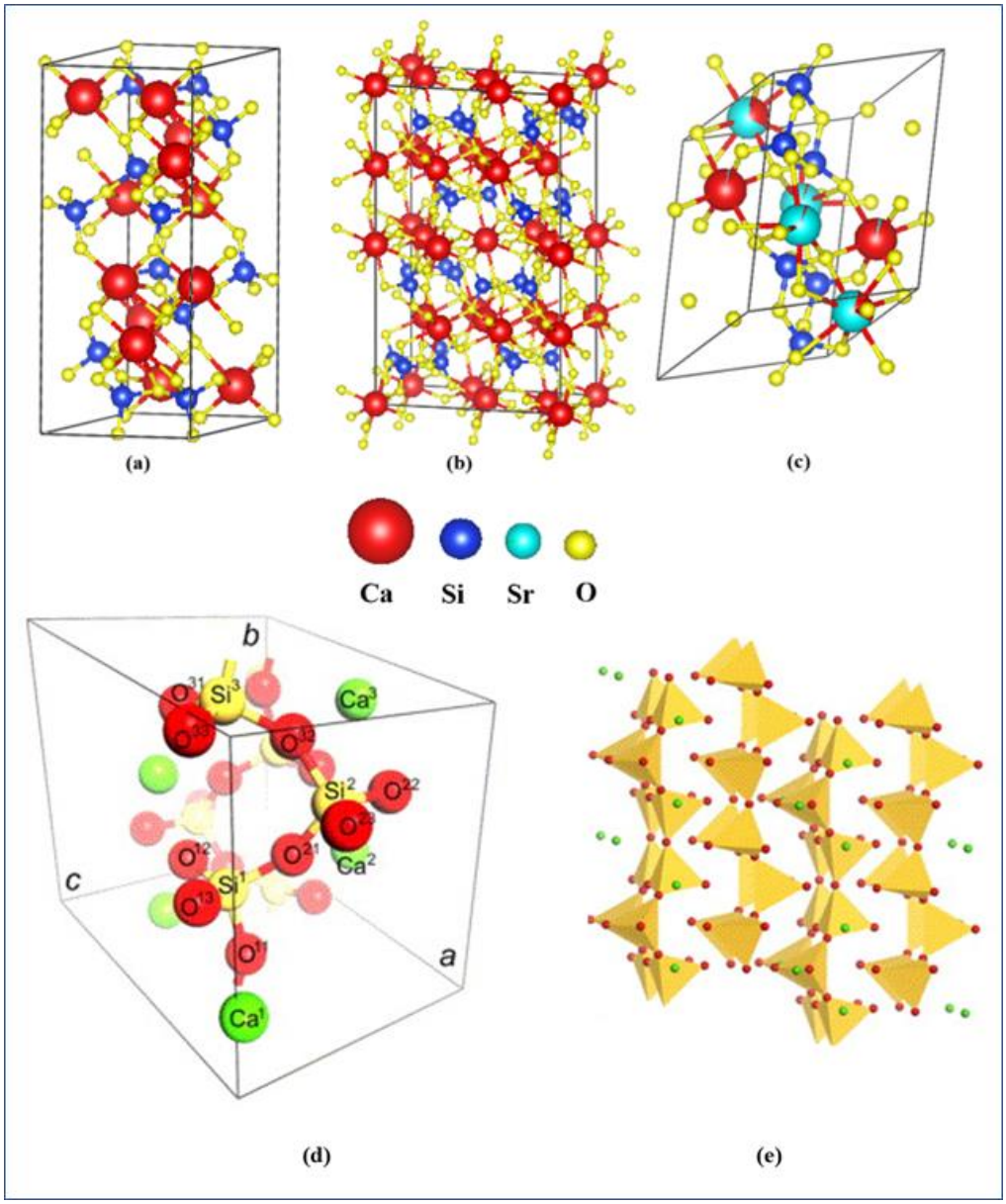

Figure 2.5. Crystal structure of $CaSiO_3$ and Sr doped $CaSiO_3$. a) Monoclinic structure of α-$CaSiO_3$ with $P2_1/a$ space group, b) Monoclinic structure of α- $CaSiO_3$ with $C2_1/c$ space group and c) Triclinic structure of $Ca_{0.43}Sr_{0.57}SiO_3$ with P-1 space group [Data are taken from refs.78, 79, 120, 121]. D) The triclinic structure of $CaSiO_3$. e) Two chains of tilted SiO_4 tetrahedra. Reproduced with permission from reference [116]. Copyright [2006, Elsevier].

2.3.2. Synthesis of $CaSiO_3$

There are many different preparation methods to synthesize the Ca-based silicate perovskite powder, such as co-precipitation, [119-123], sol-gel, [124-126], solid-state,[127] pressure less sintering [128], hydrothermal, [129, 130], and mechanochemical [131] etc. [Table 2.3].

Number of studies has been reported that the $CaSiO_3$ ceramic can be prepared by co-precipitation method with various precipitating agents such as, NH_4OH and NaOH and via calcination and sintering in the temperature range of 800 °C - 1000 °C and 1000 °C – 1400 °C, respectively [Table 2.3] [119-123]. Hayashi et al. [119] fabricated $CaSiO_3$ powder with co-precipitation route using NH_4OH precipitant and calcined at 1000 °C for 2h which led to the formation of β - $CaSiO_3$. The addition of oxalic acid restricts the formation of β- $CaSiO_3$ and promote the formation of α- $CaSiO_3$ phase [119]. Siriphannon et al. [120] synthesized $CaSiO_3$ ceramic using co-precipitation method. The β-$CaSiO_3$ has been observed at lower sintering temperature (1000 °C for 2h). However, sintering at the higher temperature (1400 °C for 2h) leads to the formation of α- $CaSiO_3$ phase. In another study, $CaSiO_3$ was synthesized using similar method with NaOH precipitant, which led to the formation of β-$CaSiO_3$ at a lower temperature range (600 °C to 800 °C) [121]. Rashid et al. [132] fabricated dense $CaSiO_3$ ceramic using limestone ($CaCO_3$) and silica sand (SiO_2) by solid-state method where, the sintering at higher temperature (1450 °C for 4h) leads to the formation of α-$CaSiO_3$. In another study, $CaSiO_3$ was synthesized using similar method with different reagents such as, CaO and SiO_2 which led to the formation of α- $CaSiO_3$ at lower sintering temperature (1150 °C /2h) [133].

From the above studies, it can be concluded that the solid-state method requires high calcination temperatures (> 1000 °C) to synthesize the $CaSiO_3$. To overcome such problems, the vapor assisted solid-state synthesis method has been proposed [134]. Kozawa et al.[135] developed single-phase β-$CaSiO_3$ at calcination temperature of 800 °C (2h) using vapor

assisted solid-state synthesis method. The sol-gel method also requires comparatively low processing temperature than solid- state method [136, 137]. Wang et al.[126] used sol-gel route to prepare $CaSiO_3$ powder which was calcined at different temperatures (800 °C - 1150 °C for 1h). At lower calcination temperature (< 1150 °C for 1h), various phases such as, $CaSiO_3$, Ca_2SiO_4, β-$CaSiO_3$ and SiO_2 were obtained. The sintering temperature of 1320 °C led to the formation of α-$CaSiO_3$. In another study, the sol-gel combustion method was used to synthesize $CaSiO_3$ using sucrose as fuel and nitric acid as an oxidant. Whereas, the formation of β- $CaSiO_3$ phase was obtained at calcination temperature of 900 °C (5 h) [138].

Huang et al. [139] fabricated $CaSiO_3$ by the citrate-nitrate combustion method, which requires lower calcination temperature. In this approach, citric acid was used as a fuel and nitrate was used as the oxidant. The formation of pure $CaSiO_3$ was observed at lower calcination temperature (650 °C/2h). Chakradhar et al. [140] synthesized $CaSiO_3$ ceramic using the solution combustion method where, β-$CaSiO_3$ and α-$CaSiO_3$ phases were formed at the calcination temperature of 950 °C and 1200 °C, respectively. In addition, the phase transformation temperature from β-$CaSiO_3$ to α-$CaSiO_3$ (1100 °C) was obtained to be comparatively lower than the other methods [141-143]. However, the effect of substitution of Mg^{2+}, Ba^{2+}, Sr^{2+}, Ag^{+} and Cu^{2+}ions at Ca^{2+} site in $CaSiO_3$ has been reported by number of studies [114, 124, 144-148]. Sun et al. [41] synthesized Mg-doped $CaSiO_3$ i.e., $Ca_{(1-x)}Mg_xSiO_3$, (x = 0.1 to 0.9) using sol-gel method which was calcined and sintered at 1100°C (4h) and 1290°C - 1300 °C (2h), respectively. In this method, the pure phases of $CaSiO_3$, $CaMgSi_2O_6$ and $MgSiO_3$ were observed at, x = 0.1, 0.5 and 0.9, respectively.

In addition, the coexistence of secondary phases such as, $Ca_3MgSi_2O_8$, $CaSiO_3$, Ca_2SiO_4 were observed at $0.2 > x < 0.4$ and $0.6 > x < 0.8$. The lattice contraction takes place in $CaSiO_3$ ceramics due to the substitution of small sized Mg^{2+} (0.76A°) at the site of Ca^{2+} (1.06A°) [41]. In another study, Sr (0 -10 mol.%) doped $CaSiO_3$ was synthesized with chemical

precipitation method and sintered at 1100°C. The lower content of Sr (< 2.5 %) doping leads to the formation of β-$CaSiO_3$. However, doping with of higher Sr (> 2.5%) content results in the formation of α- $CaSiO_3$. Also, the coexistence of two phases (β-$CaSiO_3$ and α- $CaSiO_3$) was observed at Sr content of 2.5% [147, 149]. Earlier, it was reported that the Sr ions can be used as sintering additive to enhance the densification of ceramic materials [150, 151]. Kagomhiya et al. [118] synthesized the Sr (0 to 1 mol. %) doped $CaSiO_3$ using solid-state method. The prepared powder was calcined at 1200 °C for 2h and sintered at higher temperature ranges from 1450 °C - 1540 °C for 2h, where the pure α - $CaSiO_3$ and $SrSiO_3$ phases were formed at Sr content of (0-0.4%) and (0.6-1.0%), respectively. Also, 0.5% Sr content showed the coexistence of two phases. In addition, the lattice parameters were also increased with increase in the Sr content, except for 0.5 % Sr. Kong et al.[148] synthesized Cu (2.5 %) doped $CaSiO_3$ using chemical precipitation route, followed by the calcination at 900°C for 2h. It has been observed that the incorporation of Cu results in the reduction of crystallite size of $CaSiO_3$ ceramic and thereby, increases the lattice distortion.

It has also been reported that $CaSiO_3$ shows higher densification (> 90%) at lower sintering temperature (such as, 1050 °C and 1070 °C) with the use of some additives like, Li_2CO_3 and B_2O_3 [133, 144]. Such additives consolidate $CaSiO_3$ through liquid phase sintering. From the above discussion, we concluded that it is very difficult to achieve higher densification of $CaSiO_3$ ceramics using conventional processing methods. Therefore, number of attempts have been made to obtain dense $CaSiO_3$ using advanced processing techniques, e.g., spark plasma sintering.

Such processing techniques can provide quite high densification (95 - 99%), even at lower sintering temperature (700 °C - 1200 °C /5 min with heating rate 100 - 200 °C/min). In another study, β-TCP/$CaSiO_3$ composite was prepared using different methods such as, two-

step chemical precipitation and in situ chemical co-precipitation methods at sintering temperature of 1150°C for 5h [152].

Recently, Mei et al. [130] fabricated flower-like nanostructured surface of biodegradable $CaSiO_3$ bioceramics after sintering (1100 °C), followed by hydrothermal incubation of disc in aqueous solution (pH: 7) at 180 °C for 72 h. The $CaSiO_3$/HA nanocomposite bioceramics were synthesize using two step chemical precipitation method with varying $CaSiO_3$ (10 – 90 wt. %) and calcined at 900 °C for 2 h. The formation of pure crystalline HA and β-$CaSiO_3$ was observed at sintering temperature of 1100 °C for 3h [153]. Lin et al. [154] synthesized $CaSiO_3$ nanowire (diameter 20-30 nm) with cetyltrimethyl ammonium bromide (CTAB, surfactant), n pentanol (Co-surfactant), $Ca(NO_3)_2$ and Na_2SiO_4 precursors using hydrothermal (pH: 10.8) microemulsion method, at the calcination temperature of 800 °C for 2 h. In another study, the single crystalline β-$CaSiO_3$ nanowires were developed using hydrothermal method with $Ca(NO_3)_2$ and Na_2SiO_4 precursors. The hydrothermal treatment, at 200°C for 24 h, results in the formation of $Ca_6(Si_6O_{17})(OH)_2$ (xonotlite) which completely transformed into β-$CaSiO_3$ (diameter 10-30 nm) after the calcination temperature of 800°C for 2h [155].

The sol-gel and microwave assisted methods are used to synthesize the nano sized $CaSiO_3$. Also, the wet chemical route is suitable for obtaining the nano - sized $CaSiO_3$. Table 2.3 summarizes various synthesis routes for the development of Ca- based silicates bioceramics [119, 122, 125, 132, 133, 138, 139, 143, 144, 149, 156-163].

Table 2.3. Processing parameters for Ca - based silicate bioceramics

S.N.	Synthesis route	Undoped/ doped $CaSiO_3$	Calcination temperature (°C)	Sintering temperature (°C)	% ρ_{th}	Particle size	Ref.
1	Co-precipitation	$CaSiO_3$	1000/2h	1400/ 1h	90 %	1 µm	119
2	Co-precipitation	$CaSiO_3$	900/ 2h	1400/ 2h	89 %	1.3 µm	121
3	Chemical precipitation	$CaSiO_3$	900/2h	1200/ 2h	70 %	1.15 µm	158
4	Wet-chemical technique	$CaSiO_3$ nanoparticle	1250	-		40 nm	159
5	Sol-gel method	$CaSiO_3$	800- 1150 / 1h	1320/2h	86.37 %	50-60 nm	126
6	Sol-gel combustion method	$CaSiO_3$	900/5h	-	-	51.7 nm	138
7	Citrate-nitrate combustion method	α- $CaSiO_3$	650/ 2h			356-524 nm	139
8	Precipitation method	$CaSiO_3$		1150/5 min	97.3 %	-	160
9	Chemical precipitation	Macro porous $CaSiO_3$	800	1100/3h			143
10	Solid-state method	α-$CaSiO_3$		1450/4h	97.73 %		132

11	Solid-state method	$CaSiO_3$ with 3 to 5 wt.% B_2O_3		1050/2h	97 %		133
12	Solid- state method	$Ca_{0.9}Mg_{0.1}SiO_3$ with 4wt. % Li_2CO_3 additive	1130/6h 200 °C/h	1070/4h	92.54 %		144
13	Chemical precipitation	Sr (1-10 mol. %) doped $CaSiO_3$	-	1100 / 3h			147
14	Sol- gel method	$Ca_{1-x}Mg_xSiO_3$ (0.1-0.5)	1000	1260-1320/2h	50.16 - 88.99 %		161
15	Sol-gel combustion method	$Ca_{1-x}Ag_xSiO_3$ (x = 0.00-0.05)		800/3h			156
16	Solution combustion method	Cr (1-5 mol. %) doped $CaSiO_3$	950/3h			45-32 nm	162
17	Chemical precipitation	$CaSiO_3$	800 /2h	900-970 /5 min	92 - 99 %	0.5 µm	163

2.3.3. Biocompatibility

2.3.3.1. *In vitro* response

The $CaSiO_3$ ceramics are well known for their excellent bioactivity [158, 164]. Both of the polymorphs of $CaSiO_3$, i.e., α-$CaSiO_3$ and β- $CaSiO_3$, support the formation of bone-like apatite layer on their surfaces, while soaked in SBF solution [38, 163, 165-167].

Ni et al. [24] demonstrated that both, α-$CaSiO_3$ and β-$CaSiO_3$ induce the rapid apatite layer formation in SBF and demonstrate good biodegradability (weight loss ~ 27.5 % and 27.8 %) as compared to Mg_2SiO_4 (2.5 %) and β-TCP (1.2 %) specimens, after 28 days of immersion in Tris-HCL solution. In another study, it has also been reported that the formation of HA layer on the surface of α-$CaSiO_3$ takes place within 7 days of soaking in SBF. It also shows higher weight loss (6.3 %) as compared to β-TCP (4.6 %) after immersion in ringer solution for 28 days. It has also been observed that α-$CaSiO_3$ shows higher cell proliferation and ALP activity with osteoblast cells [168]. Siriphannon et al. [120] demonstrated the higher rate of apatite formation on the surface of amorphous $CaSiO_3$ than crystalline **(**β and α)-$CaSiO_3$, after soaking in SBF solution. This is due to the rapid release of Ca^{2+} ions by the amorphous phase. It has been reported that the apatite formation ability of $CaSiO_3$ is influenced by the dissolution of Ca and Si ions. However, the crystalline phases allow the formation of comparatively dense HA layer than amorphous $CaSiO_3$ [169].

Figure 2.6 schematically illustrates the mechanism of formation of apatite layer on surface of $CaSiO_3$ in SBF. Here, H^+ and OH^- ions from SBF solution are exchanged with the Ca^{2+} and Si^{4+} ions on the surface of ceramics and consequently, the pH level of the body fluid increases. Therefore, silanols (Si-OH) rich layer develops on the surface of bioceramics. Ca^{2+} ions, in the SBF, are electrostatically attracted towards the negatively charged silica-rich layer, on the surface of bioceramics. Consequently, negatively charged PO_4^{3-}/ HPO_4^{2-} ions from the body fluid adsorbed on the previously formed Ca^{2+} rich layer which results in the formation of bone-like apatite layer onto the $CaSiO_3$ bioceramic surface [170, 171].

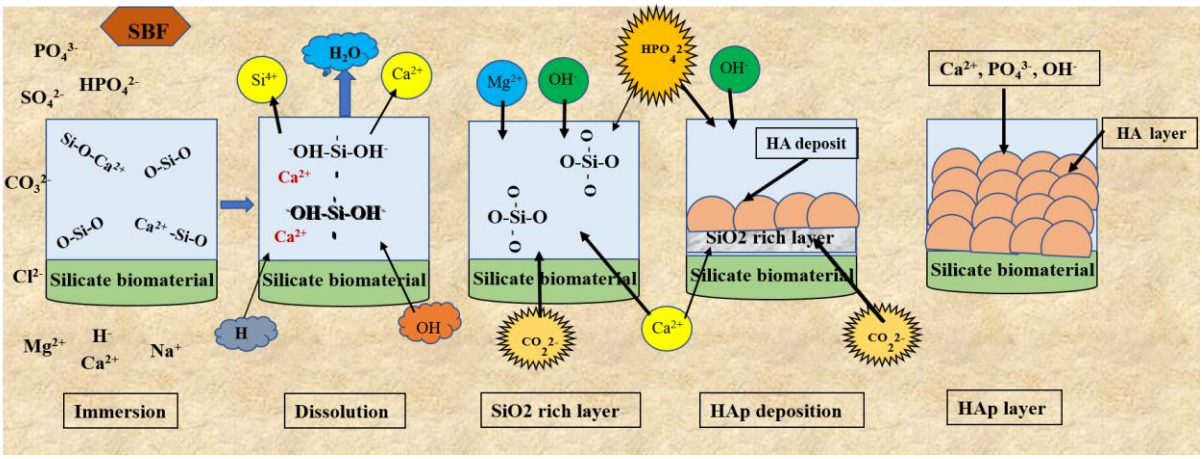

Figure 2.6. Schematic illustrating the mechanism of apatite formation on $CaSiO_3$ surface in SBF. Reproduced with permission from reference [58]. Copyright [2020, John Wiley and Sons].

Ni et al. [23] demonstrated that $CaSiO_3$ (α-$CaSiO_3$ and β-$CaSiO_3$) shows higher cell (rat osteoblast) attachment, proliferation and differentiation as compared to β-TCP (control) after 7 days, due to the higher release of Si ions. It has been reported earlier that the higher concentration of Si ions in solution promotes the metabolic activities of bone cells [172]. Lin et al. [128] reported that $CaSiO_3$ bioceramics, cultured with BMSCs show earlier cell adhesion (just after 1 day) on the surface of $CaSiO_3$ and higher cell proliferation after 5 days. *In vitro* cytotoxicity tests were performed on $CaSiO_3$ bioceramics using cord blood mesenchymal stem (CBMSCs) and BMSCs cells. It has been observed that the viability of both the cells increases with increasing the concentration of $CaSiO_3$ nano powder (20 to 80 µg/ml) [Table 2.4] [159]. The $CaSiO_3$ bioceramics also facilitates the proliferation of MG-63 cells [173]. In another study, it has been observed that the addition of $CaSiO_3$ (0 to 20 wt. %) in Mg_2SiO_4 (i.e., MgO-CaO-SiO_2) bioceramics improved its biological response [Table 2.4] [174]. $CaSiO_3$ shows earlier apatite formation i.e., just after 3 days of immersion in SBF, due to the release of Ca^{2+} ions [175]. However, the formation of apatite layer on the surface of Mg_2SiO_4 was observed after 35 days of immersion in SBF, as the Mg^{2+} ions do not play any

significant role in apatite formation. Overall, the bioactive ability depends on the dissolution behavior as well as chemical composition of the immersed samples. Peng et al. [176] examined the migration, mineralization, proliferation, and odontogenic differentiation of human dental pulp cells (hDPCs), while cultured in $CaSiO_3$ extract whereas, calcium hydroxide and culture medium without any extract were used as a control. The $CaSiO_3$ extract showed enhanced proliferation of dentine cells and upregulation of dentine genes than that of control samples, which has been suggested to be attributed to the release of Si ions from $CaSiO_3$ extract. It has also been demonstrated that the ionic products (preferably Si ions) of $CaSiO_3$ remarkably promote the immunoregulatory response of HBMSCs through activating the NF-kB pathway which further promote the differentiation of HBMSCs [177].

Recent studies reported that Sr containing calcium silicate-based compounds promote the angiogenesis of human umbilical vein endothelial cells (HUVECs) by regulating the angiogenic proteins [178, 179].

Apart from $CaSiO_3$, various studies demonstrated *in vitro* bioactivity and biocompatibility of Ca_2SiO_4 and Ca_3SiO_5 bioceramics [180-184]. Gou et al. [180] demonstrated that β-Ca_2SiO_4 surfaces result in rapid formation of carbonated hydroxyapatite layer (CHA) due to the stronger hydration, while soaked in SBF. In addition, the stronger hydration of β-Ca_2SiO_4 in SBF increases the initial stage pH values which favor faster HA layer formation. However, γ-Ca_2SiO_4 surfaces show relatively slower formation of CHA layer as compared to β-Ca_2SiO_4, due to weaker hydration [182]. Ca_2SiO_4 coating also improves the bioactivity of the surface of Ti- alloy [185].Venkatraman et al. [186] observed that Ca_2SiO_4 and $Ca_3Si_2O_7$ scaffolds demonstrate excellent differentiation and proliferation of hBMSCs cells due to the dissolution of Ca^{2+} and Si^{4+} ions. Zhong et al. [187] fabricated β-Ca_2SiO_4 by spark plasma sintering at sintering temperature of 1150 °C for 5 min. The prepared β-Ca_2SiO_4 showed comparatively higher relative density (98 %), fracture toughness (3.0 MPa m1/2), Vickers hardness (5.8

GPa) and bending strength (293 MPa) than the β-Ca_2SiO_4, prepared by conventional pressure less sintering [187]. In another study, the Ca_3SiO_5 was prepared using spark plasma sintering at the temperature of 1200 °C for 5 min which exhibited good Vickers hardness (5.8 GPa), fracture toughness (2.1 MPa $m^{1/2}$) and bending strength (168 MPa) [188]. The prepared Ca_3SiO_5 also revealed much higher bending strength than that of prepared by conventional sintering (bending strength: 98 MPa) [189]. The spark plasma sintered Ca_3SiO_5 ceramic has also shown good adhesion and proliferation of BMMMC cells [188, 189]. In another study, Sr doped $Ca_3Si_2O_5$ found to promote the proliferation of L929 cells [190].

Furthermore, few studies reported that the bioactivity of binary oxide silicate-based bioceramics (e.g., CaO-SiO_2, MgO-SiO_2 and SrO-SiO_2) decreases with the incorporation of metal ions like, Mg, Zn, and Zr due to reduction in dissolution rate [38, 191]. However, the doping of Sr (0-10 mol.%) into the $CaSiO_3$ results in decreased dissolution rate of $CaSiO_3$, without affecting the apatite formation ability in SBF [149]. Also, Sr doped $CaSiO_3$ stimulates the proliferation of HBDCs, even at lower extract concentration range (12.5 to 50 mg/ml) as compared to $CaSiO_3$ (100 to 200 mg/ml) [149]. Sr ions can easily replace Ca ions which affect the osteoblast activity due to their similarity in size and charge [192]. Therefore, Sr ions doped $CaSiO_3$ bioceramics can enhance bone regeneration, when consolidated into the synthetic bone graft material. In another study, it has also been reported that Sr substituted $CaSiO_3$ scaffold promotes the proliferation and osteogenic differentiation of rBMSCs, due to release of Sr and Si ions from the scaffold [193]. Lin et al. [194] fabricated 5 % 45S5 bioglass containing macroporous $CaSiO_3$ scaffold of reasonable compressive strength (112.5 MPa) and porosity (50 %) with controlled degradation (one third of pure macroporous $CaSiO_3$) rate [122, 157, 195]. Lin et al. [152] prepared β-TCP/$CaSiO_3$ nanocomposites powders using two-step chemical precipitation method, in situ chemical co-precipitation and mechanical milling methods, followed by the sintering at 1150 °C.

The bending strength was comparatively higher for β-TCP/$CaSiO_3$ nanocomposite, prepared via two-step chemical precipitation method (125 MPa) than those prepared by in situ chemical co-precipitation (82.3 MPa) and mechanical milling methods (33.9 MPa). In addition, the degradation rate of the nanocomposite, prepared using two-step chemical precipitation method has shown comparatively less degradation rate i.e., 9.5 %, as compared to the nanocomposites prepared by in situ chemical co-precipitation (11.6 %) and mechanical milling methods (18.5 %) [196]. It has been previously reported that the synthesis method, porosity and sintering parameters affect the degradation behavior of bioceramics [197, 198]. In another study, it has been demonstrated that with increasing the wt. % (10 – 90) of $CaSiO_3$ in $CaSiO_3$/HA composite, the porosity increases from 0.41 to 3.66 %, linear shrinkage decrease from 18.89 to 11.85 %, bending strength increases from 98.1 to 221.3 MPa and elastic modulus decreases from 18.95 to 14.91 GPa [153]. The elastic modulus of $CaSiO_3$ (10-90 wt. %) / HA is suitable for human cortical bone and comparatively less than that of monolithic HA. It has been reported that the bone graft material with elastic modulus equal to bone reduces the bone absorption [128, 196, 199]. The bone- like apatite layer on the surface of 90 wt. % $CaSiO_3$/HA was higher (> 30%) after one day immersion in SBF solution as compared to other $CaSiO_3$/HA composite. $CaSiO_3$/HA (30-90 wt%) shows higher cell proliferation as compared to 10 wt. % $CaSiO_3$/HA and pure HAP after 4 days, while cultured with MSC cells [153]. Ramaswamy et al.[200] demonstrated that Zr doped $CaSiO_3$ (i.e. $Ca_3ZrSi_2O_9$ or baghdadite) bioceramics favor the proliferation and differentiation of human osteoblast, osteoclast, and endothelial cells. The enhanced osteoclastic activity results the bone regeneration ability of $Ca_3ZrSi_2O_9$ [145]. In another study, it has also been suggested that $Ca_3ZrSi_2O_9$ coated Ti6A14V substrate shows enhanced proliferation and attachment of human osteoblast cells [201]. Gou et al.[180] reported that β-Ca_2SiO_4 and γ-Ca_2SiO_4 bioceramics promote the adhesion and proliferation of MSCs.

Sun et al. [202] demonstrated that the plasma sprayed coating of Ca_2SiO_4 on Ti substrate support the regulation of osteoclastogenic gene expression as well as proliferation and differentiation of osteoblast- like (MG-63) cells. Sun et al. [57] suggested that β- Ca_2SiO_4 - based cement (β- Ca_2SiO_4 /CSH- calcium sulfate hemihydrate) shows faster degradation and higher release of Ca and Si ions than calcium phosphate cement (CPC) and consequently, higher proliferation and differentiation of MC3T3 cells. Zhang et al.[42] examined the effect of crystal structure and time dependent release of ions from $CaSiO_3$ on the adhesion, proliferation and differentiation of hMSCs with two polymorphic forms i.e., α-$CaSiO_3$ and β-$CaSiO_3$. Initially, β-$CaSiO_3$ shows higher release of toxic Si ions (> 100 ppm) due to a three-ring silicate structure as compared α-$CaSiO_3$ ceramics with chain silicate structure (approximately 25 ppm) in both the culture media (i.e., growth and osteogenic induction media). Therefore, initially β-$CaSiO_3$ shows significantly lower viability and adhesion of hMSCs as compared to α-$CaSiO_3$.

However, the cellular response of β-$CaSiO_3$ increases with increasing the incubation time due to decrease in the concentration of Si ions as compared to α-$CaSiO_3$ (80 ppm for β-Ca_2SiO_4 and 100 ppm for α-$CaSiO_3$). It has been previously reported that Si and Ca ions, with the concentration of 19 and 200-600 ppm, respectively, are favorable for the osteoblastic differentiation [172, 203-206]. In β-$CaSiO_3$, three-ring silicate tetrahedra is covalently bonded with corner sharing oxygen however, the crystal structure of α-$CaSiO_3$ consists of corner sharing silicate tetrahedra which form chain [Figure. 2.7 (a)]. The Si-O-Si bonds are more stable in α-$CaSiO_3$ as compared to β-$CaSiO_3$ and consequently, β-$CaSiO_3$ shows higher solubility and dissolution rate as compared to α- $CaSiO_3$ [207]. These results confirm that the crystal structure of $CaSiO_3$ can control the release of Si and Ca ions and consequently, modulate the adhesion, proliferation and differentiation of hMSCs [Figure. 2.7 (b, c)]. $CaSiO_3$ -based polymer composite such as, poly (lactic co glycolic acid) or PLGA and poly

(ethylene terephthalate-co-caprolactone) or PETC, enhances the chemical stability and induces the apatite nanocrystal forming ability [208, 209]. Ni et al. [210] examined the *in vitro* response of β-$CaSiO_3$/β-$Ca_3(PO_4)_2$ composites, where β-$Ca_3(PO_4)_2$ was taken as control sample. The results reveal that the dissolution rate of β-$CaSiO_3$/β-$Ca_3(PO_4)_2$ composites enhance with increasing the amount of β-$CaSiO_3$ in composites. In addition, higher amount of β-$CaSiO_3$ in composites favors the differentiation and proliferation of osteoblast-like cells. In another study, it has been reported that $CaSiO_3$/β-$Ca_3(PO_4)_2$ composites augment the expression of osteogenic markers like, OCN and ALP activity after 10 days of culture with increasing the amount of $CaSiO_3$ (50, 80, 100 wt. %) $CaSiO_3$/β-$Ca_3(PO_4)_2$ in composites [211]. Here, the ionic concentrations of Ca and Si ions increase from 54.9- 99.7 ppm and 0-69.2 ppm, respectively, with increasing the amount of $CaSiO_3$ in composites. At the same time, the amount of P ions decreases. The dissimilar concentrations of Ca and Si ions in the composites containing lower amount of $CaSiO_3$, affect the growth of osteoblast cells which may be the reason for lower cellular response in such composites [203, 210-212]. In another study, it has been observed that the ions, dissolved from porous β-$CaSiO_3$/β-$Ca_3(PO_4)_2$, enhance the viability and differentiation of rBMSCs [213]. In addition, the soluble ions from the porous composite promote the deposition of Ca ions and ERK1/2 phosphorylation of rMBSCs. These key findings suggest that the ions, extracted from β-$CaSiO_3$/β-$Ca_3(PO_4)_2$ composite, encourage the osteogenic differentiation of rBMSCs by activating AMPK-Erk1/2 pathway [213]. Recently, Zhang et al. [214] investigated the biocompatibility and degradation properties of $CaSiO_3$/HA coated porous zirconia scaffold, fabricated by 3D printing techniques. The results showed that $CaSiO_3$/HA coated porous zirconia scaffold reveals comparatively higher compressive strength (by 55 %) with increased cell proliferation (MC3T3-E1 cell) and degradation rate as compared to uncoated porous zirconia scaffold

[211]. Ma et al. [215] studied *in vitro* bioactivity and biodegradation behavior of Mg doped ($Ca_2MgSi_2O_7$) and Zn doped ($Ca_2ZnSi_2O_7$) Ca-based silicate ceramics.

It has been observed that the apatite layer formation ability was higher in $Ca_2MgSi_2O_7$ as compared to $Ca_2ZnSi_2O_7$ after immersion in SBF solution. In addition, the weight loss was comparatively lower for $Ca_2ZnSi_2O_7$ (8.4 %) than $Ca_2MgSi_2O_7$ (12.1 %) and $CaSiO_3$ (24.8 %) ceramics, after 4 weeks of immersion in Tris-HCL solution. The higher bond energy of Zn-O as compared to Mg-O is responsible for the lower release of Zn ions than Mg ions which results in higher apatite layer formation in Mg doped calcium silicate. Recently, He et al.[216] examined the osteoclastic and osteoblastic effects on the bioceramic composite, prepared by the incorporation of Ga (2.5 mol. % gallium) and $CaSiO_3$ (5, 10 mol. %) in TCP bioceramics. In this study, it was revealed that 10 mol. % CS / 2.5 mol. % Ga - TCP composite shows higher ALP activity and mRNA gene expression such as RunX, OPN, and BSP as compared to 5 mol. % CS / 2.5 mol. % Ga - TCP and 2.5 mol. % Ga - TCP ceramics. Since, Si is well reported as excellent ions to stimulate the proliferation of osteoblasts and enhance the bone regeneration [23, 217-220]. Therefore, 10 mol. % CS / 2.5 mol. % Ga - TCP composite ceramic, due to higher amount of Si ions, prevents the osteoclastic activity and reveals the higher osteoblastic activity [216]. Recently, it has been demonstrated that the flower-like nano-structured surface of $CaSiO_3$ enhances the adhesion and osteogenic differentiation of BMSCs by activating the FAK/p38 signaling pathway [130]. In addition, the release of Ca and Si ions from the nano-structured $CaSiO_3$ was higher as compared to the micron sized $CaSiO_3$, because of reduced crystallization of grains on the surface of nano-structured $CaSiO_3$ in hydrothermal treatment. Furthermore, the nano-structured $CaSiO_3$ shows good hydrophilicity as compared to micro sized $CaSiO_3$ [221, 222]. In addition, $CaSiO_3$ nanowires, prepared using hydrothermal method, promote the osteogenesis of BMSCs [223, 224]. In another study, it has been reported that the gelatin-methacryloyl and Sr

doped xonotlite nanowire (CSH, $Ca_6(Si_6O_{17})(OH)_2$), (GelMA/Sr-CSH) composite hydrogels enhance the osteogenesis as well as angiogenesis of related cells through the activation of the ERK/p38 signaling pathway [225].

Tobermorite ($Ca_5(Si_6O_{16})(OH)_4H_2O_2$) is another calcium silicate-based nanofibers which show excellent biodegradability and bioactivity and therefore has been suggested as a potential reinforcement material for biomedical applications [226].

Huang et al. [227] performed *in vitro* biocompatibility study and investigated the surface chemistry of microscale (μ-$CaSiO_3$) and nanoscale (n-$CaSiO_3$) particles. The release of Ca ions from both, μ-$CaSiO_3$ and n-$CaSiO_3$ were comparable (2.8-5.6 mM and 2.4-5.4 mM) after 28 days of immersion in Tris-Buffer solution. In the similar period of immersion, the release of Si ions was higher from n-$CaSiO_3$ (0.9-3.0 mM) as compared to μ-$CaSiO_3$ (1.8-3.4 mM). The higher release of Si ions from n-$CaSiO_3$ takes place due to their smaller grain size and lower crystallinity. In addition, n-$CaSiO_3$ showed higher adhesion of hMSCs which may be attributed to the higher release of Si ions [228].

Overall, $CaSiO_3$ - based bioceramics reveal excellent bone forming ability and accelerate the population growth and differentiation of mesenchymal stem cells, MG-63 and human osteoblast cells.

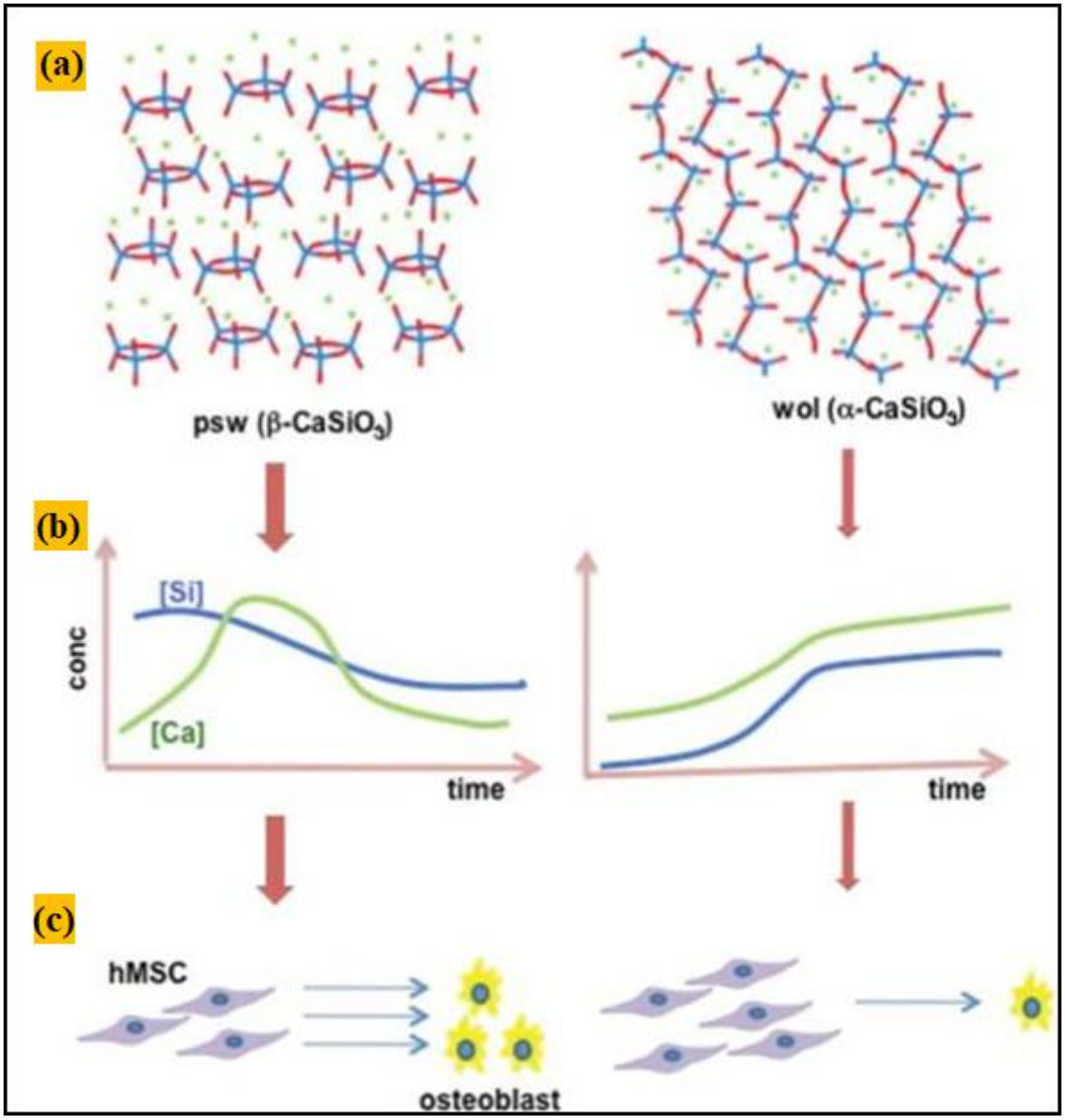

Figure 2.7. In vitro cellular response of hMSCs on β-$CaSiO_3$ and α-$CaSiO_3$. (a) Three- ring silicate and chain silicate structures of β-$CaSiO_3$ and α-$CaSiO_3$ (O-red, Si- blue and Ca-green). (b) Crystal structure dependent solubility and dissolution rate. (c) Cellular response of hMSCs, cultured on both, β-$CaSiO_3$ and α-$CaSiO_3$. Reproduced with permission from reference [42]. Copyright [2013, Royal Society of Chemistry].

2.3.3.2. In vivo response

Number of *in vivo* studies has also been performed for the $CaSiO_3$-based silicate bioceramics such as, $CaSiO_3$, Ca_2SiO_4 and Ca_3SiO_5. Aza et al. [229] demonstrated that the implantation of

α-$CaSiO_3$ in rat tibia for 12 weeks favors neo - bone formation on it's surface. Also, the implant-host interface embarks to serve as physical support. In another study, *in vivo* response of plasma- sprayed $CaSiO_3$ coated titanium alloy (Ti-6Al-4V) was studied by the implanting in dog's cortical bone, marrow, and muscle. After one month of implantation, apatite layer formation was observed on the surface of $CaSiO_3$ coated Ti alloy. In addition, $CaSiO_3$ coating induced new bone formation when implanted in the bone marrow. Also, the bone implant contact area on the $CaSiO_3$ coating (60 %) was found to be higher than the titanium coating (55%), after 12 weeks of implantation [230]. Xu et al. [231] examined the resorption and bone regenerative ability of porous β-$CaSiO_3$, while implanted in rabbit calvaria defect's site. The β- $CaSiO_3$ shows faster degradation (lower volume of residual material from 29.5 - 15.15%) as compared to β-TCP [higher volume of residual material (62.5 - 29.61%)] with increasing the implantation period (4 to 16 weeks), which suggests the faster degradation of β- $CaSiO_3$, *in vivo*. The formation of neo - bone was found to be higher on β- $CaSiO_3$ (28.36%) as compared to β- TCP bioceramics (18.80%), after 16 weeks of implantation [Figure. 2.8 (e, f)].

The β-$CaSiO_3$ shows 2 times higher resorption rate and higher bone regenerative ability as compared to β- TCP. Recently, Du et al. [232] investigated that Mg^{2+} (10 mol. %) doped $CaSiO_3$ enhances newly formed bone volume and bone mineral density by about 1.5 times than undoped $CaSiO_3$ while implanted in rabbit calvarial defect. Lin et al.[233] investigated the degradation and *in vivo* bone regeneration properties of $CaSiO_3$ and β-TCP scaffolds, while implantation in rabbit femur defect model, for 4, 8 and 12 weeks. Histomorphometric analyses revealed higher neo-bone formation on the surface of $CaSiO_3$ scaffold (7, 19, 29 %) as compared to β-TCP scaffold (1, 12, 11%) after 4, 8 and 12 weeks of implantation. Moreover, concentration of Si ions observed to be higher in $CaSiO_3$ (112, 104, 119 ppm) at 4, 8 and 12 weeks as compared to β-TCP scaffold (65, 57, 50 ppm) after operation, which may

be the prime cause of augmented bone formation on the surface of $CaSiO_3$ ceramics. It has also been suggested that at the time of degradation, $CaSiO_3$ and β-TCP ceramics produce the calcium, silicon and phosphate ions, which promote the growth in bone tissue [214].

Liu et al. [234] examined the effect of $CaSiO_3$ addition on the porous β-TCP i.e., 10, 50, 80 wt. % $CaSiO_3$ / β-TCP, while implanted in rabbit femoral condyle for 4, 12 and 26 weeks. Significant increase in the neo bone formation was observed on the surface of 80 % $CaSiO_3$ / β-TCP (25 %) and 50 % $CaSiO_3$ / β-TCP (30 %) as compared to pure β-TCP (15 %) and pure $CaSiO_3$ (5.67 %), after 26 weeks of implantation. Mirkhalaf et al.[235] examined *in vivo* biocompatibility of cylindrical scaffold of Mg doped $Ca_3ZrSi_2O_9$ ($Ca_3Mg_{0.1}Zr_{1-x}Si_2O_{8.9}$) ceramics by the implantation in rat's hind limb muscle pouch for 4 weeks. Micro-CT scanning histomorphometry analyses demonstrated that Mg-doped $Ca_3ZrSi_2O_9$ exhibits considerable neo bone volume (135 % of monolithic $Ca_3ZrSi_2O_9$). Currently, various techniques for the development of bone scaffolds such as rapid prototype, electrospinning, filament winding, thermally induced phase separation etc. are being used [236-239]. 3D printing is a very new technique for making a bone scaffold, this technique facilitates controlled pore size, void distribution and thereby, reduces the wastage of raw materials [240]. Zhang et al.[241] synthesized porous $CaSiO_3$ scaffold using 3D printing technique. The porosity of the sintered scaffold was measured to be 62 %, which is favorable for bone growth.

Moreover, the prepared scaffold exhibited the compressive strength (16.52 MPa) similar to that of cancellous bone [210]. The fabrication of bi-lineage scaffold is difficult due to different biological properties of specific tissues (such as articular cartilage) composed of different lineage [242]. Wang et al. [242] prepared Sr doped $CaSiO_3$ bi- lineage scaffold for osteochondral regeneration. The Sr doped $CaSiO_3$ scaffold significantly enhances the

regeneration of subchondral and cartilage bone, as compared to pure $CaSiO_3$, after 12 weeks of implantation in osteochondral defect of rabbit.

It was also examined that Sr doped $CaSiO_3$ scaffold showed higher (19.87 %) neo bone volume as compare to $CaSiO_3$ (15 %). It has been suggested that Sr ions positively influence the subchondral bone regeneration by inhibiting the receptor, activator responsible for human osteoarthritic such as, nuclear factor-B ligand (RANKL) and proteolytic enzymes (MMP-2 and MMP-9) [243]. In another study, it has been demonstrated that $CaSiO_3$ exhibits higher bone mineral density (800 mg/cm^3) and higher neo bone area (85 %) as compared to β-TCP (400 mg/cc, 50 %) [244]. It has been previously reported that $CaSiO_3$ shows better osteoconductive properties due to higher release of Si ions. In addition, Si ions exhibit anti-inflammatory and antioxidant properties [245]. Mei et al.[130] demonstrated that nano-structured surface of $CaSiO_3$ show higher bone volume ratio ((BV/TV) 30.98 %) and higher new bone area 4.83 mm^2 as compared to microstructured surface of $CaSiO_3$ (11.2 % and 3.5 mm^2), while implanted in critical sized defect in rats.

The biocompatibility of $CaSiO_3$-based composite and metal ion doped $CaSiO_3$ have also been examined, *in vivo* [193, 218]. Wang et al.[218] demonstrated the bone regeneration and *in vivo* degradation of β- $CaSiO_3$ and β- TCP (50 and 80 wt. % in β- TCP) composite scaffold after the implantation in rabbit femur's defect. It has been observed that the composite shows excellent osteoconductive properties and promote the rapid rate of bone formation as compared to pure β- $CaSiO_3$ and β- TCP bioceramics. Sun et al. [34] reported that β-Ca_2SiO_4 and calcium sulfate hemihydrate (CSH), i.e., (β-Ca_2SiO_4/CSH) composite shows higher neo bone formation as compared to CPC, after 12 weeks of implantation in rabbit skull defect. Also, the composite promotes the expression of osteogenic (collegen1, OCN and RUNX2) genes. These results confirm the excellent osteoconductive ability of calcium silicate-based ceramics which can promote the hard tissue regeneration. Table 2.4 summarizes the *in vitro*

and *in vivo* response of bioactive Ca silicate-based bioceramics [57, 58, 128, 158, 159, 168, 174, 193, 231, 246-249].

Overall, *in vitro* and *in vivo* results indicated that $CaSiO_3$ ceramics show excellent cellular response and favorable bone forming ability, when implanted in small and large animal models. However, prior to realizing the clinical implications, the issue of controlled biodegradability has to be addressed by means of various fabrication / substitution methods.

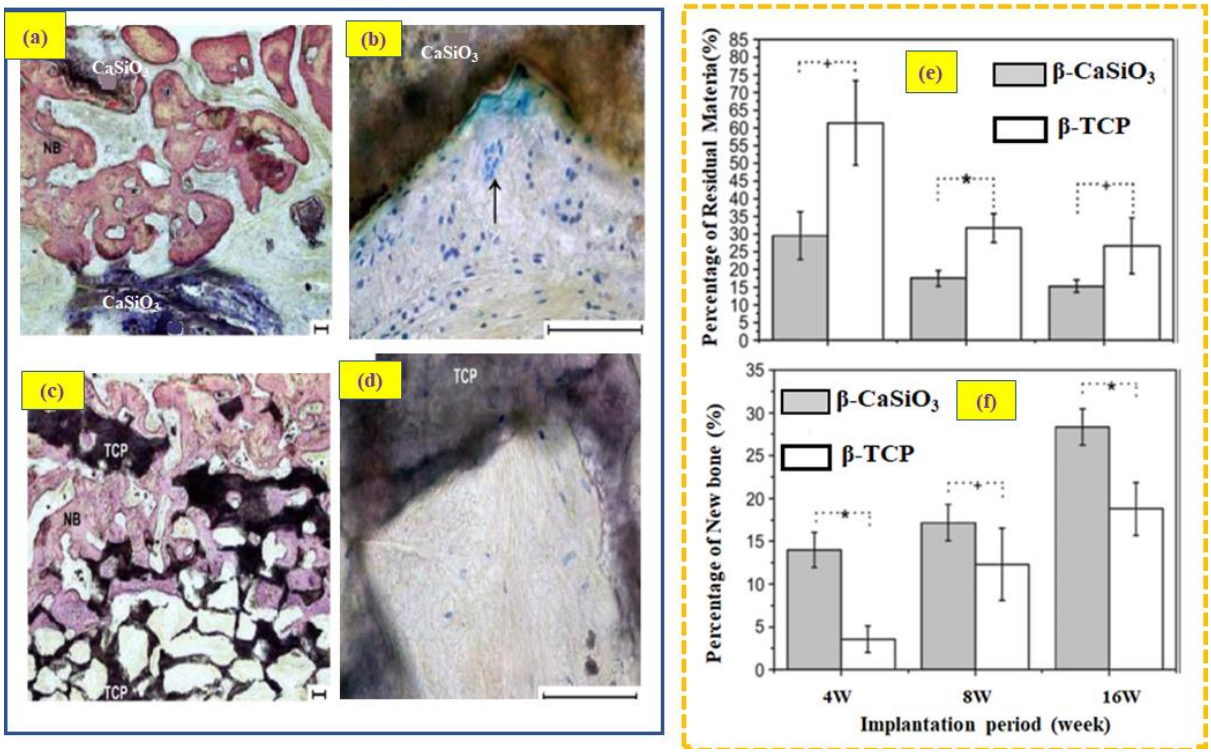

Figure 2.8. In vivo response of β - $CaSiO_3$ and β- TCP scaffolds, while implanted in rabbit calvarial defect site. Histological images of bone - tissue interface, after 16 weeks of implantation with β- $CaSiO_3$ (A, B) and β- TCP (c, d). The degradation and neo bone formation ability of β- $CaSiO_3$ and β- TCP (e, f). (NB- Neo bone) [231]. Reproduced with permission from reference [231]. Copyright [2008, Elsevier].

Table 2.4. In vitro and in vivo biocompatibility of Ca - based silicate bioceramics

S. N.	**Ca - based silicates**	**Preparation methods**	***In vitro/ in vivo* response**	**Key assessments**	**Ref.**
1	Nanostructured $CaSiO_3$	Wet chemical, Sessile drop technique	*In vitro* cytocompatibility with BMMSCs and CBMSCs	Nanostructured $CaSiO_3$ shows higher cell adhesion and proliferation for both the cells; Superhydrophobic in nature	188
2	$Ca_3Al_2O_6$/ Ca_2SiO_4 composite	Solution-polymerization route, sol -gel	Bioactivity, cytocompatibility with L929 cells	Promoted apatite layer formation after 7 days of immersion in SBF; Enhanced proliferation with 10 wt. % addition in $Ca_3Al_2O_6$.	275
3	$CaSiO_3$	Chemical precipitation	*In vitro* bioactivity	Enhanced apatite layer formation	187
4	$CaSiO_3$-Mgx (x = 6, 10, 14 mol. %)	Conventional chemical precipitation route	*In vitro* biocompatibility, ALP activity with MC3T3-E1 cells, implantation in rabbit calvarial defects	Higher Mg-doped $CaSiO_3$ shows more proliferation and differentiation; 14 wt. % Mg-$CaSiO_3$ demonstrate significantly higher neo bone regeneration (22%) as compared to pure $CaSiO_3$ (14%), after 12 weeks of implantation	58
5	$CaSiO_3$	Precipitation	*In vitro* bioactivity	Formation of HA layer on the surface of $CaSiO_3$ after 5 days of immersion in SBF solution.	276
6	Sr (0-10 mol. %) doped $CaSiO_3$	Chemical precipitation	*In vitro* bioactivity, Cytocompatibilty with HBDC cells	Sr - doped $CaSiO_3$ shows the excellent apatite formation ability and decreased the dissolution rate; Stimulated adhesion and proliferation	59

7	$CaSiO_3$/ rGO (0-1.5 wt.%) composite	Hydrothermal	*In vitro* bioactivity, ALP activity, cell adhesion and proliferation of human osteoblast cells	Dense HA layer formation on the surface of composites with increasing the rGO % as compared to pure $CaSiO_3$; Higher adhesion and proliferation of cells as compared to pure $CaSiO_3$	277
8	$CaSiO_3$	Pressureless sintering	*In vitro* cellular response with MMSC cells	Superior adhesion and proliferation	157
9	β-$CaSiO_3$/β-$Ca_3(PO_4)_2$ composite scaffold		Implantation in rabbit femur defect site	50 and 80 wt. % β-$CaSiO_3$ consisted β-TCP shows rapid bone formation; Higher neo bone formation (23.55 and 21.9%), after 26 weeks of implantation.	278
10	Sr doped (10 mol.%) $CaSiO_3$ scaffold	Chemical precipitation	*In vitro* cytocompatibility with rBMSCs, Implantation in OVX calvarial defect model	Sr doped $CaSiO_3$ shows higher ALP activity; Neo bone formation is higher in Sr-$CaSiO_3$ (11.77 ± 1.60%) as compared to pure $CaSiO_3$ (8.07 ± 2.34%) after 4 weeks of implantation.	220
11	β-$CaSiO_3$	-	Implantation in rabbit calvarial defects for (4, 8 and 16 weeks)	Higher neo bone formation (33 %) as compared to β-TCP (18 %) after 16 weeks of implantation	260
12	$CaSiO_3$ scaffolds	Chemical precipitation	*In vitro* bioactivity, ALP activity, cellular response human osteoblast cells	Enhanced adhesion, proliferation and ALP activity	197

13	$CaSiO_3$ (0, 10, 20 wt. %) addition in Mg_2SiO_4		*In vitro* bioactivity, degradability and cytocompatibilty with MG-63 cells	20 wt. % $CaSiO_3$- Mg_2SiO_4 scaffold shows higher degradability (3.64 %); dense apatite layer formation and higher adhesion and proliferation of MG-63 cells than scaffolds without $CaSiO_3$	201

2.4. Mg-Ca silicate-based ceramics

2.4.1. Crystal structure

Number of studies illustrated the structure of Mg-Ca silicate-based perovskite ceramics. Akermanite ($Ca_2MgSi_2O_7$) belongs to the melilite family with the general formula $A_2B(C)_2D_7$. Here, A represents the large cation (such as, Ca, Na, Sr, Pb), B is the tetrahedrally coordinated atom (such as, Mg, Cu, Co), C is smaller cation in tetrahedral coordination (such as, Si, Ge, Al), and D is an anion (O, S) [250]. $Ca_2MgSi_2O_7$ possesses tetragonal structure with $P42_1m$ space group and lattice parameters as, a = 7.7300 Å, c = 5.0152 Å [Figure. 2.9] [77, 251]. In another study, it has been reported that the lattice parameter of $Ca_2MgSi_2O_7$ decreases (a = 7.833 - 7.7341 Å, c = 5.0082 - 4.9215 Å) with increasing pressure upto 4.28 GPa [252]. Diopside ($CaMgSi_2O_6$) is another type of Mg-Ca based silicate bioceramics. The $CaMgSi_2O_6$ is a member of the pyroxene group with the general formula as $XY(T1)_2O_6$, where X and Y represent the large (such as, Ca, Na, Mg) and small cations (such as Mg, Co, Mn), respectively. T1 represents the Si ions (tetrahedral site) and X shows distorted cations shared with six to eight oxygen atoms, depending on the atom size and Y denotes the cation coordinates with six oxygen atoms at the octahedral site [78, 253]. The crystal structure of $CaMgSi_2O_6$ is monoclinic with C2/c space group [77, 78, 254, 255]. Monticellite ($CaMgSiO_4$)

and merwinite ($Ca_3MgSi_2O_8$) are also Mg-Ca silicate - based ceramics exhibiting the orthorhombic and monoclinic structure, respectively [80, 256].

Moore et al.[80] reported that the crystal structure of $Ca_3MgSi_2O_8$ is monoclinic with space group $P2_1/a$ and lattice parameters as, a = 13.254 Å, b = 5.293 Å, C = 9.328 Å and β = 91.90°. In merwinite structure, MgO_6 octahedra linked with each corner of SiO_4 tetrahedra. $CaMgSiO_4$ belongs to the olivine group. The crystal structure of $CaMgSiO_4$ is orthorhombic with Pnma space group and lattice parameters as, a = 11.1098 Å, b = 6.3894 Å, c = 4.821 Å [256]. Also, $CaMgSiO_4$ and $Ca_3MgSi_2O_8$ possess the hexagonal close packed structure where, the Si atom is coordinated with four oxygen atoms and both, Ca and Mg atoms are coordinated with six oxygen atoms [79, 256, 257]. The crystal structures of akermanite, diopside, monticellite and merwinite are shown in Figure. 2.9. Generally, $CaMgSi_2O_6$, $Ca_2MgSi_2O_7$, $CaMgSiO_4$ and $Ca_3MgSi_2O_8$ possess tetragonal, monoclinic and octahedral structures [20]. The crystal structure and unit cell parameters of $Ca_2MgSi_2O_7$, $CaMgSi_2O_6$, $CaMgSiO_4$ and $Ca_3MgSi_2O_8$ are presented in Table 2.1.

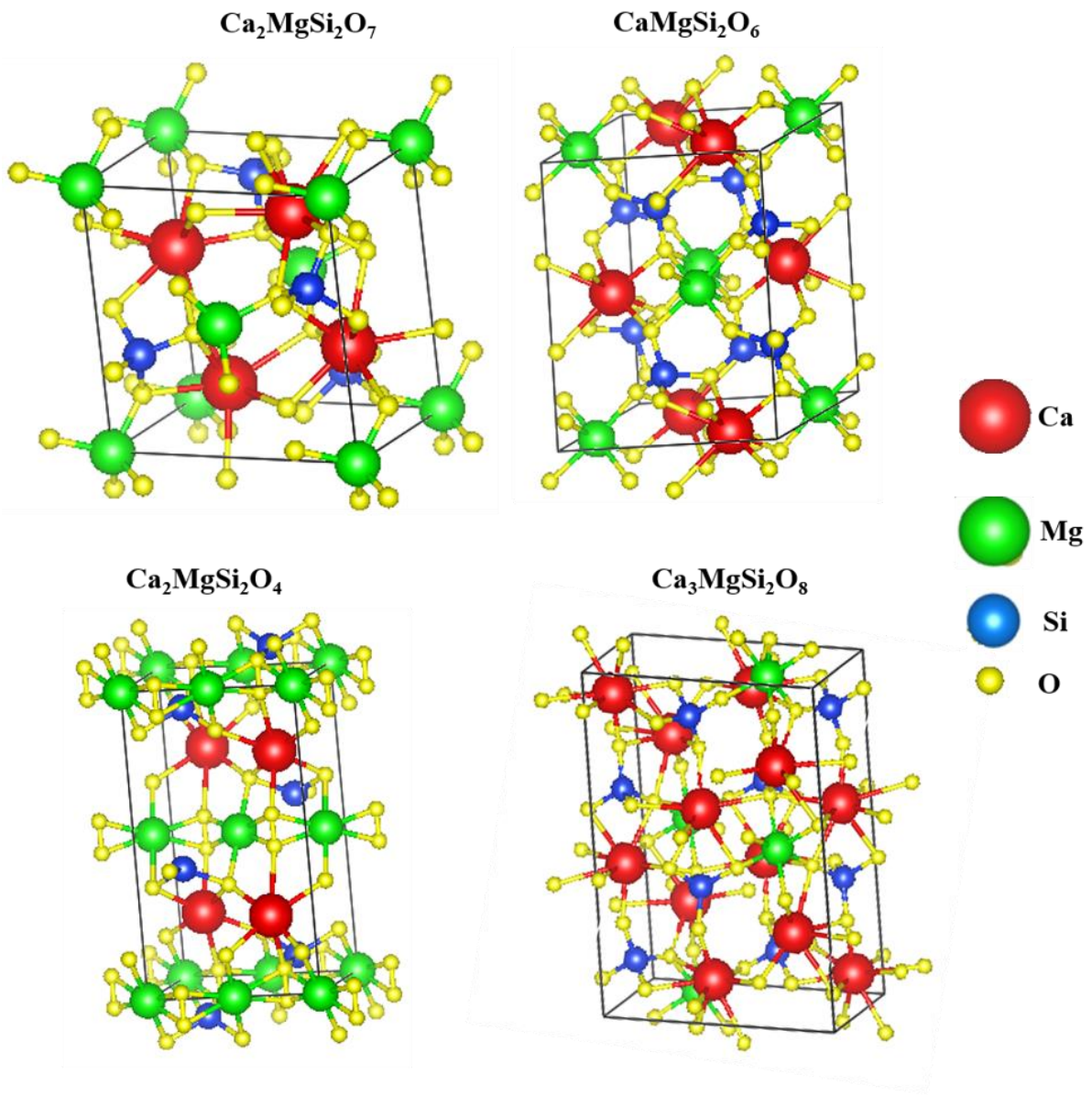

Figure 2.9. Crystal structures of akermanite, diopside, monticellite and merwinite [Data are taken from refs. 112, 113, 114, 115].

2.4.2. Synthesis

$CaMgSi_2O_6$, $Ca_2MgSi_2O_7$, $Ca_7MgSi_4O_{16}$, $CaMgSiO_4$ and $Ca_3MgSi_2O_8$ are single phase ceramics in the Ca-Mg-Si system. Number of studies reported the formation of $Ca_2MgSi_2O_7$ ceramic at the sintering temperature ranging from 1350 °C- 1370 °C (for 6 h) with the densification of about 89.57%-91.1% [258-263]. Sol-gel is the most common synthesis method to prepare $Ca_2MgSi_2O_7$ ceramics. However, it requires more expensive precursor [37,

258, 264, 265]. Therefore, Sharafabadi et al. [266] suggested new economical way to synthesize $Ca_2MgSi_2O_7$ using high energy ball milling of eggshell (calcium source), MgO and SiO_2. It has been demonstrated that pure dense $CaMgSi_2O_6$ is obtained at lower sintering (900 °C) temperature (ball milled for 6 h). In contrast, pure $Ca_2MgSi_2O_7$ phase was not obtained after sintering at 1220 °C (6 h), while processed using sol - gel method [263]. In addition, doping of Ba^{2+} (0.5 mol%) and Sr^{2+} (0.1 mol%) in $Ca_{2-x}MgSi_2O_7$ bioceramics increases the densification by 62.67 to 94.25% and 93.64 to 95.61%, respectively [171, 267].

Bredigite ($Ca_7MgSi_4O_{16}$) is also Mg and Ca containing silicate bioceramics. Various synthesis methods such as, combustion [268], mechanical activation – annealing [269], and sol-gel[264] have been adopted for the development of pure $Ca_7MgSi_4O_{16}$ ceramic. Wu et al.[270] prepared $Ca_7MgSi_4O_{16}$ ceramic by sol-gel method and obtain its pure and dense (94% of ρ_{th}) form at calcination and sintering temperature of 1150 °C (3 h) and 1350 °C (3 h), respectively. In another study, it has been reported that the pure nanocrystalline $Ca_7MgSi_4O_{16}$ phase can be obtained at lower calcination temperature (650 °C /4h) using solution combustion method [263]. In addition, doping of Ba^{2+} (0.5 mol%) and Sr^{2+} (0.1 mol%) in $Ca_{2-x}MgSi_2O_7$ bioceramics increases the densification by 62.67 to 94.25% and 93.64 to 95.61%, respectively [267, 271].

In another study, it has been reported that the pure nanocrystalline $Ca_7MgSi_4O_{16}$ phase can be obtained at lower calcination temperature (650 °C /4h) using solution combustion method [268]. Tavangarian et al.[269] synthesized the nanostructured $Ca_7MgSi_4O_{16}$ using mechanical activation - annealing process, while annealed at 1200 °C for 1 h. Various processing techniques such as, sol-gel, [272, 273], coprecipitation [274, 275] and solid-state [276] methods were used to develop the diopside ($CaMgSi_2O_6$) bioceramics. Nonami et al.[273] synthesized $CaMgSi_2O_6$ powders by sol-gel method using alkoxides [such as, $Ca(OEt)_2$, $Mg(OC_2H_4OEt)_2$ and $Si(OEt)_2$] which reveal the crystallization temperature to be 840 °C.

Iwata et al.[277] fabricated $CaMgSi_2O_6$ by sol-gel method using metal alkoxide [$Ca(NO_3)_2.4H_2O$] and metal salts ($MgCl_2.6H_2O$) with calcination at 700 °C. After sintering (1100 °C for 2h), single phase $CaMgSi_2O_6$ was observed. The crystallization temperature of $CaMgSi_2O_6$ has lowered (751.4^0C) using metal alkoxide and metal salts. However, $CaMgSi_2O_6$ were prepared using similar method, without metal salts, which shows higher crystallization temperature (840 °C) [273]. Recently, Srinath et al.[255] prepared $CaMgSi_2O_6$ using natural waste (rice husk ash and eggshell) via sol-gel method and demonstrated the lower crystallization temperature (776°C) than other synthesis methods for $CaMgSi_2O_6$. In another study, it has been reported that the pure phase of $CaMgSi_2O_6$ can be prepared by coprecipitation method using metal alkoxide and metal salts at lower calcination (700 °C for 2h) and sintering temperatures (1000 °C for 2h) [274].

Recently, Mg-Ca silicate - based ceramics such as, $Ca_2MgSi_2O_7$, $Ca_7MgSi_4O_{16}$, $CaMgSi_2O_6$, $CaMgSiO_4$ and $Ca_3MgSi_2O_8$ were prepared by sol - gel route. It has been observed that single phase $Ca_2MgSi_2O_7$, $CaMgSiO_4$ and $Ca_3MgSi_2O_8$ can be obtained at higher sintering temperatures of 1350 °C, 1450 °C and 1400 °C (for 6 h), respectively [20, 262]. Also, the single phase merwinite ceramic was obtained using sol-gel route with different calcination (700, 1000, 1100, 1300 and 400 °C) and sintering (1300 °C for 2 h) temperatures [278-280]. In another study, dense (93.7%) merwinite ceramic was obtained at calcination and sintering temperatures of 1100 °C (2 h) and 1400 °C (5 h), respectively [281]. Monticellite is another Mg-Ca based bioceramics, which was synthesized using sol-gel method [282-284]. Chen et al. [282] reported that the single phase monticellite was obtained at sintering temperature of 1480 °C (6 h) using sol-gel method.

2.4.3. Biocompatibility

2.4.3.1. *In vitro* response

The ceramics, enriched with Ca, Mg, and Si ions, show excellent mechanical response and manageable degradation rate, even better than β- TCP, which is quite important for bone tissue engineering applications [261, 285].

Recently, it has been recognized that Mg-Ca containing bioceramics such as, akermanite ($Ca_2MgSi_2O_7$), bredigite ($Ca_7MgSi_4O_{16}$), diopside ($CaMgSi_2O_6$), monticellite ($CaMgSiO_4$) and merwinite ($Ca_3MgSi_2O_8$) possess reasonably higher mechanical properties (e.g. bending strength, fracture toughness), biodegradability and apatite forming ability as compared to HA and $CaSiO_3$ ceramics [209, 257-260, 264, 277, 286, 287]. Wu et al.[261] examined *in vitro* bioactivity, degradation, and cytocompatibility of $CaMgSi_2O_6$, $Ca_7MgSi_4O_{16}$, and $Ca_2MgSi_2O_7$ ceramics. It has been observed that diopside ceramics show higher degradation and excellent bioactivity as compared to bredigite and akermanite. Also, ceramics containing Ca, Mg, and Si ions can potentially stimulate osteoblast cell proliferation at lower extract concentration (1.25 and 12.5 mg/ml) and prohibit cell proliferation at higher extract concentration (100 mg/ml). Mg plays an important role in degradation and bioactivity of bioceramics [261]. $CaMgSi_2O_6$, $Ca_7MgSi_4O_{16}$, and $Ca_2MgSi_2O_7$ ceramics have different crystal structures, such as monoclinic, tetragonal and orthorhombic. The degradation rate is also dependent on the crystal structures of these ceramics, which affect the release of various ions (Ca, Mg, and Si) [20, 288-290]. Mg-Ca silicate ceramics show comparatively slower dissolution rate and higher mechanical strength than $CaSiO_3$. The primary reason for the slow dissolution rate of Ca-Mg-Si ceramics is associated with the lower bond energy of Ca-O than the Mg-O bond energy, which inhibits the rapid dissolution rate and makes the crystal structure more stable [291]. Therefore, such ceramics can be treated as a potential alternative for prosthetic orthopedic implants.

Wu et al.[292] reported that in contrast to $Ca_2MgSi_2O_7$, $CaSiO_3$ shows apatite layer formation after 5 days of immersion in SBF. However, after 20 days, the thickness of apatite layer, formed on $Ca_2MgSi_2O_7$ (130 μm) was similar to that of $CaSiO_3$ (110 μm) [292]. Therefore, such ceramics can be treated as a potential alternative for prosthetic orthopedic implants. Wu et al.[259] reported that in contrast to $Ca_2MgSi_2O_7$, $CaSiO_3$ shows apatite layer formation after 5 days of immersion in SBF. However, after 20 days, the thickness of apatite layer, formed on $Ca_2MgSi_2O_7$ (130 μm) was similar to that of $CaSiO_3$ (110 μm) [259]. The compositional difference between the $Ca_2MgSi_2O_7$ and $CaSiO_3$ ceramics is the presence of Mg. Earlier, it has been reported that the release of Mg ions inhibit the crystallization and growth of apatite at initial stage [291, 293].

However, with increasing the soaking period, the concentration of Ca increases at higher rate as compared to that of Mg, which favors apatite formation [170]. In another study, it has also been reported that the doping of Ba^{2+} (x = 0.1, 0.3, 0.5%) in $Ca_{2-x}MgSi_2O_7$ shows better apatite formation ability when immersed in SBF solution than $Ca_2MgSi_2O_7$ [267]. $Ca_2MgSi_2O_7$ ceramic, cultured with osteoblast and fibroblast (L929) cells, considerably enhances cell proliferation due to release of Ca, Mg and Si ions at a certain concentration. Therefore, the proliferation rate of osteoblast cells increases with increasing the culture duration for $Ca_2MgSi_2O_7$ ceramics [259]. Wu et al.[286] prepared 90% porous $Ca_2MgSi_2O_7$ scaffold which promotes the formation of HA layer after immersion in SBF for 10 days. In addition, significantly higher weight loss (17 %) was observed after 28 days of immersion in Ringer's solution. Also, the dissolution of Si, Mg and Ca ions from $Ca_2MgSi_2O_7$ ceramic, stimulates the proliferation and differentiation of BMSCs. In another study, it has been reported that human adipose-derived stem cells (hASCs) adhered and well proliferated on $Ca_2MgSi_2O_7$ ceramics. Also, after 10 days, the osteogenic differentiation of hASCs increases in both, growth and osteogenic media [294]. Likewise, Huang et al.[88] demonstrated that

$Ca_2MgSi_2O_7$ ceramic shows significantly higher proliferation and ALP activity as compared to β- TCP, when cultured with hBMSCs for 20 days. $Ca_2MgSi_2O_7$ extract upregulate the expression of osteogenic gene (osteopontin, bone sialoprotein and osteocalcin) as compared to β-TCP [88] [295]. It has been suggested that the proliferation and differentiation of bone marrow stem cells also increase due to the release of Si and Mg ions. The doping of Mg in β-TCP has been reported to stimulate the adhesion and proliferation of osteoblast cells [295, 296]. Lunguo et al.[28] illustrated that the $Ca_2MgSi_2O_7$ ceramic, cultured with human periodontal ligament cells (hPDLCs) shows significant enchantment in osteogenic differentiation and proliferation as compared to β- TCP. In addition, doping of Sr (x=0.1%) in $Ca_{2-x}MgSi_2O_7$ shows the enhancement in the cell viability of human fetal osteoblast (hFOB) cells which was attributed due to the dissolution of Sr^{2+} ions [271].

In another study, it has been observed that porous $Ca_2MgSiO_7/Ca_3MgSi_2O_8$ scaffold shows higher cell proliferation and ALP activity, while cultured with BMSCs cells. The porous structure facilitates the tissue growth, cell attachment and vascularization [297]. $Ca_7MgSi_4O_{16}$ is also Mg, Ca containing silicate bioceramic which has the ability to form the bone-like apatite after immersion in SBF [264]. In another study, Wu et al.[270] reported that $Ca_7MgSi_4O_{16}$ disc develops compact HA crystals on its surface, with length and diameter of 200-300 nm and 100 nm, respectively, after 10 days of immersion in SBF. It has also been suggested that the ionic products (Ca, Mg and Si), released from $Ca_7MgSi_4O_{16}$ ceramics, enhance the proliferation of L929 cells at lower concentrations (6.25 to 50 mg/ml) and inhibit the proliferation at higher concentrations (100 to 200 mg/ml) [270]. Huang et al.[268] demonstrated that $Ca_7MgSi_4O_{16}$ ceramic, prepared using combustion method, shows the faster rate of apatite layer formation in SBF, as compared to $Ca_2MgSi_2O_7$ ceramic, prepared by sol-gel method. The $CaMgSi_2O_6$ is the first recognized Mg containing bioactive silicate bioceramics, which shows the excellent bioactivity [298, 299].

Iwata et al.[274] demonstrated the apatite layer formation on the surface of sintered $CaMgSi_2O_6$ when soaked in SBF where, the concentration of Mg^{2+} ions initially increased rapidly and then remain constant as the soaking period increases. These studies confirm that the apatite formation ability of $CaMgSi_2O_6$ does not depend on Mg^{2+} ions. Kobayashi et al.[298] examined the cytocompatibility of $CaMgSi_2O_6$ using osteogenic MC3T3-E1 cells where, the reasonably good ALP activity was observed [30, 298, 300]. Srinath et al.[255] reported that $CaMgSi_2O_6$ bioceramic, prepared using rice husk ash and eggshell, shows excellent apatite formation ability in SBF and enhanced proliferation for MG-63 cells. Also, the doping of Ce and Sr in $CaMgSi_2O_6$ improves the apatite formation ability [266, 301].

Later on, Zhai et al.[31] demonstrated that the ionic dissolution of $Ca_2MgSi_2O_7$, $Ca_7MgSi_4O_{16}$ and $CaMgSi_2O_6$ ceramics stimulate the proliferation and osteogenic differentiation of hBMSCs and angiogenesis of hAECs. Among $Ca_7MgSi_4O_{16}$ and $CaMgSi_2O_6$ ceramics, $Ca_7MgSi_4O_{16}$ shows higher osteogenesis and angiogenesis, as compared to diopside due to the higher extract concentration of Si in $Ca_7MgSi_4O_{16}$ [31].These results confirm that the extract concentration of Si (> 0.034 $mmol^{-1}$) stimulates osteogenic differentiation and angiogenesis as compared to β-TCP. Bakhsheshi et al.[302] examined that the $CaMgSiO_4$ – (3%) ciprofloxacin scaffold exhibits good apatite formation ability, additionally, composite scaffold shows excellent attachment and proliferation of MG-63 cells. It has been suggested that Si ions play an important role in the stimulation of osteogenic differentiation, proliferation, and angiogenesis.

Other Mg-Ca silicate-based bioceramics such as $Ca_3MgSi_2O_8$ and $CaMgSiO_4$ also show excellent bioactivity and biocompatibility [278, 279, 282, 303]. Also, the concentration of ions, released from $Ca_3MgSi_2O_8$ and $CaMgSiO_4$ appreciably stimulate the adhesion and proliferation of osteoblast cells [264, 281].

Recently, Mg, Si- and Ca-containing bioceramics gained significant attention due to their tunable degradation rate and bone mimicking mechanical properties [25]. Overall, it can be suggested that the release of different ions (Mg, Ca and Si) from Mg-Ca silicate-based bioceramics stimulates the adhesion, proliferation and differentiation of various cell types.

2.4.3.2. In vivo response

Several studies examined *in vivo* biocompatibility of Mg- Ca silicate-based bioceramics. Huang et al.[88] reported that the $Ca_2MgSi_2O_7$ scaffold shows higher neo bone formation as compared to β-TCP, after 16 weeks of implantation in femur defect site of rabbit. The Van Gieson's picric-fuchsine staining confirms that the degradation and neo bone formation are more obvious on $Ca_2MgSi_2O_7$ as compared to β-TCP [Figure. 2.10 (a, b, c and d)]. Furthermore, $Ca_2MgSi_2O_7$ shows the faster neo bone formation as compared to β-TCP, preferably due to their degradation behavior [Figure. 2.10 (e)]. Also, the $Ca_2MgSi_2O_7$ have faster degradation rate (lower volume of residual material) as compared to β-TCP (higher volume of residual material) after 8 and 16 weeks, which suggest the rapid degradation of $Ca_2MgSi_2O_7$ implant [Figure. 2.10 (f)]. In another study, the osteogenic performance of the $Ca_2MgSi_2O_7$ ceramics has been observed after implantation in OVX rat defect [304].The Van Gieson's picric-fuchsine staining confirms that the degradation and neo bone formation are more evident on $Ca_2MgSi_2O_7$ as compared to β-TCP [Figure 2.10 (a1, a2, b1 and b2)]. After 8 weeks of implantation, the neo bone formation was higher (24 ± 3.8%) on $Ca_2MgSi_2O_7$ ceramic as compared to β-TCP (14.29 ± 2.98%), which was used as control [Figure. 2.10 (c1)]. Also, the newly developed blood vessel area was higher in $Ca_2MgSi_2O_7$ (1.93 ± 0.35%) as compared to β-TCP (1.08 ± 0.19%) [Figure. 2.10 (d1)]. In addition, the degradation rate of $Ca_2MgSi_2O_7$ was faster (lower volume of residual material) as compared to β-TCP (higher volume of residual material) [Figure. 2.10 (e1)].

It can be suggested that the release of Mg and Si ions from the $Ca_2MgSi_2O_7$ ceramics promotes the biodegradability and consequently, the biocompatibility of $Ca_2MgSi_2O_7$ ceramics. In a recent study, the nano-structured $Ca_2MgSi_2O_7$ coated Ti-6Al-4V implant showed higher neo bone formation (40 %) as compared to microstructured $Ca_2MgSi_2O_7$ (35 %) and HA (20 %) coated implant, after 12 weeks of implantation in rabbit bone defect of tibiae [305]. The histomorphometric analyses reveal that the bone-implant contact ratio (%) was higher on the nano-structured $Ca_2MgSi_2O_7$ coated Ti-6Al-4V (~ 36 %) as compared to $Ca_2MgSi_2O_7$ (~ 26 %) and HA coated (~ 14 %) implant. Therefore, it can be realized that the nanostructured surface and the release of bioactive ions synergistically promote the neo bone formation. Hafezi et al. [35] implanted the merwinite ceramics in rat femoral defect site and observed that the degradation rate and new bone formation was higher in $Ca_3MgSi_2O_8$ ceramic as compared to HA, after 8 weeks of implantation. The $Ca_3MgSi_2O_8$ ceramic shows higher degradation and induces osteogenesis [35].

$CaMgSi_2O_6$ has been demonstrated as a potential material which induces the neo bone formation after implantation in rabbits, monkey and greater trochanter of rabbits [30, 31, 298, 306]. Also, $Ca_3MgSi_2O_8$ and $CaMgSiO_4$ bioceramics enhance the proliferation and cell growth of osteoblast cells. The *in vivo* studies confirm that $Ca_3MgSi_2O_8$ ceramic shows enhanced bone regeneration due to their superior degradation [35, 281, 282]. Few studies also reported increased apatite layer formation on the surface of $CaMgSi_2O_6$ ceramics, while implanted in monkeys and rabbits [30]. From the above results, it can be concluded that akermanite, bredigite and diopside bioceramics stimulate the angiogenesis and osteogenesis both, *in vitro* and *in vivo*. Figure. 2.11 illustrates a glimpse of *in vivo* studies on Mg-Ca silicate - based bioceramics on small, medium and large animal models. Table 2.5 summarizes the *in vitro* and *vivo* response of Mg-Ca silicate - based bioceramics [88, 213, 246, 258, 259, 286, 294, 307-310].

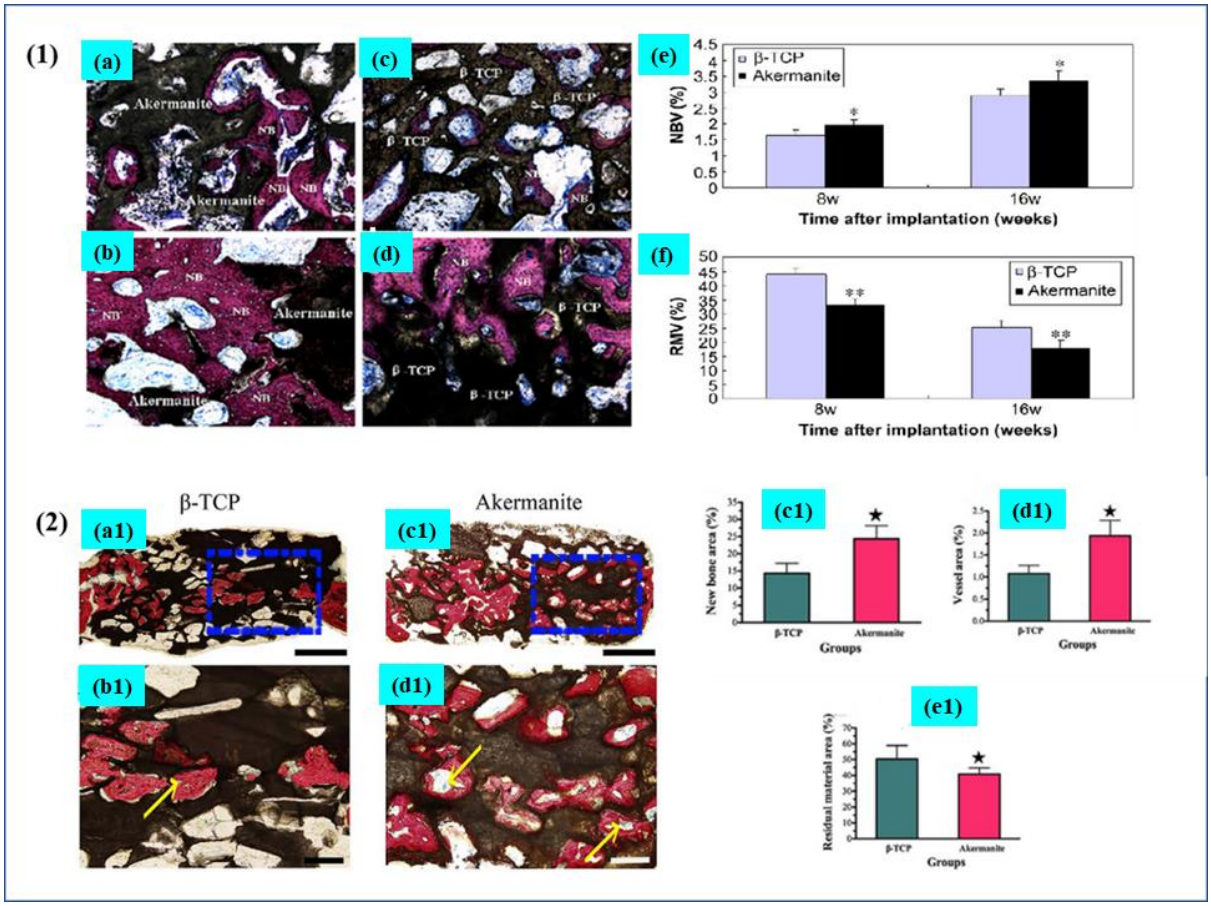

Figure 2.10. In vivo response of akermanite ceramic, while implanted in rabbit femur and ovx rat defect site. *Van Gieson's picric-fuchsine staining images demonstrating new bone formation area around akermanite (a, b) and β-TCP (c, d). The histomorphometric analyses illustrate the neo bone volume and volume of residual material (e, f) on akermanite and β-TCP ceramics, while implanted in rabbit femur defect for 8 and 16 weeks. Reproduced with permission from reference [88]. Copyright [2009, Elsevier]. Histological images representing the neo bone formation area on akermanite (a1, a2) and β-TCP (b1, b2), implanted in calvarial defect area for 8 weeks. (c1), (d1) and (e1) represent the neo bone area, vessel area as well as residual material area of akermanite and β-TCP ceramics. Reproduced with permission from reference [304]. Copyright [2016, Springer Nature].*

Figure 2.11 A glimpse of in vivo studies, performed on Mg-Ca- based biomaterials using small, medium and large animal models.

Table 2.5. In vitro and in vivo biocompatibility of Mg-Ca silicate- based bioceramics

S. N.	Mg-Ca based materials	Preparation methods	*In vitro/ in vivo* response	Key assessments	Ref.
1	$Ca_2MgSi_2O_7$	Sol-gel	*In vitro* bioactivity	HA layer formation after 10 days soaking in SBF	250
2	$Ca_2MgSi_2O_7$	Polymer spongy	*In vitro* bioactivity, biodegradability and cytocompatibility with BMSC cells	Higher weight loss (18 %) after 28 days of immersion; formation of HA layer (100 nm) after 10 days; Higher adhesion, proliferation and ALP activity as compared to control, after 7 days.	288
3	$Ca_2MgSi_2O_7$	Sol- gel	*In vitro* bioactivity, proliferation, ALP activity with L929 fibroblast cells	Apatite layer formation after 20 days; Significantly higher adhesion and proliferation as compared to $CaSiO_3$, after 7 days of culture	259
4	Poly(lactide-co-glycolide) (PLGA) / $Ca_2MgSi_2O_7$ composite	Sol-gel	*In vitro* bioactivity, cytocompatibility with hBMSCs	PLGA/ $Ca_2MgSi_2O_7$ composite shows higher ALP activity; Higher cell proliferation as compared to PLGA after 14 days.	246
5	$Ca_2MgSi_2O_7$	Sol-gel	Bioactivity and cellular response with hASCs	$Ca_2MgSi_2O_7$ increases the cell proliferation and differentiation; Ca, Mg and Si ions induce the differentiation of hASCs.	213
6	$Ca_2MgSi_2O_7$ glass sphere	Sol -gel	*In vitro* bioactivity, proliferation and	Excellent bioactivity after soaking for 7 days;	307

			ALP activity with MC3T3- E1 cells	$Ca_2MgSi_2O_7$ sphere reveal higher proliferation and differentiation after 7 days.	
7	$Ca_2MgSi_2O_7$		*In vitro* cytocompatibility with hASCs	Higher cell proliferation and higher ALP activity in both, osteogenic (121 %) and growth (128 %) media as compared to β-TCP, after 10 days.	294
8	$Ca_2MgSi_2O_7$		Cellular response and ALP activity with hBMSCs. Implantation in rabbit femur defect model	Enhanced osteogenic differentiation and higher proliferation of hBMSCs, than on β-TCP; Significantly higher new bone formation (3.5%) as compared to β-TCP (3%), after 16 weeks.	88
9	$Ca_7MgSi_4O_{16}$	Sol-gel	Bioactivity, cellular response with L929 cell	Extract concentration (6.25-25 m/ml) of $Ca_7MgSi_4O_{16}$ increases the attachment and proliferation of L929 cells after 6 days; HA layer formation (80-100 nm) after 20 days	270
10	$Ca_7MgSi_4O_{16}$ scaffold with biometric apatite layer (BATP)	Polymer sponge	*In vitro* bioactivity, biodegradability, cell proliferation and differentiation, ALP activity with osteoblast cells	$Ca_7MgSi_4O_{16}$ ceramic shows higher weight loss (18 %) after 30 days; Apatite layer formation after 10 days; Enhance the cell adhesion, proliferation and ALP	308

				activity after 7 days.	
11	$Ca_7MgSi_4O_{16}$	Sol- gel	*In vitro* bioactivity	HA layer formation after 10 days	264
12	$CaMgSi_2O_6$		Cellular response with MC3T3-E1 cells. Implantation in rabbits defect model for 12 weeks	$CaMgSi_2O_6$ shows higher ALP activity as compared to control; Significant neo bone formation after 20 weeks	28
13	$CaMgSi_2O_6$		Implantation in jaw bone of rabbits and Japanese monkey for 12 weeks	$CaMgSi_2O_6$ forms a uniform junction with newly grown bone	30
14	$CaMgSi_2O_6$	Coprecip itation method	*In vitro* bioactivity	Leaf-like apatite particle formation on the surface of $CaMgSi_2O_6$ after 3 and 7 days of immersion	277
15	$CaMgSi_2O_6$		Implantation in greater trochanter of rabbits	$CaMgSi_2O_6$ coating on AZ91 Mg alloy enhance the new bone formation	306
17	Mg doped $Ca_3ZrSi_2O_9$ ($Ca_3Mg_{0.1}Zr_{0.9}Si_2O_{8.9}$)		Implantation in the rat hind limb muscle pouch of Wistar rats	$Ca_3ZrSi_2O_9$ shows higher new bone volume (35%) as compared to $CaMgSi_2O_6$ after 4 weeks of implantation	235
17	$CaMgSi_2O_6$		Implantation in the femur of Wistar rats	Higher amount of new bone formation as compared to β-TCP after 4 weeks of implantation	310
18	$Ca_3MgSi_2O_8$		Implantation in rat femoral defect site	Higher osteogenesis and higher new bone formation as compared to HA	35

2.5. Influence of surface charge and electrodynamic stimulation on cellular response

Recently, polarization induced enhanced biocompatibility of piezoelectric bioceramics has been recognized as a potential strategy for the creation of electroactive prosthetic orthopaedic implants [47, 311-314]. It has been demonstrated that the combined effect of electrostatic and electrodynamic simulation remarkably enhances the functionality of osteoblast-like cells as well as human bone marrow mesenchymal stem cells (MSC) [315-319]. Negatively charged surfaces enhanced the adhesion of osteoblast cells through electrostatic interactions, where the negative charges attract Ca^{2+} ions, promoting cellular adhesion [320]. Dubey et al.[316] reported that, after 48 h of cell culture on the negatively polarized HA-x BT (with x = 20 and 40 wt. %), composites the density of L929 cells rises significantly by 40% and 62%, respectively. Verma et al.[317] reported that, electrostatically and electrodynamically treated HA-$Na_{0.5}K_{0.5}NbO_3$ (NKN) composites bioceramics show the significant enhancement in viability of MG-63 cells, after 5 and 7 days of incubation.

In another study, it has been reported that polarized HA (negatively charged) has been shown to promote the proliferation of MC3T3-E1 osteoblast cells, after 7 days of incubation period [321]. Bodhak et al. [322] reported that the proliferation of hFOB cells is significantly higher on negatively polarized HA as compared to positively polarized HA after 11 days of incubation period, with negatively polarized HA showing an almost twofold increase in cell growth [322]. Verma et al.[323] demonstrated that electrostatic and electrodynamic stimulation enhances the proliferation and adhesion of MG-63 cells, while cultured on the surface of NKN in 1393 bioglass (1393 BG) composite. It has been reported that, the charged surfaces of HA doubles the rate of apatite layer development in HA, in comparison to uncharged HA [324]. It has been revealed that the application of external stimuli and surface polarization has been established to significantly enhance the proliferation of osteoblast cells.

2.6. Influence of surface charge on antibacterial response

It is known that the stress-induced surface charges in our bone help in regulating its metabolic activities [325, 326]. The nature and amount of these stress-induced charges depend on the type of load applied to the bone, i.e, compressive or tensile. Compressive loads produce negative charges on the bone surface, whereas tensile loads produce positive charges. The amount of charge depends on the extent of the applied load [327, 328]. Therefore, the development of polarizable prosthetic implants has attracted significant attention in recent years [311, 317, 329-331].

In orthopedic implants, the predominant portion (65%) of bacterial infections is attributed to GP bacteria, specially, Staphylococcus epidermidis (*S. epidermidis*) and Staphylococcus aureus (*S. aureus*). However, GN bacteria, such as Escherichia coli (*E. coli*) and Pseudomonas aeruginosa (*P. aeruginosa*) are responsible for approximately 11% of total bacterial infections in prosthetic implants [6, 332-335]. GN bacteria possess a dual-layered architecture comprising a slim peptidoglycan layer (~ 5-10 nm) encased by a lipopolysaccharide layer. In contrast, the cell wall of GP bacteria is primarily constituted by a substantial peptidoglycan layer (~ 20-80 nm) without any additional outer layers [336-338]. While both types of bacterial cells exhibit a negative charge, the transmembrane potential of GN bacteria is approximately 1.5 times more than that of GP bacteria [339, 340]. Bacteria respond to external electric or magnetic fields due to their surface potentials, which triggers the production of reactive oxygen species (ROS) Figure [333]. The production of ROS damages to the bacterial cell wall [341-343]. In addition, bacteria communicate with electret surfaces through their electrical potential and micro electric field of charged surface of bacterial membrane [344-346]. Also, the application of external electric field (1 V/cm)

improves the antibacterial response by preventing the development of biofilm on the implant site [344, 347].

Recently, Deepak et al. [338] demonstrated the antibacterial efficacy of charged piezoelectric $Na_{0.5}K_{0.5}NbO_3$ bioceramics. It has been observed that the population of both, *E. coli* and *S. aureus* bacteria are reduced on the negatively and positively charged surfaces, respectively. Also, the charged (polarized at 4.5 KV/cm) surfaces of $BaTiO_3$ – HA bioceramics demonstrate the antibacterial response for the *P. aeruginosa*, *S. aureus* and *E. coli*, bacteria in comparison to their uncharged surfaces. Swin et al. [346] examined the antibacterial response of the positively charged HA- (40/60 wt%) $BaTiO_3$ composite against *S. aureus*, *E. coli* and *P. aeruginosa* bacteria. The results suggested that the population of these bacterial cell decreases on the positive surface of HA- $BaTiO_3$ composite. It has been suggested that the papulation of both, *S. aureus* and *E. coli* bacterial cells decreased by 53 % and 40 %, respectively, on negative surfaces of 7.5 wt% ZnO-HA bioceramics composite [348]. The adherence and proliferation of bacterial infections are largely determined by the surface characteristics and composition of biomaterials [349].

Typically, bacteria colonize on the implant surface by traveling through blood vessels, often enclosed within a capsule composed of extracellular matrix (ECM) proteins. This protective capsule aids in the initial colonization of bacteria, leading to the formation of a three-dimensional bacterial biofilm on the surface of the implant [350-352].

2.7. Closure

Mg and Ca - based silicate bioceramics such as $MgSiO_3$, Mg_2SiO_4, $CaSiO_3$, Ca_2SiO_4, Ca_3SiO_5, $CaMgSi_2O_6$, $Ca_2MgSi_2O_7$, $Ca_7MgSi_4O_{16}$, $CaMgSiO_4$ and $Ca_3MgSi_2O_8$, Zn and Sr doped $MgSiO_3$ and $MgSiO_3$ and $CaSiO_3$-based polymer composites are the appealing choices for bone tissue engineering applications. However, despite of notable potential as prosthetic implants, the underlying mechanisms, associated with the processing and surface chemistry

that stimulate the formation of new bone as well as healing process in the vicinity of such implant, are still need to be well established.

The biocompatibility of these ceramics can be tuned by tailoring the release rate of Ca, Mg and Si etc. ions, adapting specific synthesis routes as well as elemental doping at A and B sites of these perovskites. In addition, the crystal structure of these perovskites also plays an important role in deciding their biocompatibility. The dissolution rate of ions can be controlled by the compositional modifications as well as advanced processing techniques. Also, the wide spectra of *in vivo* degradation behavior of Ca, Mg etc. ions for these silicate bioceramics need to be established.

Recently, the development of piezoelectric biomaterials gained significant attention, owing to the piezoelectric nature of living bone. Piezoelectricity plays a critical role in controlling/regulating number of bone metabolic activities. There are number of reports which suggested that the tailored piezoelectricity can potentially improve the biocompatibility. Some of the above discussed perovskites such as $MgSiO_3$, NKN, $CaSiO_3$ etc. are piezoelectric in nature. However, the piezoelectricity dependent biocompatibility of these perovskite bioceramics systems has to be explored.

The surface charge has been demonstrated to augment biocompatibility as well as induce the antibacterial response. In this perspective, the potentiality of piezoelectric silicate perovskites can be realized as a new generation prosthetic implant. However, nature and amount of surface charge and consequently, the polarization parameters need to be optimized which can accelerate the osteogenesis with the desired antibacterial response. Further, the effect of combined action of electrostatic (surface charge) and electrodynamic electrical stimulation on osteogenesis and other related activities need to be explored.

This study attempted to understand the synergistic impact of electrostatic surface polarization and electrodynamic stimulation, combined with compositional modification towards

augmenting the osteogenic response of Ca and Zr doped $MgSiO_3$ bioceramics ($Mg_{1-x}Ca_xSi_{1-x}Zr_xO_3$; MCSZO-X).

These MCSZO-X ceramics were fabricated using solid state synthesis route via cold isostatic pressing at a pressure of 330 MPa. Furthermore, the study explores how the combined influence of surface charge and variations in Ca and Zr contents (ranging from x = 0.0 to 0.4) in biocompatible MCSZO-X ceramics contributes to enhancing their antibacterial properties. In addition, *vivo* investigation to evaluate the local and systemic toxicity of MCSZO-X nanoparticulate using a rat model.

Bibliography

[1] Sheikh Z, Najeeb S, Khurshid Z, Verma V, Rashid H and Glogauer M 2015 Biodegradable materials for bone repair and tissue engineering applications *Materials* **8** 5744-94

[2] Ratner B D, Hoffman A S, Schoen F J and Lemons J E 2004 *Biomaterials science: an introduction to materials in medicine*: Elsevier)

[3] Chanlalit C, Shukla D R, Fitzsimmons J S, An K-N and O'Driscoll S W 2012 Stress shielding around radial head prostheses *The Journal of hand surgery* **37** 2118-25

[4] Hutmacher D, Hürzeler M B and Schliephake H 1996 A review of material properties of biodegradable and bioresorbable polymers and devices for GTR and GBR applications *International Journal of Oral & Maxillofacial Implants* **11**

[5] Hench L L 2013 Chronology of bioactive glass development and clinical applications

[6] Saini M, Singh Y, Arora P, Arora V and Jain K 2015 Implant biomaterials: A comprehensive review *World Journal of Clinical Cases: WJCC* **3** 52

[7] Liu X and Ma P X 2004 Polymeric scaffolds for bone tissue engineering *Annals of biomedical engineering* **32** 477-86

[8] Nabiyouni M, Brückner T, Zhou H, Gbureck U and Bhaduri S B 2018 Magnesium-based bioceramics in orthopedic applications *Acta biomaterialia* **66** 23-43

[9] Lutton P and Ben-Nissan B 1997 The status of biomaterials for orthopedic and dental applications: Part I–Materials *Materials Technology* **12** 59-64

[10] Saad M, Akhtar S and Srivastava S 2018 Composite polymer in orthopedic implants: A review *Materials Today: Proceedings* **5** 20224-31

[11] Alexander R and Theodos L 1993 Fracture of the bone-grafted mandible secondary to stress shielding: Report of a case and review of the literature *Journal of oral and maxillofacial surgery* **51** 695-7

[12] Sumner D 2015 Long-term implant fixation and stress-shielding in total hip replacement *Journal of Biomechanics* **48** 797-800

[13] Haase K and Rouhi G 2013 Prediction of stress shielding around an orthopedic screw: Using stress and strain energy density as mechanical stimuli *Computers in Biology and Medicine* **43** 1748-57

[14] Christensen F B, Dalstra M, Sejling F, Overgaard S and Bünger C 2000 Titanium-alloy enhances bone-pedicle screw fixation: mechanical and histomorphometrical results of titanium-alloy versus stainless steel *European Spine Journal* **9** 97-103

[15] Marti C, Imhoff A, Bahrs C and Romero J 1997 Metallic versus bioabsorbable interference screw for fixation of bone-patellar tendon-bone autograft in arthroscopic anterior cruciate ligament reconstruction A preliminary report: A preliminary report *Knee Surgery, Sports Traumatology, Arthroscopy* **5** 217-21

[16] Eppley B L and Sadove A M 1995 A comparison of resorbable and metallic fixation in healing of calvarial bone grafts *Plastic and reconstructive surgery* **96** 316-22

[17] Diba M, Goudouri O-M, Tapia F and Boccaccini A R 2014 Magnesium-containing bioactive polycrystalline silicate-based ceramics and glass-ceramics for biomedical applications *Current opinion in solid state and materials science* **18** 147-67

[18] Venkatraman S K and Swamiappan S 2020 Review on calcium-and magnesium-based silicates for bone tissue engineering applications *Journal of Biomedical Materials Research Part A* **108** 1546-62

[19] Bavya Devi K, Nandi S K and Roy M 2019 Magnesium silicate bioceramics for bone regeneration: a review *Journal of the Indian Institute of Science* **99** 261-88

[20] Chen C, Watkins-Curry P, Smoak M, Hogan K, Deese S, McCandless G T, Chan J Y and Hayes D J 2015 Targeting calcium magnesium silicates for polycaprolactone/ceramic composite scaffolds *ACS Biomaterials Science & Engineering* **1** 94-102

[21] Sun T-W, Yu W-L, Zhu Y-J, Yang R-L, Shen Y-Q, Chen D-Y, He Y-H and Chen F 2017 Hydroxyapatite nanowire@ magnesium silicate core–shell hierarchical nanocomposite: Synthesis and application in bone regeneration *ACS Applied Materials & Interfaces* **9** 16435-47

[22] Jin X, Chang J, Zhai W and Lin K 2011 Preparation and characterization of clinoenstatite bioceramics *Journal of the American Ceramic Society* **94** 66-70

[23] Ni S, Chang J, Chou L and Zhai W 2007 Comparison of osteoblast-like cell responses to calcium silicate and tricalcium phosphate ceramics in vitro *Journal of Biomedical Materials Research Part B: Applied Biomaterials: An Official Journal of the Society for Biomaterials, The Japanese Society for Biomaterials, and the Australian Society for Biomaterials and the Korean Society for Biomaterials* **80** 174-83

[24] Ni S and Chang J 2009 In vitro degradation, bioactivity, and cytocompatibility of calcium silicate, dimagnesium silicate, and tricalcium phosphate bioceramics *Journal of biomaterials applications* **24** 139-58

[25] Zadehnajar P, Mirmusavi M H, Soleymani Eil Bakhtiari S, Bakhsheshi-Rad H R, Karbasi S, RamaKrishna S and Berto F 2021 Recent advances on akermanite calcium-silicate ceramic for biomedical applications *International Journal of Applied Ceramic Technology* **18** 1901-20

[26] Pietak A, Mahoney P, Dias G J and Staiger M P 2008 Bone-like matrix formation on magnesium and magnesium alloys *Journal of materials science: materials in medicine* **19** 407-15

[27] Wu C and Chang J 2013 A review of bioactive silicate ceramics *Biomedical materials* **8** 032001

[28] Xia L, Zhang Z, Chen L, Zhang W, Zeng D, Zhang X, Chang J and Jiang X 2011 Proliferation and osteogenic differentiation of human periodontal ligament cells on akermanite and β-TCP bioceramics *Eur Cell Mater* **22** e82

[29] Zhai W, Lu H, Chen L, Lin X, Huang Y, Dai K, Naoki K, Chen G and Chang J 2012 Silicate bioceramics induce angiogenesis during bone regeneration *Acta Biomaterialia* **8** 341-9

[30] Nonami T and Tsutsumi S 1999 Study of diopside ceramics for biomaterials *Journal of Materials Science: Materials in Medicine* **10** 475-9

[31] Zhai W, Lu H, Wu C, Chen L, Lin X, Naoki K, Chen G and Chang J 2013 Stimulatory effects of the ionic products from Ca–Mg–Si bioceramics on both osteogenesis and angiogenesis in vitro *Acta biomaterialia* **9** 8004-14

[32] Devi K B, Tripathy B, Kumta P N, Nandi S K and Roy M 2018 In vivo biocompatibility of zinc-doped magnesium silicate bio-ceramics *ACS Biomaterials Science & Engineering* **4** 2126-33

[33] Devi K B, Tripathy B, Roy A, Lee B, Kumta P N, Nandi S K and Roy M 2018 In vitro biodegradation and in vivo biocompatibility of forsterite bio-ceramics: Effects of strontium substitution *ACS Biomaterials Science & Engineering* **5** 530-43

[34] Sun M, Liu A, Ma C, Shao H, Yu M, Liu Y, Yan S and Gou Z 2016 Systematic investigation of β-dicalcium silicate-based bone cements in vitro and in vivo in comparison with clinically applied calcium phosphate cement and Bio-Oss® *RSC advances* **6** 586-96

[35] Hafezi M, Talebi A R, Miresmaeili S M, Sadeghian F and Fesahat F 2013 Histological analysis of bone repair in rat femur via nanostructured merwinite granules *Ceramics International* **39** 4575-80

[36] Bretado L, Cortés D, Ortega W and Renteria D 2009 Effect of magnesium content in simulated body fluid on apatite forming ability of wollastonite ceramics *Advances in Applied Ceramics* **108** 194-7

[37] Mirhadi S, Tavangarian F and Emadi R 2012 Synthesis, characterization and formation mechanism of single-phase nanostructure bredigite powder *Materials Science and Engineering: C* **32** 133-9

[38] Wu C, Chang J and Xiao Y 2013 *Advanced bioactive inorganic materials for bone regeneration and drug delivery*: CRC Press)

[39] Devi K B, Lee B, Roy A, Kumta P N and Roy M 2017 Effect of zinc oxide doping on in vitro degradation of magnesium silicate bioceramics *Materials Letters* **207** 100-3

[40] Bandyopadhyay A, Bernard S, Xue W and Bose S 2006 Calcium phosphate-based resorbable ceramics: Influence of MgO, ZnO, and SiO2 dopants *Journal of the American Ceramic Society* **89** 2675-88

[41] Sun H, Zhang Q, Yang H and Zou J 2007 (Ca1− xMgx) SiO3: A low-permittivity microwave dielectric ceramic system *Materials Science and Engineering: B* **138** 46-50

[42] Zhang N, Molenda J A, Mankoci S, Zhou X, Murphy W L and Sahai N 2013 Crystal structures of CaSiO 3 polymorphs control growth and osteogenic differentiation of human mesenchymal stem cells on bioceramic surfaces *Biomaterials science* **1** 1101-10

[43] Bigham A, Saudi A, Rafienia M, Rahmati S, Bakhtiyari H, Salahshouri F, Sattary M and Hassanzadeh-Tabrizi S A 2019 Electrophoretically deposited mesoporous

magnesium silicate with ordered nanopores as an antibiotic-loaded coating on surface-modified titanium *Materials Science and Engineering: C* **96** 765-75

[44] Li J, Song Y, Zhang S, Zhao C, Zhang F, Zhang X, Cao L, Fan Q and Tang T 2010 In vitro responses of human bone marrow stromal cells to a fluoridated hydroxyapatite coated biodegradable Mg–Zn alloy *Biomaterials* **31** 5782-8

[45] Feng S, Li J, Jiang X, Li X, Pan Y, Zhao L, Boccaccini A R, Zheng K, Yang L and Wei J 2016 Influences of mesoporous magnesium silicate on the hydrophilicity, degradability, mineralization and primary cell response to a wheat protein based biocomposite *Journal of Materials Chemistry B* **4** 6428-36

[46] Kang Y G, Wei J, Shin J W, Wu Y R, Su J, Park Y S and Shin J-W 2018 Enhanced biocompatibility and osteogenic potential of mesoporous magnesium silicate/polycaprolactone/wheat protein composite scaffolds *International Journal of Nanomedicine* **13** 1107-17

[47] Khare D, Basu B and Dubey A K 2020 Electrical stimulation and piezoelectric biomaterials for bone tissue engineering applications *Biomaterials* **258** 120280

[48] Wu Z, Tang T, Guo H, Tang S, Niu Y, Zhang J, Zhang W, Ma R, Su J, Liu C and Wei J 2014 In vitro degradability, bioactivity and cell responses to mesoporous magnesium silicate for the induction of bone regeneration *Colloids and Surfaces B: Biointerfaces* **120** 38-46

[49] Wilkins M R, Sanchez J C, Gooley A A, Appel R D, Humphery-Smith I, Hochstrasser D F and Williams K L 1996 Progress with proteome projects: why all proteins expressed by a genome should be identified and how to do it *Biotechnol Genet Eng Rev* **13** 19-50

[50] Deng F, Zhai W, Yin Y, Peng C and Ning C 2021 Advanced protein adsorption properties of a novel silicate-based bioceramic: A proteomic analysis *Bioactive Materials* **6** 208-18

[51] Othman Z, Pastor B C, van Rijt S and Habibovic P 2018 Understanding interactions between biomaterials and biological systems using proteomics *Biomaterials* **167** 191-204

[52] Wang J, Chen Y, Zhu X, Yuan T, Tan Y, Fan Y and Zhang X 2014 Effect of phase composition on protein adsorption and osteoinduction of porous calcium phosphate ceramics in mice *Journal of biomedical materials research Part A* **102** 4234-43

[53] Maehira F, Miyagi I and Eguchi Y 2009 Effects of calcium sources and soluble silicate on bone metabolism and the related gene expression in mice *Nutrition* **25** 581-9

[54] Dufrane D, Delloye C, McKay I J, De Aza P N, De Aza S, Schneider Y-J and Anseau M 2003 Indirect cytotoxicity evaluation of pseudowollastonite *Journal of Materials Science: Materials in Medicine* **14** 33-8

[55] Macphee D E and Lachowski E E 2003 Cement components and their phase *Lea's chemistry of cement and concrete* **95**

[56] Oates T 2000 Lime and limestone *Kirk-Othmer encyclopedia of chemical technology*

[57] Sun M, Liu A, Shao H, Yang X, Ma C, Yan S, Liu Y, He Y and Gou Z 2016 Systematical evaluation of mechanically strong 3D printed diluted magnesium doping wollastonite scaffolds on osteogenic capacity in rabbit calvarial defects *Scientific reports* **6** 34029

[58] Shen T, Dai Y, Li X, Xu S, Gou Z and Gao C 2017 Regeneration of the osteochondral defect by a wollastonite and macroporous fibrin biphasic scaffold *ACS biomaterials science & engineering* **4** 1942-53

[59] Smyth J R 1974 Experimental study on the polymorphism of enstatite *American Mineralogist: Journal of Earth and Planetary Materials* **59** 345-52

[60] Mielcarek W, Nowak-Woźny D and Prociów K 2004 Correlation between MgSiO3 phases and mechanical durability of steatite ceramics *Journal of the European Ceramic Society* **24** 3817-21

[61] Song M E, Kim J S, Joung M R, Nahm S, Kim Y S, Paik J H and Choi B H 2008 Synthesis and microwave dielectric properties of MgSiO3 ceramics *Journal of the American Ceramic Society* **91** 2747-50

[62] Kanzaki M and Xue X 2017 Protoenstatite in MgSiO3 samples prepared by conventional solid state reaction *Journal of Mineralogical and Petrological Sciences* **112** 359-64

[63] Sadanaga R, Okamura F P and Takeda H 1969 X-ray study of the phase transformations of enstatite *Mineralogical Journal* **6** 110-30

[64] Kushiro I 1972 Determination of liquidus relations in synthetic silicate systems with electron probe analysis: the system forsterite-diopside-silica at 1 atmosphere *American Mineralogist: Journal of Earth and Planetary Materials* **57** 1260-71

[65] Smith J V 1959 The crystal structure of proto-enstatite, MgSiO3 *Acta Crystallographica* **12** 515-9

[66] Hawthorne F C and Ito J 1978 Refinement of the crystal structures of (Mg0. 776Co0. 224) SiO3 and (Mg0. 925Mn0. 075) SiO3 *Acta Crystallographica Section B: Structural Crystallography and Crystal Chemistry* **34** 891-3

[67] Vitos L, Magyari-Köpe B, Ahuja R, Kollár J, Grimvall G and Johansson B 2006 Phase transformations between garnet and perovskite phases in the Earth's mantle: a theoretical study *Physics of the Earth and Planetary Interiors* **156** 108-16

[68] Jung D Y and Schmidt M W 2011 Solid solution behaviour of CaSiO 3 and MgSiO 3 perovskites *Physics and Chemistry of Minerals* **38** 311-9

[69] Ullah A, Liu H, Hao H, Iqbal J, Yao Z, Cao M and Xu Q 2017 Effect of Zn substitution on the sintering temperature and microwave dielectric properties of MgSiO3-based ceramics *Ceramics International* **43** 484-90

[70] Ullah A, Liu H, Pengcheng Z, Hao H, Iqbal J, Cao M, Yao Z, Ahmad A S and Manan A 2019 Influence of Co substitution on the phase, microstructure, and microwave dielectric properties of MgSiO 3 ceramics *Journal of Materials Science: Materials in Electronics* **30** 6469-74

[71] Ullah A, Liu H, Hao H, Iqbal J, Yao Z, Cao M and Xu Q 2016 Phase and Microstructure Evaluation and Microwave Dielectric Properties of Mg 1− x Ni x SiO 3 Ceramics *Journal of Electronic Materials* **45** 5133-9

[72] Stephenson D A, Sclar C B and Smith J V 1966 Unit cell volumes of synthetic orthoenstatite and low clinoenstatite *Mineralogical magazine and journal of the Mineralogical Society* **35** 838-46

[73] Smith J V 1969 Magnesium pyroxenes at high temperature: Inversion in clinoenstatite *Nature* **222** 256-7

[74] Edrees S J, Shukur M M and Obeid M M 2018 First-principle analysis of the structural, mechanical, optical and electronic properties of wollastonite monoclinic polymorph *Computational Condensed Matter* **14** 20-6

[75] Trojer F J 1968 The crystal structure of parawollastonite *Zeitschrift für Kristallographie-Crystalline Materials* **127** 291-308

[76] Yang H and Prewitt C T 1999 On the crystal structure of pseudowollastonite (CaSiO3) *American Mineralogist* **84** 929-32

[77] Warren B 1930 XV. The Structure of Melilite (Ca, Na) 2 (Mg, Al) 1 (Si, Al) 2O7 *Zeitschrift für Kristallographie-Crystalline Materials* **74** 131-8

[78] Cameron M and Papike J J 1981 Structural and chemical variations in pyroxenes *American Mineralogist* **66** 1-50

[79] Pilati T, Demartin F and Gramaccioli C M 1995 Thermal parameters for minerals of the olivine group: their implication on vibrational spectra, thermodynamic functions and transferable force fields *Acta Crystallographica Section B: Structural Science* **51** 721-33

[80] Moore P B and Araki T 1972 Atomic arrangement of merwinite, Ca3Mg [SiO4] 2, an unusual dense-packed structure of geophysical interest *American Mineralogist: Journal of Earth and Planetary Materials* **57** 1355-74

[81] Huang C M, Kuo D H, Kim Y J and Kriven W M 1994 Phase stability of chemically derived enstatite (MgSiO3) powders *Journal of the American Ceramic Society* **77** 2625-31

[82] Lee W E and Heuer A H 1987 On the polymorphism of enstatite *Journal of the American Ceramic Society* **70** 349-60

[83] Atlas L 1952 The polymorphism of MgSiO3 and solid-state equilibria in the system MgSiO3-CaMgSi2O6 *The Journal of Geology* **60** 125-47

[84] Sarver J F and Hummel F A 1962 Stability relations of magnesium metasilicate polymorphs *Journal of the American Ceramic Society* **45** 152-6

[85] Ullah A, Liu H, Zhai P, Hao H, Iqbal J, Cao M, Yao Z, Ahmad S and Manan A 2019 Influence of Co substitution on the phase, microstructure, and microwave dielectric properties of MgSiO3 ceramics *Journal of Materials Science: Materials in Electronics* **30**

[86] Lin L, Min Y, Chaoshu S, Weiping Z and Baogui Y 2006 Synthesis and luminescence properties of red phosphors: Mn2+ doped MgSiO3 and Mg2SiO4 prepared by sol-gel method *Journal of Rare Earths* **24** 104-7

[87] Volpe S L 2013 Magnesium in disease prevention and overall health *Advances in nutrition* **4** 378S-83S

[88] Huang Y, Jin X, Zhang X, Sun H, Tu J, Tang T, Chang J and Dai K 2009 In vitro and in vivo evaluation of akermanite bioceramics for bone regeneration *Biomaterials* **30** 5041-8

[89] Wu C, Chen Z, Wu Q, Yi D, Friis T, Zheng X, Chang J, Jiang X and Xiao Y 2015 Clinoenstatite coatings have high bonding strength, bioactive ion release, and osteoimmunomodulatory effects that enhance in vivo osseointegration *Biomaterials* **71** 35-47

[90] He D, Dong W, Tang S, Wei J, Liu Z, Gu X, Li M, Guo H and Niu Y 2014 Tissue engineering scaffolds of mesoporous magnesium silicate and poly (ε-caprolactone)–poly (ethylene glycol)–poly (ε-caprolactone) composite *Journal of Materials Science: Materials in Medicine* **25** 1415-24

[91] Wu Z, Zheng K, Zhang J, Tang T, Guo H, Boccaccini A and wei j 2016 Effects of magnesium silicate on mechanical property, biocompatibility, bioactivity, degradability, osteogenesis of poly(butylene succinate) based composite scaffolds for bone repair *J. Mater. Chem. B* **4**

[92] Niu Y, Dong W, Guo H, Deng Y, Guo L, An X, He D, Wei J and Li M 2014 Mesoporous magnesium silicate-incorporated poly(ε-caprolactone)-poly(ethylene glycol)-poly(ε-caprolactone) bioactive composite beneficial to osteoblast behaviors *Int J Nanomedicine* **9** 2665-75

[93] Hsu F-Y, Weng R-C, Lin H-M, Lin Y-H, Lu M-R, Yu J-L and Hsu H-W 2015 A biomimetic extracellular matrix composed of mesoporous bioactive glass as a bone graft material *Microporous and Mesoporous Materials* **212** 56-65

[94] Niu Y, Dong W, Guo H, Deng Y, Guo L, an X, He D, Wei J and Li M 2014 Mesoporous magnesium silicate-incorporated poly(ε-caprolactone)-poly(ethylene glycol)-poly(ε-caprolactone) bioactive composite beneficial to osteoblast behaviors *International journal of nanomedicine* **9 Suppl 1** 2665-75

[95] Kang Y, Wei J, Shin J, Wu Y, Su J-C, Park Y and Shin J-w 2018 Enhanced biocompatibility and osteogenic potential of mesoporous magnesium silicate/polycaprolactone/wheat protein composite scaffolds *International Journal of Nanomedicine* **Volume 13** 1107-17

[96] Tavangarian F and Emadi R 2011 Improving degradation rate and apatite formation ability of nanostructure forsterite *Ceramics International* **37** 2275-80

[97] Tavangarian F and Emadi R 2011 Nanostructure effects on the bioactivity of forsterite bioceramic *Materials Letters* **65** 740-3

[98] Jurkić L M, Cepanec I, Pavelić S K and Pavelić K 2013 Biological and therapeutic effects of ortho-silicic acid and some ortho-silicic acid-releasing compounds: New perspectives for therapy *Nutrition & Metabolism* **10** 2

[99] Szurkowska K and Kolmas J 2017 Hydroxyapatites enriched in silicon – Bioceramic materials for biomedical and pharmaceutical applications *Progress in Natural Science: Materials International* **27** 401-9

[100] O'Neill E, Awale G, Daneshmandi L, Umerah O and Lo K W H 2018 The roles of ions on bone regeneration *Drug Discovery Today* **23** 879-90

[101] Hartwig A 2001 Role of magnesium in genomic stability *Mutation Research/Fundamental and Molecular Mechanisms of Mutagenesis* **475** 113-21

[102] Rude R K, Gruber H E, Wei L Y, Frausto A and Mills B G 2003 Magnesium deficiency: effect on bone and mineral metabolism in the mouse *Calcified tissue international* **72** 32-41

[103] Rude R K, Gruber H E, Norton H J, Wei L Y, Frausto A and Kilburn J 2006 Reduction of dietary magnesium by only 50% in the rat disrupts bone and mineral metabolism *Osteoporosis international : a journal established as result of cooperation between the European Foundation for Osteoporosis and the National Osteoporosis Foundation of the USA* **17** 1022-32

[104] Hoppe A, Güldal N S and Boccaccini A R 2011 A review of the biological response to ionic dissolution products from bioactive glasses and glass-ceramics *Biomaterials* **32** 2757-74

[105] Middleton J C and Tipton A J 2000 Synthetic biodegradable polymers as orthopedic devices *Biomaterials* **21** 2335-46

[106] Wuisman P I and Smit T H 2006 Bioresorbable polymers: heading for a new generation of spinal cages *European spine journal : official publication of the European Spine Society, the European Spinal Deformity Society, and the European Section of the Cervical Spine Research Society* **15** 133-48

[107] Liu X, Morra M, Carpi A and Li B 2008 Bioactive calcium silicate ceramics and coatings *Biomedicine & Pharmacotherapy* **62** 526-9

[108] Azarov G M, Maiorova E V, Oborina M A and Belyakov A V 1995 Wollastonite raw materials and their applications (a review) *Glass and Ceramics* **52** 237-40

[109] Yagi T, Kusanagi S, Tsuchida Y and Fukai Y 1989 Isothermal Compression and Stability of Perovskite-type CaSiO₃ *Proceedings of the Japan Academy, Series B* **65** 129-32

[110] Magyari-Köpe B, Vitos L, Grimvall G, Johansson B and Kollár J 2002 Low-temperature crystal structure of ${\mathrm{CaSiO}}_{3}$ perovskite: An ab initio total energy study *Physical Review B* **65** 193107

[111] TROJER F J 1968 The crystal structure of parawollastonite *Zeitschrift für Kristallographie - Crystalline Materials* **127** 291-308

[112] Yamanaka T and Mori H 1981 The structure and polytypes of α-CaSiO3 (pseudowollastonite) *Acta Crystallographica Section B: Structural Crystallography and Crystal Chemistry* **37** 1010-7

[113] Karki B B and Crain J 1998 First-principles determination of elastic properties of CaSiO3 perovskite at lower mantle pressures *Geophysical research letters* **25** 2741-4

[114] Stixrude L, Cohen R E, Yu R and Krakauer H 1996 Prediction of phase transition in CaSiO3 perovskite and implications for lower mantle structure *American Mineralogist* **81** 1293-6

[115] Akber-Knutson S, Bukowinski M S and Matas J 2002 On the structure and compressibility of CaSiO3 perovskite *Geophysical Research Letters* **29** 4-1-4-

[116] Henriques J M, Caetano E W S, Freire V N, da Costa J A P and Albuquerque E L 2006 Structural and electronic properties of CaSiO3 triclinic *Chemical Physics Letters* **427** 113-6

[117] Dörsam G, Liebscher A, Wunder B, Franz G and Gottschalk M 2009 Crystal structure refinement of synthetic Ca0.43Sr0.57[SiO3]-walstromite and walstromite–fluid Ca–Sr distribution at upper-mantle conditions *European Journal of Mineralogy* **21** 705-14

[118] Kagomiya I, Suzuki I and Ohsato H 2009 Microwave Dielectric Properties of (Ca1-xSrx)SiO3 Ring Silicate Solid Solutions *Japanese Journal of Applied Physics* **48** 09KE2

[119] HAYASHI S, OKADA K and OTSUKA N 1991 Preparation of CaSiO3 powders by coprecipitation method and their sinterability *Journal of the Ceramic Society of Japan* **99** 1224-7

[120] Siriphannon P, Kameshima Y, Yasumori A, Okada K and Hayashi S 2002 Formation of hydroxyapatite on CaSiO3 powders in simulated body fluid *Journal of the European Ceramic Society* **22** 511-20

[121] Siriphannon P, Hayashi S, Yasumori A and Okada K 2011 Preparation and sintering of CaSiO3 from coprecipitated powder using NaOH as precipitant and its apatite formation in simulated body fluid solution *Journal of Materials Research* **14** 529-536

[122] Limori Y, Kameshima Y, Yasumori A and Okada K 2004 Comparative Study of Apatite Formation on CaSiO3 Ceramics Prepared by Glass Crystallization and Sintering Methods in Simulated Body Fluid *Key Engineering Materials* **264-268** 1965-8

[123] Morsy R 2016 Synthesis and in vitro bioactivity mechanism of synthetic α-wollastonite and β-wollastonite bioceramics *Journal of Ceramic Science and Technology* **7** 65-70

[124] Day S J, Thompson S P, Evans A, Parker J E, Connor L D and Tang C C 2013 Thermal processing and crystallization of amorphous Mg-Ca silicates *Meteoritics & Planetary Science* **48** 1459-71

[125] Meiszterics A and Sinkó K 2008 Sol–gel derived calcium silicate ceramics *Colloids and Surfaces A: Physicochemical and Engineering Aspects* **319** 143-8

[126] Wang H, Zhang Q, Yang H and Sun H 2008 Synthesis and microwave dielectric properties of CaSiO3 nanopowder by the sol–gel process *Ceramics International* **34** 1405-8

[127] Ahn S, Seo D and Lee J K 2015 Fabrication of dense β-wollastonite bioceramics by MgSiO3 addition *Journal of Ceramic Processing Research* **16** 548-54

[128] Lin K, Zhai W, Ni S, Chang J, Zeng Y and Qian W 2005 Study of the mechanical property and in vitro biocompatibility of CaSiO3 ceramics *Ceramics International* **31** 323-6

[129] Pei L Z, Yang L J, Yang Y, Fan C G, Yin W Y, Chen J and Zhang Q F 2010 A green and facile route to synthesize calcium silicate nanowires *Materials Characterization* **61** 1281-5

[130] Mei P, Jiang S, Mao L, Zhou Y, Gu K, Zhang C, Wang X, Lin K, Zhao C and Zhu M 2022 In situ construction of flower-like nanostructured calcium silicate bioceramics for enhancing bone regeneration mediated via FAK/p38 signaling pathway *Journal of Nanobiotechnology* **20** 162

[131] Singh S P and Karmakar B 2011 Mechanochemical Synthesis of Nano Calcium Silicate Particles at Room Temperature *New Journal of Glass and Ceramics* **1**

[132] Abd Rashid R, Shamsudin R, Abdul Hamid M A and Jalar A 2014 Low temperature production of wollastonite from limestone and silica sand through solid-state reaction *Journal of Asian Ceramic Societies* **2** 77-81

[133] Harabi A and Chehlatt S 2013 Preparation process of a highly resistant wollastonite bioceramics using local raw materials *Journal of Thermal Analysis and Calorimetry* **111** 203-11

[134] Kozawa T, Onda A and Yanagisawa K 2009 Accelerated formation of β-dicalcium silicate by solid-state reaction in water vapor atmosphere *Chemistry letters* **38** 476-7

[135] Kozawa T, Yanagisawa K, Yoshida A, Onda A and Suzuki Y 2013 Preparation of β-CaSiO3 powder by water vapor-assisted solid-state reaction *Journal of the Ceramic Society of Japan* **121** 103-5

[136] Roy R 1987 Ceramics by the solution-sol-gel route *Science* **238** 1664-9

[137] Fang Q, Cheng H, Huang K, Wang J, Li R and Jiao Y 2005 Doping effect on crystal structure and magnetic properties of chromium-substituted strontium hexaferrite nanoparticles *Journal of magnetism and magnetic materials* **294** 281-6

[138] Lakshmi R, Velmurugan V and Sasikumar S 2013 Preparation and phase evolution of wollastonite by sol-gel combustion method using sucrose as the fuel *Combustion Science and Technology* **185** 1777-85

[139] Huang X-H and Chang J 2009 Synthesis of nanocrystalline wollastonite powders by citrate–nitrate gel combustion method *Materials Chemistry and Physics* **115** 1-4

[140] Sreekanth Chakradhar R P, Nagabhushana B M, Chandrappa G T, Ramesh K P and Rao J L 2006 Solution combustion derived nanocrystalline macroporous wollastonite ceramics *Materials Chemistry and Physics* **95** 169-75

[141] Kanzaki M, Stebbins J F and Xue X 1991 Characterization of quenched high pressure phases in CaSiO3 system by XRD and 29Si NMR *Geophysical Research Letters* **18** 463-6

[142] Yun Y H, Yun S D, Park H R, Lee Y K and Youn Y N 2002 Preparation of β-Wollastonite Glass-Ceramics *Journal of Materials Synthesis and Processing* **10** 205-9

[143] Lin K, Chang J, Zeng Y and Qian W 2004 Preparation of macroporous calcium silicate ceramics *Materials Letters* **58** 2109-13

[144] Zhao X H, Wang M J, Zhang Q L and Yang H 2014 Low-Temperature Sintering and Microwave Dielectric Properties of (Ca0.9Mg0.1)SiO3 Ceramic with Li2CO3 Addition *Key Engineering Materials* **602-603** 748-51

[145] Dhoble S J, Dhoble N S and Pode R B 2003 Preparation and characterization of Eu3+ activated CaSiO3, (CaA)SiO3 [A = Ba or Sr] phosphors *Bulletin of Materials Science* **26** 377-82

[146] Wei F and Jia Q 2015 Synthesis and Characteristics of Al2O3-doped α-CaSiO3 Ceramics *Ferroelectrics* **474** 120-7

[147] Wu C T and Zreiqat H 2007 Preparation and Characteristics of Strontium Containing Bioactive CaSiO3 Ceramics *Key Engineering Materials* **330-332** 499-502

[148] Kong N, Lin K, Li H and Chang J 2014 Synergy effects of copper and silicon ions on stimulation of vascularization by copper-doped calcium silicate *Journal of Materials Chemistry B* **2** 1100-10

[149] Wu C, Ramaswamy Y, Kwik D and Zreiqat H 2007 The effect of strontium incorporation into CaSiO3 ceramics on their physical and biological properties *Biomaterials* **28** 3171-81

[150] Chen T-Y, Chu S-Y and Juang Y-D 2002 Effects of sintering temperature on the dielectric and piezoelectric properties of Sr additive Sm-modified PbTiO3 ceramics *Sensors and Actuators A: Physical* **102** 6-10

[151] Li J, Liao H and Hermansson L 1996 Sintering of partially-stabilized zirconia and partially-stabilized zirconia—hydroxyapatite composites by hot isostatic pressing and pressureless sintering *Biomaterials* **17** 1787-90

[152] Lin K, Chang J and Shen R 2009 The effect of powder properties on sintering, microstructure, mechanical strength and degradability of β-tricalcium phosphate/calcium silicate composite bioceramics *Biomedical Materials* **4** 065009

[153] Lin K, Zhang M, Zhai W, Qu H and Chang J 2011 Fabrication and Characterization of Hydroxyapatite/Wollastonite Composite Bioceramics with Controllable Properties for Hard Tissue Repair *Journal of the American Ceramic Society* **94** 99-105

[154] Lin K, Chang J and Lu J 2006 Synthesis of wollastonite nanowires via hydrothermal microemulsion methods *Materials Letters* **60** 3007-10

[155] Lin K, Chang J, Chen G, Ruan M and Ning C 2007 A simple method to synthesize single-crystalline β-wollastonite nanowires *Journal of Crystal Growth* **300** 267-71

[156] Reddy M V and Pathak M 2018 Sol-gel combustion synthesis of Ag doped CaSiO3: in vitro bioactivity, antibacterial activity and cytocompatibility studies for biomedical applications *Materials Technology* **33** 38-47

[157] Siriphannon P, Hayashi S, Yasumori A and Okada K 1999 Preparation and sintering of CaSiO3 from coprecipitated powder using NaOH as precipitant and its apatite formation in simulated body fluid solution *Journal of Materials Research* **14** 529-36

[158] Hazar A B Y 2007 Preparation and in vitro bioactivity of CaSiO3 powders *Ceramics International* **33** 687-92

[159] Jagadale P N, Kulal S R, Joshi M G, Jagtap P P, Khetre S M and Bamane S R 2013 Synthesis and characterization of nanostructured CaSiO3 biomaterial *Materials Science-Poland* **31** 269-75

[160] Wan X, Hu A, Li M, Chang C and Mao D 2008 Performances of CaSiO3 ceramic sintered by Spark plasma sintering *Materials Characterization* **59** 256-60

[161] Huan-ping W, QiLong Z, Hui Y and Huiping S 2007 Synthesis and Microwave Dielectric Properties of (Ca 1- x Mg x)SiO 3 Ceramic by Sol-Gel Process *Acta Physico-chimica Sinica* **23** 609-13

[162] Madesh Kumar M, Nagabhushana H, Nagabhushana B M, Suriyamurthy N, Sharma S C, Shivakumara C and Hari Krishna R 2014 Synthesis, characterization and spectroscopic investigation of Cr3+ doped wollastonite nanophosphor *Spectrochimica Acta Part A: Molecular and Biomolecular Spectroscopy* **128** 403-7

[163] Long L H, Chen L D, Bai S Q, Chang J and Lin K L 2006 Preparation of dense β-CaSiO3 ceramic with high mechanical strength and HAp formation ability in simulated body fluid *Journal of the European Ceramic Society* **26** 1701-6

[164] de Aza P N, Guitian F and de Aza S 1994 Bioactivity of wollastonite ceramics: In vitro evaluation *Scripta Metallurgica et Materialia* **31** 1001-5

[165] Zhang N, Molenda J A, Fournelle J H, Murphy W L and Sahai N 2010 Effects of pseudowollastonite (CaSiO3) bioceramic on in vitro activity of human mesenchymal stem cells *Biomaterials* **31** 7653-65

[166] Magallanes-Perdomo M, De Aza A H, Mateus A Y, Teixeira S, Monteiro F J, De Aza S and Pena P 2010 In vitro study of the proliferation and growth of human bone marrow cells on apatite–wollastonite-2M glass ceramics *Acta Biomaterialia* **6** 2254-63

[167] Palakurthy S, K V G R, Samudrala R K and P A A 2019 In vitro bioactivity and degradation behaviour of β-wollastonite derived from natural waste *Materials Science and Engineering: C* **98** 109-17

[168] Ni S, Chang J and Chou L 2006 A novel bioactive porous CaSiO3 scaffold for bone tissue engineering *Journal of Biomedical Materials Research Part A* **76A** 196-205

[169] Kokubo T and Takadama H 2006 How useful is SBF in predicting in vivo bone bioactivity? *Biomaterials* **27** 2907-15

[170] Liu X, Ding C and Chu P K 2004 Mechanism of apatite formation on wollastonite coatings in simulated body fluids *Biomaterials* **25** 1755-61

[171] Mohammadi H, Hafezi M, Nezafati N, Heasarki S, Nadernezhad A, Ghazanfari S and Sepantafar M 2014 Bioinorganics in Bioactive Calcium Silicate Ceramics for Bone Tissue Repair: Bioactivity and Biological Properties.

[172] Keeting P E, Oursler M J, Wiegand K E, Bonde S K, Spelsberg T C and Riggs B L 1992 Zeolite a increases proliferation, differentiation, and transforming growth factor β production in normal adult human osteoblast-like cells in vitro *Journal of Bone and Mineral Research* **7** 1281-9

[173] Palakurthy S, Azeem A, Reddy K, Penugurti V and Manavathi B 2019 A Comparative study on in vitro behaviour of calcium silicate ceramics synthesised from bio-waste resources *Journal of the American Ceramic Society*

[174] Sun H, He S, Wu P, Gao C, Feng P, Xiao T, Deng Y and Shuai C 2016 A Novel MgO-CaO-SiO_2 System for Fabricating Bone Scaffolds with Improved Overall Performance *Materials (Basel, Switzerland)* **9**

[175] Choudhary R, Venkatraman S K, Bulygina I, Senatov F, Kaloshkin S, Anisimova N, Kiselevskiy M, Knyazeva M, Kukui D, Walther F and Swamiappan S 2021 Biomineralization, dissolution and cellular studies of silicate bioceramics prepared from eggshell and rice husk *Materials Science and Engineering: C* **118** 111456

[176] Peng W, Huan Z, Pei G, Li J, Cao Y, Jiang L and Zhu Y 2022 Silicate bioceramics elicit proliferation and odonto-genic differentiation of human dental pulp cells *Dental materials journal* **41** 27-36

[177] Li H, Wang W and Chang J 2021 Calcium silicate enhances immunosuppressive function of MSCs to indirectly modulate the polarization of macrophages *Regenerative biomaterials* **8** rbab056

[178] Liu L, Yu F, Li L, Zhou L, Zhou T, Xu Y, Lin K, Fang B and Xia L 2021 Bone marrow stromal cells stimulated by strontium-substituted calcium silicate ceramics: release of exosomal miR-146a regulates osteogenesis and angiogenesis *Acta Biomater* **119** 444-57

[179] Zhao F, Lei B, Li X, Mo Y, Wang R, Chen D and Chen X 2018 Promoting in vivo early angiogenesis with sub-micrometer strontium-contained bioactive microspheres through modulating macrophage phenotypes *Biomaterials* **178** 36-47

[180] Gou Z, Chang J and Zhai W 2005 Preparation and characterization of novel bioactive dicalcium silicate ceramics *Journal of the European Ceramic Society* **25** 1507-14

[181] Gou Z, Chang J, Zhai W and Wang J 2005 Study on the self-setting property and the in vitro bioactivity of beta-Ca2SiO4 *Journal of biomedical materials research. Part B, Applied biomaterials* **73** 244-51

[182] Gou Z and Chang J 2004 Synthesis and in vitro bioactivity of dicalcium silicate powders *Journal of the European Ceramic Society* **24** 93-9

[183] Zhao W, Wang J, Zhai W, Wang Z and Chang J 2005 The self-setting properties and in vitro bioactivity of tricalcium silicate *Biomaterials* **26** 6113-21

[184] Zhao W and Chang J 2004 Sol–gel synthesis and in vitro bioactivity of tricalcium silicate powders *Materials Letters* **58** 2350-3

[185] Liu X, Tao S and Ding C 2002 Bioactivity of plasma sprayed dicalcium silicate coatings *Biomaterials* **23** 963-8

[186] Venkatraman S K, Choudhary R, Krishnamurithy G, Raghavendran H R B, Murali M R, Kamarul T, Suresh A, Abraham J and Swamiappan S 2021 Biomineralization, mechanical, antibacterial and biological investigation of larnite and rankinite bioceramics *Materials Science and Engineering: C* **118** 111466

[187] Zhong H, Wang L, Fan Y, He L, Lin K, Jiang W, Chang J and Chen L 2011 Mechanical properties and bioactivity of β-Ca2SiO4 ceramics synthesized by spark plasma sintering *Ceramics International* **37** 2459-65

[188] Zhong H, Wang L, He L, Jiang W, Zhai W, Lin K, Chen L and Chang J 2011 Fabrication and Characterization of Tricalcium Silicate Bioceramics with High Mechanical Properties by Spark Plasma Sintering *International Journal of Applied Ceramic Technology* **8** 501-10

[189] Zhao W and Chang J 2005 Preparation and characterization of novel tricalcium silicate bioceramics *Journal of Biomedical Materials Research Part A* **73A** 86-9

[190] Liu W-C, Hu C-C, Tseng Y-Y, Sakthivel R, Fan K-S, Wang A-N, Wang Y-M and Chung R-J 2020 Study on strontium doped tricalcium silicate synthesized through sol-gel process *Materials Science and Engineering: C* **108** 110431

[191] Jodati H, Yilmaz B and Evis Z 2020 Calcium zirconium silicate (baghdadite) ceramic as a biomaterial *Ceramics International* **46** 21902-9

[192] Saint-Jean S, Camiré C, Nevsten P, Hansen S and Ginebra M-P 2005 Study of the reactivity and in vitro bioactivity of Sr-substituted α-TCP cements *Journal of materials science. Materials in medicine* **16** 993-1001

[193] Lin K, Xia L, Li H, Jiang X, Pan H, Xu Y, Lu W W, Zhang Z and Chang J 2013 Enhanced osteoporotic bone regeneration by strontium-substituted calcium silicate bioactive ceramics *Biomaterials* **34** 10028-42

[194] Lin K, Chang J, Liu Z, Zeng Y and Shen R 2009 Fabrication and characterization of 45S5 bioglass reinforced macroporous calcium silicate bioceramics *Journal of the European Ceramic Society* **29** 2937-43

[195] Hench L L A W, June *An Introduction to Bioceramics*

[196] Hench L L 1991 Bioceramics: From Concept to Clinic *Journal of the American Ceramic Society* **74** 1487-510

[197] Koerten H K and van der Meulen J 1999 Degradation of calcium phosphate ceramics *Journal of biomedical materials research* **44** 78-86

[198] Lu J, Descamps M, Dejou J, Koubi G, Hardouin P, Lemaitre J and Proust J-P 2002 The biodegradation mechanism of calcium phosphate biomaterials in bone *Journal of biomedical materials research* **63** 408-12

[199] Niinomi M 2008 Mechanical biocompatibilities of titanium alloys for biomedical applications *Journal of the Mechanical Behavior of Biomedical Materials* **1** 30-42

[200] Ramaswamy Y, Wu C, Van Hummel A, Combes V, Grau G and Zreiqat H 2008 The responses of osteoblasts, osteoclasts and endothelial cells to zirconium modified calcium-silicate-based ceramic *Biomaterials* **29** 4392-402

[201] Pham D Q, Berndt C C, Cizek J, Gbureck U, Zreiqat H, Lu Z and Ang A S M 2021 Baghdadite coating formed by hybrid water-stabilized plasma spray for bioceramic applications: Mechanical and biological evaluations *Materials science & engineering. C, Materials for biological applications* **122** 111873

[202] Sun J, Wei L, Liu X, Li J, Li B, Wang G and Meng F 2009 Influences of ionic dissolution products of dicalcium silicate coating on osteoblastic proliferation, differentiation and gene expression *Acta Biomaterialia* **5** 1284-93

[203] Maeno S, Niki Y, Matsumoto H, Morioka H, Yatabe T, Funayama A, Toyama Y, Taguchi T and Tanaka J 2005 The effect of calcium ion concentration on osteoblast viability, proliferation and differentiation in monolayer and 3D culture *Biomaterials* **26** 4847-55

[204] Xynos I D, Edgar A J, Buttery L D, Hench L L and Polak J M 2000 Ionic products of bioactive glass dissolution increase proliferation of human osteoblasts and induce insulin-like growth factor II mRNA expression and protein synthesis *Biochemical and biophysical research communications* **276** 461-5

[205] Christodoulou I, Buttery L D, Saravanapavan P, Tai G, Hench L L and Polak J M 2005 Dose- and time-dependent effect of bioactive gel-glass ionic-dissolution products on human fetal osteoblast-specific gene expression *Journal of biomedical materials research. Part B, Applied biomaterials* **74** 529-37

[206] Tsigkou O, Jones J R, Polak J M and Stevens M M 2009 Differentiation of fetal osteoblasts and formation of mineralized bone nodules by 45S5 Bioglass conditioned medium in the absence of osteogenic supplements *Biomaterials* **30** 3542-50

[207] Casey W H, Westrich H R, Banfield J F, Ferruzzi G and Arnold G W 1993 Leaching and reconstruction at the surfaces of dissolving chain-silicate minerals *Nature* **366** 253-6

[208] Zhao L, Lin K, Zhang M, Xiong C, Bao Y, Pang X and Chang J 2011 The influences of poly(lactic-co-glycolic acid) (PLGA) coating on the biodegradability, bioactivity, and biocompatibility of calcium silicate bioceramics *Journal of Materials Science* **46** 4986-93

[209] Suebwongnat S, Monvisade P and Siriphannon P 2013 Mechanical properties and bioactivity of calcium silicate/poly(ethylene terephthalate-co-caprolactone) composites *Materials Research Innovations* **17** s118-s23

[210] Ni S-y, Lin K L, Chang J and Chou L 2008 β-CaSiO3/β-Ca3(PO4)2 composite materials for hard tissue repair: In vitro studies *Journal of Biomedical Materials Research Part A* **85** 72-82

[211] Fei L, Wang C, Xue Y, Lin K, Chang J and Sun J 2012 Osteogenic differentiation of osteoblasts induced by calcium silicate and calcium silicate/β-tricalcium phosphate composite bioceramics *Journal of Biomedical Materials Research Part B: Applied Biomaterials* **100B** 1237-44

[212] Farley J R, Hall S L, Tanner M A and Wergedal J E 1994 Specific activity of skeletal alkaline phosphatase in human osteoblast-line cells regulated by phosphate, phosphate esters, and phosphate analogs and release of alkaline phosphatase activity inversely regulated by calcium *Journal of bone and mineral research : the official journal of the American Society for Bone and Mineral Research* **9** 497-508

[213] Wang C, Lin K, Chang J and Sun J 2014 The stimulation of osteogenic differentiation of mesenchymal stem cells and vascular endothelial growth factor secretion of

endothelial cells by β-CaSiO3/β-Ca3(PO4)2 scaffolds *Journal of biomedical materials research. Part A* **102** 2096-104

[214] Zhang H, Jiao C, He Z, Ge M, Tian Z, Wang C, Wei Z, Shen L and Liang H 2021 Fabrication and properties of 3D printed zirconia scaffold coated with calcium silicate/hydroxyapatite *Ceramics International* **47** 27032-41

[215] Ma J, Wang C, Huang B, Zhao X, Chen C and Yu H 2020 In vitro degradation and apatite formation of magnesium and zinc incorporated calcium silicate prepared by sol-gel method *Materials Technology* **36** 1-10

[216] He F, Qiu C, Lu T, Shi X and Ye J 2021 Conjunction of gallium doping and calcium silicate mediates osteoblastic and osteoclastic performances of tricalcium phosphate bioceramics *Biomedical materials (Bristol, England)* **17**

[217] Han P, Wu C and Xiao Y 2013 The effect of silicate ions on proliferation, osteogenic differentiation and cell signalling pathways (WNT and SHH) of bone marrow stromal cells *Biomaterials Science* **1** 379-92

[218] Wang C, Xue Y, Lin K, Lu J, Chang J and Sun J 2012 The enhancement of bone regeneration by a combination of osteoconductivity and osteostimulation using β-CaSiO3/β-Ca3(PO4)2 composite bioceramics *Acta Biomaterialia* **8** 350-60

[219] Shao H, Yu X, Lin T, Peng J, Wang A, Zhang Z, Zhang Y, Liu S and Zhao M 2020 Effect of PCL concentration on PCL/CaSiO3 porous composite scaffolds for bone engineering *Ceramics International* **46** 13082-7

[220] Knabe C, Adel-Khattab D, Hübner W D, Peters F, Knauf T, Peleska B, Barnewitz D, Genzel A, Kusserow R, Sterzik F, Stiller M and Müller-Mai C 2019 Effect of silicon-doped calcium phosphate bone grafting materials on bone regeneration and osteogenic marker expression after implantation in the ovine scapula *Journal of biomedical materials research. Part B, Applied biomaterials* **107** 594-614

[221] Zhao R, Chen S, Zhao W, Yang L, Yuan B, Ioan V S, Iulian A V, Yang X, Zhu X and Zhang X 2020 A bioceramic scaffold composed of strontium-doped three-dimensional hydroxyapatite whiskers for enhanced bone regeneration in osteoporotic defects *Theranostics* **10** 1572-89

[222] Barrias C C, Martins M C, Almeida-Porada G, Barbosa M A and Granja P L 2009 The correlation between the adsorption of adhesive proteins and cell behaviour on hydroxyl-methyl mixed self-assembled monolayers *Biomaterials* **30** 307-16

[223] Dou Y, Wu C and Chang J 2012 Preparation, mechanical property and cytocompatibility of poly(L-lactic acid)/calcium silicate nanocomposites with controllable distribution of calcium silicate nanowires *Acta Biomater* **8** 4139-50

[224] Zhang N, Zhai D, Chen L, Zou Z, Lin K and Chang J 2014 Hydrothermal synthesis and characterization of Si and Sr co-substituted hydroxyapatite nanowires using strontium containing calcium silicate as precursors *Materials science & engineering. C, Materials for biological applications* **37** 286-91

[225] Yu X, Wang X, Li D, Sheng R, Qian Y, Zhu R, Wang X and Lin K 2022 Mechanically reinforced injectable bioactive nanocomposite hydrogels for in-situ bone regeneration *Chemical Engineering Journal* **433** 132799

[226] Lin K, Chang J and Cheng R 2007 In vitro hydroxyapatite forming ability and dissolution of tobermorite nanofibers *Acta Biomater* **3** 271-6

[227] Huang Y-R, Wu I T, Chen C-C and Ding S-J 2020 In vitro comparisons of microscale and nanoscale calcium silicate particles *Journal of Materials Chemistry B* **8** 6034-47

[228] Shie M Y, Ding S J and Chang H C 2011 The role of silicon in osteoblast-like cell proliferation and apoptosis *Acta Biomater* **7** 2604-14

[229] De Aza P N, Luklinska Z B, Martinez A, Anseau M R, Guitian F and De Aza S 2000 Morphological and structural study of pseudowollastonite implants in bone *Journal of microscopy* **197** 60-7

[230] Xue W, Liu X, Zheng X and Ding C 2005 In vivo evaluation of plasma-sprayed wollastonite coating *Biomaterials* **26** 3455-60

[231] Xu S, Lin K, Wang Z, Chang J, Wang L, Lu J and Ning C 2008 Reconstruction of calvarial defect of rabbits using porous calcium silicate bioactive ceramics *Biomaterials* **29** 2588-96

[232] Du Z, Leng H, Guo L, Huang Y, Zheng T, Zhao Z, Liu X, Zhang X, Cai Q and Yang X 2020 Calcium silicate scaffolds promoting bone regeneration via the doping of Mg2+ or Mn2+ ion *Composites Part B: Engineering* **190** 107937

[233] Lin K, Liu Y, Huang H, Chen L, Wang Z and Chang J 2015 Degradation and silicon excretion of the calcium silicate bioactive ceramics during bone regeneration using rabbit femur defect model *Journal of Materials Science: Materials in Medicine* **26** 197

[234] Liu S, Jin F, Lin K, Lu J, Sun J, Chang J, Dai K and Fan C 2013 The effect of calcium silicate on in vitro physiochemical properties and in vivo osteogenesis, degradability and bioactivity of porous β-tricalcium phosphate bioceramics *Biomedical materials (Bristol, England)* **8** 025008

[235] Mirkhalaf M, Goldsmith J, Ren J, Dao A, Newman P, Schindeler A, Woodruff M A, Dunstan C R and Zreiqat H 2021 Highly substituted calcium silicates 3D printed with complex architectures to produce stiff, strong and bioactive scaffolds for bone regeneration *Applied Materials Today* **25** 101230

[236] Duan B, Wang M, Zhou W Y, Cheung W L, Li Z Y and Lu W W 2010 Three-dimensional nanocomposite scaffolds fabricated via selective laser sintering for bone tissue engineering *Acta Biomater* **6** 4495-505

[237] Tong H-W and Wang M 2010 Electrospinning of fibrous polymer scaffolds using positive voltage or negative voltage: a comparative study *Biomedical Materials* **5** 054110

[238] O'flaherty E J 1992 Modeling bone mineral metabolism, with special reference to calcium and lead *Neurotoxicology* **13 4** 789-97

[239] Fan H, Tao H, Wu Y, Hu Y, Yan Y and Luo Z 2010 TGF-β3 immobilized PLGA-gelatin/chondroitin sulfate/hyaluronic acid hybrid scaffold for cartilage regeneration *Journal of biomedical materials research. Part A* **95** 982-92

[240] Hollister S J 2005 Porous scaffold design for tissue engineering *Nature materials* **4** 518-24

[241] Zhang Z, Shao H, Lin T, Zhang Y, He J and Wang L 2019 3D gel printing of porous calcium silicate scaffold for bone tissue engineering *Journal of Materials Science* **54** 10430-6

[242] Wang C, Chen B, Wang W, Zhang X, Hu T, He Y, Lin K and Liu X 2019 Strontium released bi-lineage scaffolds with immunomodulatory properties induce a pro-regenerative environment for osteochondral regeneration *Materials Science and Engineering: C* **103** 109833

[243] Tat S K, Pelletier J P, Mineau F, Caron J and Martel-Pelletier J 2011 Strontium ranelate inhibits key factors affecting bone remodeling in human osteoarthritic subchondral bone osteoblasts *Bone* **49** 559-67

[244] Zhou P, Xia D, Ni Z, Ou T, Wang Y, Zhang H, Mao L, Lin K, Xu S and Liu J 2021 Calcium silicate bioactive ceramics induce osteogenesis through oncostatin M *Bioactive Materials* **6** 810-22

[245] Kim E J, Bu S Y, Sung M K, Kang M H and Choi M K 2013 Analysis of antioxidant and anti-inflammatory activity of silicon in murine macrophages *Biological trace element research* **156** 329-37

[246] Liu G, Wu C, Fan W, Miao X, Sin D-C, Crawford R and Xiao Y 2011 The effects of bioactive akermanite on physiochemical, drug-delivery, and biological properties of poly(lactide-co-glycolide) beads *Journal of Biomedical Materials Research Part B: Applied Biomaterials* **96B** 360-8

[247] Siriphannon P, Kameshima Y, Yasumori A, Okada K and Hayashi S 2000 Influence of Preparation Conditions on the Microstructure and Bioactivity of ??-CaSiO3 Ceramics *Journal of Biomedical Materials Research Part A* **52** 30-9

[248] Mehrali M, Moghaddam E, Shirazi S F, Baradaran S, Mehrali M, Latibari S T, Metselaar H S, Kadri N A, Zandi K and Osman N A 2014 Synthesis, mechanical properties, and in vitro biocompatibility with osteoblasts of calcium silicate-reduced graphene oxide composites *ACS Appl Mater Interfaces* **6** 3947-62

[249] Wang C, Lin K, Chang J and Sun J 2013 Osteogenesis and angiogenesis induced by porous β-CaSiO3/PDLGA composite scaffold via activation of AMPK/ERK1/2 and PI3K/Akt pathways *Biomaterials* **34** 64-77

[250] Roethlisberger F, Seifert F M and Czank M 1990 Chemical control of the commensurate-incommensurate phase transition in synthetic melilites *European Journal of Mineralogy* **2** 585-94

[251] Bhatkar V B and Bhatkar N V 2011 Combustion synthesis and photoluminescence study of silicate biomaterials *Bulletin of Materials Science* **34** 1281-4

[252] Yang H, Hazen R, Downs R and Finger L 1997 Structural change associated with the incommensurate-normal phase transition in akermanite, Ca 2 MgSi 2 O 7 , at high pressure *Physics and Chemistry of Minerals - PHYS CHEM MINER* **24** 510-9

[253] Thompson R M and Downs R T 2004 Model pyroxenes II: Structural variation as a function of tetrahedral rotation *American Mineralogist* **89** 614-28

[254] Finger L W and Ohashi Y 1976 The thermal expansion of diopside to 800 degrees C and a refinement of the crystal structure at 700 degrees C *American Mineralogist* **61** 303-10

[255] Srinath P, Azeem P A, Reddy K V, Chiranjeevi P, Bramanandam M and Rao R P 2021 A novel cost-effective approach to fabricate diopside bioceramics: A promising ceramics for orthopedic applications *Advanced Powder Technology* **32** 875-84

[256] Sharp Z D, Hazen R M and Finger L W 1987 High-pressure crystal chemistry of monticellite, CaMgSiO4 *American Mineralogist* **72** 748-55

[257] Brown G B and West J X. The structure of monticellite (MgCaSiO4) *Zeitschrift für Kristallographie - Crystalline Materials* **66** 154 - 61

[258] Wu C and Chang J 2004 Synthesis and apatite-formation ability of akermanite *Materials Letters* **58** 2415-7

[259] Wu C, Chang J, Ni S and Wang J 2006 In vitro bioactivity of akermanite ceramics *Journal of biomedical materials research. Part A* **76** 73-80

[260] Wu C and Chang J 2006 A novel akermanite bioceramic: preparation and characteristics *J Biomater Appl* **21** 119-29

[261] Wu C and Chang J 2007 Degradation, bioactivity, and cytocompatibility of diopside, akermanite, and bredigite ceramics *Journal of Biomedical Materials Research Part B: Applied Biomaterials* **83B** 153-60

[262] Chen X, Ou J, Yan W, Huang Z, Kang Y and Yin G 2010 Effect of MgO contents on the mechanical properties and biological performances of bioceramics in the MgO-CaO-SiO2 system *Journal of materials science. Materials in medicine* **21** 1463-71

[263] Choudhary R, Koppala S and Swamiappan S 2015 Bioactivity studies of calcium magnesium silicate prepared from eggshell waste by sol–gel combustion synthesis *Journal of Asian Ceramic Societies* **3** 173-7

[264] Wu C and Chang J 2007 Synthesis and in vitro bioactivity of bredigite powders *J Biomater Appl* **21** 251-63

[265] Tavangarian F, Zolko C and Davami K 2021 Synthesis, characterization and formation mechanisms of nanocrystalline akermanite powder *Journal of Materials Research and Technology* **11**

[266] Sharafabadi A K, Abdellahi M, Kazemi A, Khandan A and Ozada N 2017 A novel and economical route for synthesizing akermanite (Ca2MgSi2O7) nano-bioceramic *Materials Science and Engineering: C* **71** 1072-8

[267] Myat-Htun M, Noor A F M, Kawashita M and Ismail Y M B 2020 Enhanced sinterability and in vitro bioactivity of barium-doped akermanite ceramic *Ceramics International* **46** 19062-8

[268] Huang X-H and Chang J 2008 Preparation of nanocrystalline bredigite powders with apatite-forming ability by a simple combustion method *Materials Research Bulletin* **43** 1615-20

[269] Tavangarian F and Emadi R 2011 Mechanism of nanostructure bredigite formation by mechanical activation with thermal treatment *Materials Letters* **65** 2354-6

[270] Wu C, Chang J, Wang J, Ni S and Zhai W 2005 Preparation and characteristics of a calcium magnesium silicate (bredigite) bioactive ceramic *Biomaterials* **26** 2925-31

[271] Mohammadi H, Baba Ismail Y M, Shariff K A and Mohd Noor A-F 2021 Effect of strontium substitution on structural, sinterability, physicomechanical and biological properties of akermanite ceramic *Journal of the Mechanical Behavior of Biomedical Materials* **116** 104379

[272] Wei J, Lu J, Yan Y, Li H, Ma J, Wu X, Dai C and Liu C 2011 Preparation and characterization of well ordered mesoporous diopside nanobiomaterial *Journal of nanoscience and nanotechnology* **11** 10746-9

[273] Nonami T, Takahashi C and Yamazaki J 1995 Synthesis of Diopside by Alkoxide Method and Coating on Titanium *Journal of the Ceramic Society of Japan* **103** 703-8

[274] Iwata N Y, Lee G H, Tokuoka Y and Kawashima N 2004 Sintering behavior and apatite formation of diopside prepared by coprecipitation process *Colloids and surfaces. B, Biointerfaces* **34** 239-45

[275] Shahrouzifar M and Salahinejad E 2019 Strontium doping into diopside tissue engineering scaffolds *Ceramics International* **45** 10176-81

[276] Nonami T 1991 Developmental study of diopside for use as implant material *MRS Online Proceedings Library (OPL)* **252** 87

[277] Iwata N Y, Lee G-H, Tsunakawa S, Tokuoka Y and Kawashima N 2004 Preparation of diopside with apatite-forming ability by sol–gel process using metal alkoxide and metal salts *Colloids and Surfaces B: Biointerfaces* **33** 1-6

[278] Hafezi-Ardakani M, Moztarzadeh F, Rabiee M and Talebi A R 2011 Synthesis and characterization of nanocrystalline merwinite (Ca3Mg (SiO4) 2) via sol–gel method *Ceramics International* **37** 175-80

[279] Hafezi-Ardakani M, Moztarzadeh F, Rabiee M, Talebi A R, Abasi-shahni M, Fesahat F and Sadeghian F 2010 Sol-gel synthesis and apatite-formation ability of

nanostructure merwinite (Ca3MgSi2O8) as a novel bioceramic *J. Ceram. Process. Res* **11** 765-8

[280] Praharaj S, Venkatraman S K, Vasantharaman R and Swamiappan S 2021 Sol-gel combustion synthesis of merwinite and its biomedical applications *Materials Letters* **300** 130108

[281] Ou J, Kang Y, Huang Z, Chen X, Wu J, Xiao R and Yin G 2008 Preparation and in vitro bioactivity of novel merwinite ceramic *Biomedical Materials* **3** 015015

[282] Chen X, Ou J, Kang Y, Huang Z, Zhu H, Yin G and Wen H 2008 Synthesis and characteristics of monticellite bioactive ceramic *Journal of Materials Science: Materials in Medicine* **19** 1257-63

[283] Kalantari E, Naghib S M, Naimi-Jamal M R, Aliahmadi A, Iravani N J and Mozafari M 2018 Nanostructured monticellite for tissue engineering applications-Part I: Microstructural and physicochemical characteristics *Ceramics International* **44** 12731-8

[284] Kalantari E and Naghib S M 2019 A comparative study on biological properties of novel nanostructured monticellite-based composites with hydroxyapatite bioceramic *Materials Science and Engineering: C* **98** 1087-96

[285] Kokubo T 1991 Bioactive glass ceramics: properties and applications *Biomaterials* **12** 155-63

[286] Wu C, Chang J, Zhai W, Ni S and Wang J 2006 Porous akermanite scaffolds for bone tissue engineering: preparation, characterization, and in vitro studies *Journal of Biomedical Materials Research Part B: Applied Biomaterials: An Official Journal of The Society for Biomaterials, The Japanese Society for Biomaterials, and The Australian Society for Biomaterials and the Korean Society for Biomaterials* **78** 47-55

[287] Collin M S, Venkatraman S K, Sriramulu M, Shanmugam S, Drweesh E A, Elnagar M M, Mosa E and Sasikumar S 2021 Solution combustion synthesis of functional diopside, akermanite, and merwinite bioceramics: Excellent biomineralization, mechanical strength, and antibacterial ability *Materials Today Communications* **27** 102365

[288] Radin S and Ducheyne P 1993 The effect of calcium phosphate ceramic composition and structure on in vitro behavior. II. Precipitation *Journal of biomedical materials research* **27** 35-45

[289] Ducheyne P, Radin S and King L 1993 The effect of calcium phosphate ceramic composition and structure on in vitro behavior. I. Dissolution *Journal of biomedical materials research* **27** 25-34

[290] Radin S and Ducheyne P 1994 Effect of bioactive ceramic composition and structure on in vitro behavior. III. Porous versus dense ceramics *Journal of biomedical materials research* **28** 1303-9

[291] Vallet-Regi M, Salinas A, Roman J and Gil M 1999 Effect of magnesium content on the in vitro bioactivity of CaO-MgO-SiO 2-P 2 O 5 sol-gel glasses *Journal of Materials Chemistry* **9** 515-8

[292] Wu C, Chang J, Ni S and Wang J 2006 In Vitro Bioactivity of Akermanite Ceramics *Journal of biomedical materials research. Part A* **76** 73-80

[293] Pérez-Pariente J, Balas F and Vallet-Regí M 2000 Surface and Chemical Study of SiO2⊙ P2O5⊙ CaO⊙(MgO) Bioactive Glasses *Chemistry of materials* **12** 750-5

[294] Liu Q, Cen L, Yin S, Chen L, Liu G, Chang J and Cui L 2008 A comparative study of proliferation and osteogenic differentiation of adipose-derived stem cells on akermanite and β-TCP ceramics *Biomaterials* **29** 4792-9

[295] Sun H, Wu C, Dai K, Chang J and Tang T 2006 Proliferation and osteoblastic differentiation of human bone marrow-derived stromal cells on akermanite-bioactive ceramics *Biomaterials* **27** 5651-7

[296] Sader M S, LeGeros R Z and Soares G A 2009 Human osteoblasts adhesion and proliferation on magnesium-substituted tricalcium phosphate dense tablets *Journal of Materials Science: Materials in Medicine* **20** 521-7

[297] Ansari M, Malmir F and Salati A 2020 Preparation and characterization of akermanite/merwinite scaffolds for bone tissue repair *Journal of Biomimetics, Biomaterials and Biomedical Engineering* **44** 73-81

[298] Kobayashi T, Okada K, Kuroda T and Sato K 1997 Osteogenic cell cytotoxicity and biomechanical strength of the new ceramic diopside *Journal of Biomedical Materials Research: An Official Journal of The Society for Biomaterials and The Japanese Society for Biomaterials* **37** 100-7

[299] Miake Y, Yanagisawa T, Yajima Y, Noma H, Yasui N and Nonami T 1995 High-resolution and analytical electron microscopic studies of new crystals induced by a bioactive ceramic (diopside) *Journal of dental research* **74** 1756-63

[300] Nonami T, Takahashi C and Yamazaki J 1995 Synthesis of diopside by alkoxide method and coating on titanium *Journal of the Ceramic Society of Japan* **103** 703-8

[301] Su Y-H, Pan C-T, Tseng Y-S, Zhang J and Chen W-F 2021 Rare earth element cerium substituted Ca–Si–Mg system bioceramics: From mechanism to mechanical and degradation properties *Ceramics International* **47** 19414-23

[302] Bakhsheshi-Rad H, Chen X, Ismail A, Aziz M, Hamzah E and Najafinezhad A 2019 A new multifunctional monticellite-ciprofloxacin scaffold: preparation, bioactivity, biocompatibility, and antibacterial properties *Materials Chemistry and Physics* **222** 118-31

[303] Chen X, Yin G and Ou J 2007 In vitro bioactivity of merwinite prepared by sol-gel process *JOURNAL OF FUNCTIONAL MATERIALS* **38** 435

[304] Xia L, Yin Z, Mao L, Wang X, Liu J, Jiang X, Zhang Z, Lin K, Chang J and Fang B 2016 Akermanite bioceramics promote osteogenesis, angiogenesis and suppress osteoclastogenesis for osteoporotic bone regeneration *Scientific reports* **6** 22005

[305] Cui J, Xia L, Lin K and Wang X 2021 In situ construction of a nano-structured akermanite coating for promoting bone formation and osseointegration of Ti–6Al–4V implants in a rabbit osteoporosis model *Journal of Materials Chemistry B* **9** 9505-13

[306] Razavi M, Fathi M, Savabi O, Beni B H, Vashaee D and Tayebi L 2014 Surface microstructure and in vitro analysis of nanostructured akermanite (Ca2MgSi2O7) coating on biodegradable magnesium alloy for biomedical applications *Colloids and Surfaces B: Biointerfaces* **117** 432-40

[307] Wu C, Zhang M, Zhai D, Yu J, Liu Y, Zhu H and Chang J 2013 Containerless processing for preparation of akermanite bioceramic spheres with homogeneous structure, tailored bioactivity and degradation *Journal of Materials Chemistry B* **1** 1019-26

[308] Wu C, Chang J, Zhai W and Ni S 2007 A novel bioactive porous bredigite (Ca 7 MgSi 4 O 16) scaffold with biomimetic apatite layer for bone tissue engineering *Journal of Materials Science: Materials in Medicine* **18** 857-64

[309] Razavi M, Fathi M, Savabi O, Razavi S M, Heidari F, Manshaei M, Vashaee D and Tayebi L 2014 In vivo study of nanostructured diopside (CaMgSi2O6) coating on magnesium alloy as biodegradable orthopedic implants *Applied Surface Science* **313** 60-6

[310] Luo T, Wu C and Zhang Y 2012 The in vivo osteogenesis of Mg or Zr-modified silicate-based bioceramic spheres *Journal of Biomedical Materials Research Part A* **100** 2269-77

[311] Baxter F R, Bowen C R, Turner I G and Dent A C 2010 Electrically active bioceramics: a review of interfacial responses *Annals of biomedical engineering* **38** 2079-92

[312] Singh A, Singh P and Dubey A K 2022 Effect of incorporation of piezoelectric phases on antibacterial and cellular response of borate bioactive glass *Open Ceramics* **9** 100234

[313] More N and Kapusetti G 2017 Piezoelectric material–a promising approach for bone and cartilage regeneration *Medical hypotheses* **108** 10-6

[314] Srirussamee K 2020 *Direct Electrical Stimulation Approaches for Bone Repair and Regeneration*: The University of Manchester (United Kingdom))

[315] Khare D, Singh P and Dubey A K 2022 Interplay of surface polarization charge, dynamic electrical stimulation and compositional modification towards accelerated osteogenic response of NaxK1-xNbO3 piezo-bioceramics *Biomaterials Advances* **140** 213042

[316] Dubey A K and Basu B 2014 Pulsed electrical stimulation and surface charge induced cell growth on multistage spark plasma sintered hydroxyapatite-barium titanate piezobiocomposite *Journal of the American Ceramic Society* **97** 481-9

[317] Verma A S, Sharma A, Kumar A, Mukhopadhyay A, Kumar D and Dubey A K 2020 Multifunctional response of piezoelectric sodium potassium niobate (NKN)-toughened hydroxyapatite-based biocomposites *ACS Applied Bio Materials* **3** 5287-99

[318] Griffin M, Iqbal S A, Sebastian A, Colthurst J and Bayat A 2011 Degenerate wave and capacitive coupling increase human MSC invasion and proliferation while reducing cytotoxicity in an in vitro wound healing model *PloS one* **6** e23404

[319] Srirussamee K, Xue R, Mobini S, Cassidy N J and Cartmell S H 2021 Changes in the extracellular microenvironment and osteogenic responses of mesenchymal stem/stromal cells induced by in vitro direct electrical stimulation *Journal of Tissue Engineering* **12** 2041731420974147

[320] Kumar D, Gittings J, Turner I G, Bowen C, Bastida-Hidalgo A and Cartmell S 2010 Polarization of hydroxyapatite: Influence on osteoblast cell proliferation *Acta biomaterialia* **6** 1549-54

[321] Ohgaki M, Kizuki T, Katsura M and Yamashita K 2001 Manipulation of selective cell adhesion and growth by surface charges of electrically polarized hydroxyapatite *Journal of Biomedical Materials Research: An Official Journal of The Society for Biomaterials, The Japanese Society for Biomaterials, and The Australian Society for Biomaterials and the Korean Society for Biomaterials* **57** 366-73

[322] Bodhak S, Bose S and Bandyopadhyay A 2009 Role of surface charge and wettability on early stage mineralization and bone cell–materials interactions of polarized hydroxyapatite *Acta Biomaterialia* **5** 2178-88

[323] Verma A S, Kumar D and Dubey A K 2020 Antibacterial and cellular response of piezoelectric Na0. 5K0. 5NbO3modified 1393 bioactive glass *Materials Science and Engineering: C* **116** 111138

[324] Atanasoska L, Radhakrishnan R and Schewe S 2014 Medical devices employing piezoelectric materials for delivery of therapeutic agents. Google Patents)

[325] Frost H M 1994 Wolff's Law and bone's structural adaptations to mechanical usage: an overview for clinicians *The Angle Orthodontist* **64** 175-88

[326] Hu S, Jia F, Marinescu C, Cimpoesu F, Qi Y, Tao Y, Stroppa A and Ren W 2017 Ferroelectric polarization of hydroxyapatite from density functional theory *RSC advances* **7** 21375-9

[327] Turner C, Wang T and Burr D 2001 Shear strength and fatigue properties of human cortical bone determined from pure shear tests *Calcified tissue international* **69**

[328] Halperin C, Mutchnik S, Agronin A, Molotskii M, Urenski P, Salai M and Rosenman G 2004 Piezoelectric effect in human bones studied in nanometer scale *Nano Letters* **4** 1253-6

[329] Verma A S, Singh A, Kumar D and Dubey A K 2020 Electro-mechanical and Polarization-Induced Antibacterial Response of 45S5 Bioglass–Sodium Potassium Niobate Piezoelectric Ceramic Composites *ACS Biomaterials Science & Engineering* **6** 3055-69

[330] Rajabi A H, Jaffe M and Arinzeh T L 2015 Piezoelectric materials for tissue regeneration: A review *Acta biomaterialia* **24** 12-23

[331] Jacob J, More N, Kalia K and Kapusetti G 2018 Piezoelectric smart biomaterials for bone and cartilage tissue engineering *Inflammation and regeneration* **38** 2

[332] Costerton J W, Stewart P S and Greenberg E P 1999 Bacterial biofilms: a common cause of persistent infections *science* **284** 1318-22

[333] Singh A and Dubey A K 2018 Various biomaterials and techniques for improving antibacterial response *ACS Applied Bio Materials* **1** 3-20

[334] Choudhary R, Chatterjee A, Venkatraman S K, Koppala S, Abraham J and Swamiappan S 2018 Antibacterial forsterite (Mg2SiO4) scaffold: A promising bioceramic for load bearing applications *Bioactive Materials* **3** 218-24

[335] Avram A, Rapuntean S, Gorea M, Tomoaia G, Mocanu A, Horovitz O, Rapuntean G and Tomoaia-Cotisel M 2022 In vitro antibacterial effect of forsterite nanopowder:

synthesis and characterization *Environmental Science and Pollution Research* **29** 77097-112

[336] Baron S 1996 Medical microbiology

[337] Nikaido H and Nakae T 1980 The outer membrane of Gram-negative bacteria *Advances in microbial physiology* **20** 163-250

[338] Khare D, Singh A and Dubey A K 2021 Influence of Na and K contents on the antibacterial response of piezoelectric biocompatible NaxK1-xNbO3 (x= 0.2–0.8) *Materials Today Communications* **27** 102317

[339] Sonohara R, Muramatsu N, Ohshima H and Kondo T 1995 Difference in surface properties between Escherichia coli and Staphylococcus aureus as revealed by electrophoretic mobility measurements *Biophysical chemistry* **55** 273-7

[340] Kłodzińska E, Szumski M, Dziubakiewicz E, Hrynkiewicz K, Skwarek E, Janusz W and Buszewski B 2010 Effect of zeta potential value on bacterial behavior during electrophoretic separation *Electrophoresis* **31** 1590-6

[341] Nakahara T, Yaguchi H, Yoshida M and Miyakoshi J 2002 Effects of exposure of CHO-K1 cells to a 10-T static magnetic field *Radiology* **224** 817-22

[342] Bajpai I, Saha N and Basu B 2012 Moderate intensity static magnetic field has bactericidal effect on E. coli and S. epidermidis on sintered hydroxyapatite *Journal of Biomedical Materials Research Part B: Applied Biomaterials* **100** 1206-17

[343] Bajpai I, Balani K and Basu B 2014 Synergistic effect of static magnetic field and HA-Fe3O4 magnetic composites on viability of S. aureus and E. coli bacteria *Journal of Biomedical Materials Research Part B: Applied Biomaterials* **102** 524-32

[344] Tan G, Wang S, Zhu Y, Zhou L, Yu P, Wang X, He T, Chen J, Mao C and Ning C 2016 Surface-Selective Preferential Production of Reactive Oxygen Species on Piezoelectric Ceramics for Bacterial Killing *ACS Appl Mater Interfaces* **8** 24306-9

[345] Yao T, Chen J, Wang Z, Zhai J, Li Y, Xing J, Hu S, Tan G, Qi S, Chang Y, Yu P and Ning C 2019 The antibacterial effect of potassium-sodium niobate ceramics based on controlling piezoelectric properties *Colloids and Surfaces B: Biointerfaces* **175** 463-8

[346] Swain S, Padhy R N and Rautray T R 2020 Polarized piezoelectric bioceramic composites exhibit antibacterial activity *Materials Chemistry and Physics* **239** 122002

[347] Liu W K, Brown M R and Elliott T S 1997 Mechanisms of the bactericidal activity of low amperage electric current (DC) *The Journal of antimicrobial chemotherapy* **39** 687-95

[348] Singh A, Reshma K and Dubey A K 2020 Combined effect of surface polarization and ZnO addition on antibacterial and cellular response of Hydroxyapatite-ZnO composites *Materials Science and Engineering: C* **107** 110363

[349] Ribeiro M, Monteiro F and Ferraz M 2012 Infection of orthopedic implants with emphasis on bacterial adhesion process and techniques used in studying bacterial-material interactions *Biomatter* **2** 176-94

[350] Baier R, Meyer A, Natiella J, Natiella R and Carter J 1984 Surface properties determine bioadhesive outcomes: methods and results *Journal of biomedical materials research* **18** 337-55

[351] Flock J-I 1999 Extracellular-matrix-binding proteins as targets for the prevention of Staphylococcus aureus infections *Molecular medicine today* **5** 532-7

[352] Alam F and Balani K 2017 Adhesion force of staphylococcus aureus on various biomaterial surfaces *Journal of the Mechanical Behavior of Biomedical Materials* **65** 872-80